Mechanics of Needle-free Drug Delivery

Anna Henley

Master of Engineering

Supervised by Prof. Luc Mongeau

Department of Biological and Biomedical Engineering
McGill University
Montreal, Québec
2020-11-15

A dissertation submitted to McGill University in partial fulfillment of the requirements for the degree of Master of Engineering.

I TABLE OF CONTENTS

II LIST OF FIGURES

III ABSTRACT

Despite its long history and widespread applications, particularly for animal injections, needle-free pneumatic jet injection remains under-utilized in healthcare systems worldwide. The detailed mechanisms and physics of needle free injection are poorly understood. Improved understanding of conventional needle-based and pneumatic needle-free injection may improve clinical outcomes by informing evidence-based clinical techniques. Increased uptake associated with improved outcomes may then benefit clinicians by eliminating the risk of needle-stick injuries and transfection. Patients will benefit from a pain-free alternative, potentially avoiding complications associated with needle phobia, a condition which results in avoidance of necessary medical procedures in some patients.

In the present study, a needle-free liquid jet injection device (MED-Jet Meso-Jet, MIT Canada Inc., 80-220 psi supply pressure, orifice diameter 120 μm) was characterized for dental local anesthesia application. First, a soft tissue phantom was selected based on the properties of fresh porcine oral tissue. Viscoelastic and mechanical properties were measured using torsional rheometry. Scanning electron microscopy was used to characterize the phantom pore size and morphology. Candidate phantom materials included type-II bovine gelatin hydrogel, type-II bovine gelatin cryogel, glycol chitosan hydrogel, and polyhydroxyethylmethacrylate (pHEMA) hydrogel. This tissue phantom was then used to compare needle-based and jet injection via a test apparatus comprising a strain gauge transducer, linear motorized traverse, and high-speed camera. Outcomes included the injection forces developed inside the phantom, wound morphology, and the dispersion profile of injected fluid. The same set-up was then used to characterize the effects of injection parameters such as injection volume (0.1-1 mL) and pneumatic supply pressure (413.7-1241.1 kPa or 60-180 psi) on the dynamics of jet injection, and parameters such as insertion speed

(2-37.5 mm/s), needle geometry (18-27 gauge, flat and beveled tips), injection volume (0.3 mL or 1 mL), and volumetric flow rate (0.9 mL/minute or 7.2 mL/minute) on needle injection. It was found that type-II bovine gelatin (5% mass concentration) provided a reasonable facsimile for the storage modulus and viscosity of porcine oral tissue. The wound morphology created in the gelatin phantom, however, was found to differ from that developed in tissue. A porous pHEMA phantom was then evaluated and found to adequately mimic the mechanical properties and porous characteristics of porcine oral mucosa; the associated wound morphology better approximated that of injection into tissue than non-porous phantoms. The characteristics of needle insertion, needle injection, and injection via NFLJI system were investigated in the gelatin and pHEMA phantoms. With respect to needle insertion, it was found that increasing needle gauge corresponded with decreased insertion forces and fracture toughness, while a beveled tip geometry decreased insertion forces and fracture toughness. The relationship between insertion speed and insertion force amplitude was found to be nonlinear. Increased needle injection volume produced a greater injection force amplitude, and a greater impulse as calculated from the recorded force time histories. The relationship between injection volume and work of injection was non-linear. Increased volumetric flow rate was found to correlate with a decrease in impulse of injection, due to the decreased injection duration, and an increase in work of injection associated with the increased work of fluid delivery. Injection volume did not cause any significant change in the magnitude of injection forces developed. Finally, the effects of pneumatic supply pressure and injection volume on the injection forces and work of jet injection were evaluated. It was found that increased injection volume resulted in increased injection force amplitude, impulse, and work of injection. Increased pneumatic supply pressure to the NFLJI system was found to linearly increase the impulse, work, and injection force amplitude for injection volumes of 0.1 mL and 0.3 mL.

Increasing pneumatic supply pressure was also found to increase the penetration depth of the jet into the soft tissue phantom. Regurgitation of fluid following NFLJI was found to be the greatest at low injection volumes in the gelatin phantom.

The injection force amplitudes produced by needle injection and NFLJI as methods of fluid delivery into the soft tissue phantom were found to be comparable; however, the injection duration of NFLJI delivery was significantly shorter than that of needle injection. It was also found that NFLJI produced vibrations in the tissue, absent in needle injection, which should be further explored in future work. In comparing the energy delivered to the phantom, characterized as the work of injection via each method, it was found that the energy was comparable for an injection volume of 0.3 mL with needle volumetric flow rate of 7.2 mL/minute and NFLJI pneumatic supply pressure of 413.7 kPa. For other configurations, including the clinical benchmark parameters of pneumatic supply pressure of 620.5 kPa for the NFLJI system and volumetric flow rate of 7.2 mL/minute for needle injection, a 1 mL injection corresponded with greater energy when delivered via NFLJI system. Increased energy associated with fluid delivery relative to needle injection may indicate greater tissue damage. Clinical investigations have indicated decreased injection pain associated with delivery via NFLJI, indicating that the temporal aspect of pain sensation may be more relevant to injection than the energetic aspect. Results from this investigation are in use to inform clinical pilot testing of the jet injection device for local anesthesia at the McGill Dental Clinic. They will help define best clinical practices and safe injection pressure limits for the widespread use of needle-free pneumatic jet injection.

IV ABRÉGÉ

Malgré une longue histoire et de nombreuses applications, en particulier pour les injections animales, l'injection à jet pneumatique sans-aiguille reste sous-utilisée dans les systèmes de santé. Les mécanismes physiques de l'injection sans-aiguille sont toujours mal compris. Une meilleure compréhension de l'injection conventionnelle à base d'aiguille et pneumatique sans-aiguille est nécessaire afin d'améliorer les résultats cliniques. L'injection par aiguille pourrait contribuer à éliminer les blessures par piqûre d'aiguille et réduire les risques de transfection. Elle constitue une alternative indolore aux aiguilles, évitant éventuellement les complications associées à la phobie des aiguilles, une condition qui peut parfois conduire des patients à éviter des procédures médicales nécessaires.

Dans l'étude présente, un dispositif d'injection à jet liquide sans-aiguille (MED-Jet Meso-Jet, MIT Canada Inc., pression d'alimentation 80-220 psi, diamètre de buse 120 µm) a été caractérisé pour l'anesthésie locale dans les applications dentaires. Tout d'abord, un fantôme de tissu mou a été sélectionné en fonction des propriétés du tissu buccal porcin frais. Les propriétés viscoélastiques et mécaniques ont été mesurées par rhéométrie de torsion. La microscopie électronique à balayage a été utilisée pour caractériser la taille et la morphologie des pores. Les candidats de matériaux fantômes comprenaient l'hydrogel de gélatine bovine de type II, le cryogel de gélatine bovine de type II, l'hydrogel de glycol chitosane et l'hydrogel de polyhydroxyéthylméthacrylate (pHEMA). Ce fantôme de tissu a ensuite été utilisé pour comparer l'injection à base d'aiguille et l'injection par jet via un appareil de test comprenant un capteur de force à jauge de contrainte, une traverse motorisée linéaire et deux caméras à grande vitesse. Les résultats obtenus incluent les forces d'injection développées à l'intérieur du fantôme, la morphologie de la plaie et le profil de dispersion du fluide injecté. La même configuration a ensuite été utilisée pour caractériser les effets des

paramètres d'injection tels que le volume (0,1-1 ml) et la pression d'alimentation pneumatique (413,7-1241,1 kPa ou 60-180 psi) sur la dynamique de l'injection par jet, et des paramètres comme la vitesse d'insertion (2-37,5 mm / s), la géométrie de l'aiguille (calibre 18-27, pointes plates et biseautées), le volume (0,3 ml ou 1 ml) et le débit volumétrique (0,9 ml / minute ou 7,2 ml / minute) pour l'injection à l'aiguille. On a découvert que la gélatine bovine de type II (concentration massique de 5%) semble être un facsimilé raisonnable du tissu oral porcin en ce qui a trait au module de stockage et la viscosité. Cependant, la morphologie de la plaie créée dans le fantôme de gélatine différe de celle développée dans les tissus. Un fantôme pHEMA poreux a ensuite été évalué. Ce dernier se trouve à imiter de manière adéquate les propriétés mécaniques et les caractéristiques poreuses de la muqueuse buccale porcine, en plus de présenter une morphologie de la plaie qui approche celle de l'injection dans les tissus. Les caractéristiques de l'insertion de l'aiguille, de l'injection d'aiguille et de l'injection via le système IJLSA ont été étudiées dans les fantômes de gélatine et de pHEMA. En ce qui concerne l'insertion de l'aiguille, on a trouvé que l'augmentation du calibre de l'aiguille offre des forces d'insertion et à une résistance à la fracture réduites, tandis qu'une géométrie de pointe biseautée diminue les forces d'insertion et la ténacité à la fracture. La relation entre la vitesse d'insertion et l'amplitude de la force d'insertion s'est avérée non linéaire. En ce qui concerne l'injection à l'aiguille, il a été trouvé qu'un volume d'injection accru correspondait à une plus grande amplitude de force d'injection et à une plus grande impulsion d'injection calculée, tandis que la relation entre le volume d'injection et le travail d'injection était aussi non linéaire. L'augmentation du débit volumétrique s'est avérée corrélée à une diminution de l'impulsion d'injection, due à la diminution de la durée de l'injection, et à une augmentation du travail associé à la distribution du fluide. Le volume d'injection n'a pas provoqué de changement significatif dans l'amplitude des forces d'injection développées. Enfin, les effets de la pression d'alimentation pneumatique et du volume d'injection sur les forces d'injection et le travail d'injection par jet ont été évalués. Il a été constaté qu'une augmentation du volume d'injection entraînait une augmentation de l'amplitude de la force d'injection, de l'impulsion et du travail d'injection. L'augmentation de la pression d'alimentation pneumatique au système IJLSA s'est avérée augmenter l'amplitude de l'impulsion, du travail et de la force d'injection de façon linéaire pour des volumes d'injection de 0,1 ml et 0,3 ml, mais non pour 1 ml. On a également trouvé que l'augmentation de la pression d'alimentation pneumatique était en corrélation avec l'augmentation de la profondeur de pénétration du jet dans le fantôme des tissus mous. La régurgitation du liquide après IJLSA s'est avérée être la plus élevée à de faibles volumes d'injection dans le fantôme de gélatine.

Les amplitudes de la force d'injection étant comparables, la durée d'injection de IJLSA était beaucoup plus courte que celle de l'aiguille. Il a également été constaté que le IJLSA produisait des vibrations dans le tissu, absentes lors de l'injection à l'aiguille. En comparant l'énergie fournie au fantôme, caractérisée comme le travail d'injection via chaque méthode, il a été constaté que l'énergie était comparable à un volume d'injection de 0,3 ml avec un débit volumétrique à l'aiguille de 7,2 ml / minute et une pression d'alimentation pneumatique IJLSA de 413,7 kPa. Pour d'autres configurations, incluant en particulier une pression d'alimentation pneumatique de 620,5 kPa pour le système IJLSA et un débit volumétrique de 7,2 ml / minute pour l'injection par aiguille, une injection de 1 ml requiert une plus grande énergie lorsqu'elle est administrée via le système IJLSA. Cette énergie accrue associée à la distribution de fluide par rapport à l'injection d'aiguille pourrait engendrer une plus grande lésion tissulaire. Les investigations cliniques ont indiqué une diminution de la douleur associée à l’injection via IJLSA, indiquant que l'aspect temporel de la sensation de douleur peut être plus pertinent pour l'injection que l'aspect énergétique.

Les résultats de la présente étude seront utilisés pour éclairer des futurs essais cliniques pilotes du dispositif d'injection à jet pour l'anesthésie locale à la clinique dentaire de McGill. Ils aideront à définir les meilleures pratiques cliniques et les limites de pression d'injection en toute confiance pour l'utilisation généralisée et sécuritaire de l'injection à jet pneumatique sans-aiguille.

V ACKNOWLEDGEMENTS

I must first thank Prof. Luc Mongeau for his endless patience, guidance, and support. The privilege of his supervision and mentorship has been invaluable, and I have learned an incredible amount. I must also immensely thank Qiman Gao for her fearless partnership – she has been the best co-investigator one could ask for! Thanks go as well to Zixin He for his invaluable assistance in test apparatus design and modification, and his willingness as a sounding board for research ideas. I am also grateful to Swen Groen and Rani Taher, whose excellent foundational work laid the path for my research to follow. I was immensely lucky to be surrounded by a group of excellent and inspiring colleagues in the McGill Biomechanics Lab: Guangyu Bao, Sareh Taheri, Sepideh Mohammadi, Alda Profka, Alicia Reyes Valenzuela, Rayane Ait Oubahou, Hana Mirvakili, Mehdi Shamshiri, Mitchell Strong, Abigail Vikstrom, Pooya Tavakoli-Saberi, Ksenia Kolosova, Zhengdong Lei, and Huijie Wang. To all of you, thank you for your friendship, support, and willingness to answer research-related questions at all hours of the night and weekend.

To my family, thank you for your endless support and guidance as I navigated these formative years of my life and education. To my friends, especially my partner and Abrégé editor extraordinaire Canon Wan Chun Wah, thank you especially for putting up with me throughout the thesis-drafting process.

I would like to acknowledge the support provided to this project by the Natural Sciences and Engineering Research Council of Canada (NSERC) Engage Grant (EGP 543972-19) obtained in collaboration with Medical International Technologies (MIT Canada) Inc. Many thanks to Mr. Karim Menassa and the team at Medical International Technologies (MIT Canada) Inc. for their support as the industrial partners of this research.

I would also like to acknowledge the educational software licenses provided which supported this research. BioVinci, provided free of cost to researchers by BioTuring, was utilized for preparation of figures and Dragonfly, free of cost to researchers from Object Research Systems, was used for computerized tomography image segmentation.

Finally, I must acknowledge that this land which has become my home amid these most formative years of my education has been a site of meeting and exchange for centuries, long before Canada and McGill University came to be. I must express my gratitude to the traditional stewards of these unceded lands and waters, the Kanien’kehà:ka. McGill University and its students owe the Kanien’kehà:ka an immense and continuing debt, which must be meaningfully acknowledged and respected by each of the many minds shaped by this institution if we are to move forward in the spirit of peace, truth, and reconciliation.

VI CONTRIBUTION TO ORIGINAL KNOWLEDGE

The present project sought to address gaps in the literature surrounding the mechanism of transdermal drug delivery via NFLJI system and needle injection. As such, it is novel that these mechanisms were compared directly using the same experimental approach and soft tissue phantom. In previous engineering investigations, only a parametric study of each injection method individually was presented. Additionally, to the knowledge of the author, previous engineering investigations lacked emphasis on clinically relevant injection parameters and did not include clinical needle geometry and realistic volume flow rates. The present work is also the first introduction of polyhydroxymethylethacrylate (pHEMA) as a soft tissue phantom candidate for engineering investigations of needle-free injection. Finally, the segmentation and metrological analysis performed to characterize the injection path of the inferior alveolar nerve block injection presented in this work is a novel approach to optimization of the injection technique and the first published method to quantitatively investigate the space surrounding the mandibular foramen.

VII CONTRIBUTION OF AUTHORS

The present work comprises the engineering investigation component of an interdisciplinary project in collaboration with co-investigator Qiman Gao, a PhD candidate in the McGill University Faculty of Dentistry co-supervised by Professors Faleh Tamini and Luc Mongeau. The project entails a comprehensive clinical and engineering investigation of needle-free liquid jet injection technology. The clinical features of the project, including ongoing clinical pilot testing (McGill IRB A09-M36-18A) performed in the McGill Faculty of Dentistry by co-investigator Qiman Gao, are not addressed in the present work. The project was originated by former students in the McGill Biomechanics Lab, Swen Groen, Rani Taher, and Zixin He, who constructed the first iteration of the test apparatus. Preliminary data for the project was collected by Qiman Gao and Zixin He. As described in Section 3.2.1, Zixin He modified the test apparatus to include a syringe pump for needle injection tests. Qiman Gao performed the measurements pertaining to regurgitation of injected fluid. The protocol for synthesis of glycol chitosan was developed by Neda Latifi [1]. The synthesis of Polyhydroxyethylmethacrylate hydrogel was based on a protocol described in [2] by Guangyu Bao. Guangyu Bao provided additional assistance in sample preparation and imaging of porcine tissue via Scanning Electron Microscopy. In the present work, Section 2.1.2 Clinical Investigations encompasses information obtained in a clinical literature review performed by Qiman Gao.

1 INTRODUCTION

Effective and reliable drug delivery is essential to modern medical practice. This is commonly achieved via needle injection which, while effective and supported by extensive clinical experience, encompasses significant drawbacks. These include pain associated with needle injection, needle phobia, needle stick injuries and transfection for clinicians, and the expenses incurred managing and disposing of needles. Alternative systems of transdermal drug delivery have been proposed to address these issues, including needle-free liquid jet injection (NFLJI). NFLJI systems deliver drugs via penetration of the skin by a liquid jet typically 50-360 µm in diameter with a peak velocity greater than 100 m/s [3]. It is estimated that penetration of the human skin requires a minimum pressure of 15 MPa [4]. In addition to eliminating the risk of needle stick injuries, NFLJI studies have indicated that this injection method may cause less pain [5]–[8]. In the case of local anesthetic delivery in the dental clinic, it is well-documented that some dental patients avoid necessary treatments due to needle-related pain and anxiety. This phenomenon that is even more relevant in pediatric dentistry [9]. It has been reported that 24% of parents and 63% of children indicate a fear of needles, in some cases resulting in non-compliance with clinical care [10]. In the dental setting, drug delivery via needles often requires general anesthesia of young or difficult pediatric patients. Routine dental procedures thus become a traumatic experience for the patient and a financial burden for the healthcare system. By reducing needle phobia, NFLJI offers a promising alternative which may improve patient experience while simultaneously reducing the impact of needle injection complications.

The diameter of the jet produced by a typical NFLJI system is six times smaller than that of a typical clinical hypodermic needle. The interaction between tissue and delivery device involves no needle penetration in NFJJI. It is hypothesized that the decreased diameter and injection time associated with NFLJI drug delivery may contribute to decreased injection pain by reducing mechanical trauma and distension damage to the tissue relative to conventional needle injection [11]. NFLJI systems may thus reduce the effects of needle pain, needle phobia, and needle disposal costs and hazards.

Despite its apparent promise, however, NFLJI has seen limited adoption since its first introduction in 1936. Following decades of development and applications in fields as diverse as dermatology, vaccination, and diabetes management, uptake of the technology has been impeded by several factors [12]–[15]. Firstly, clinical injection protocols have not been adapted for needle-free devices to ensure delivery at the targeted location, limiting successful and painless delivery. This aspect is being addressed in the clinical arm of the project, and not elaborated here. A better understanding of the mechanics of NFLJI is needed to inform clinical protocols. Existing models address only skin rupture and jet penetration depth, with little investigation of injection dynamics, diffusion profile, and tissue damage. A series of mechanical experiments was therefore conducted to characterize the injection dynamics of both NFLJI and needle-based injection. The goal was to compare the location, distribution and concentration of the delivered drug for representative host tissues. A suitable tissue phantom was first identified. A common material choice in the literature for developing a soft tissue phantom is gelatin hydrogel; however, this material has limitations including a brittle nature and lack of porous structure. To identify a better phantom, the mechanical properties of porcine oral tissue were characterized and phantom materials selected to better reproduce the tissue characteristics.

The results of the present study provide a better understanding of the clinical and engineering aspects of the PIS. They will contribute to the clinical and regulatory knowledge base supporting NFLJI, possibly sparking wider adoption. Characterizing the mechanism of drug delivery via NFLJI may contribute to understanding the clinical outcomes of injection pain and wound healing. In turn, healthcare systems may benefit from reduced patient avoidance of treatment due to needle anxiety, reduced costs associated with needle disposal, and reduced risk of needle-related incidents such as transfection and needle stick injuries.

1.1 RESEARCH OBJECTIVES

1.1.1 Soft Tissue Phantom Design

The first aim of this project was to identify a suitable soft tissue phantom. Oral mucosa tissue itself is scarce, opaque, and prone to inter-subject variation. The phantom must adequately represent the mechanical properties of soft tissue, specifically the oral mucosa and surrounding soft tissues involved in dental local anesthesia application. To this end, the modulus and viscoelastic response of excised porcine oral soft tissue were characterized via rheometer and compared to those of candidate hydrogels including type II bovine gelatin, gelatin cryogel, glycol chitosan, and polyhydroxymethylethacrylate (pHEMA). The porosity structure porcine oral soft tissues was characterized via scanning electron microscopy and compared to that of the porous phantoms: gelatin cryogel, glycol chitosan, and pHEMA. Finally, needle and NFLJI injections were performed in both porcine soft tissue and each phantom candidate, and the results compared via computerized tomography scanning and three-dimensional reconstruction of the “wound” created. A suitable soft tissue phantom candidate was then selected which best represented the modulus and viscoelastic behavior, the porosity structure, and the injection wound morphology of oral soft tissues.

1.1.2 *In Vitro* Comparison of Transdermal Drug Delivery via Needle Injection and NLFJI System

The second aim was to understand how NFLJI differs from conventional needle injection. The soft tissue phantom was employed in conjunction with a customized test apparatus for collection of force and high-speed camera data. A customized force balance apparatus was used to record the dynamic force response of injection into the phantom. A high-speed camera was used to capture the penetration characteristics. Computerized tomography (CT) scanning was utilized to reconstruct the three-dimensional profile of the injection volume and morphology. First, needle insertion into the phantom, and the effect of needle gauge and insertion rate was assessed via fracture toughness measurement [16], [17]. Needle injection was performed , via introduction of a syringe pump to the test apparatus. The test apparatus was used to capture the dynamic force response, penetration behavior, and regurgitation characteristics of injection with the NFLJI device and evaluate the effects of pneumatic supply pressure, injection volume, and injection angle. The resulting dynamic force profiles, penetration behavior, and wound morphology were then compared between needle injection and NFLJI.

1.1.3 Improved Protocol for Dental Local Anesthesia: Pilot Study in Humans

Ongoing clinical pilot testing of dental local anesthesia via NFLJI (McGill IRB A09-M36-18A) have raised issues which may be assessed *in vitro*. One such issue was investigated, namely the persistent difficulty of drug reaching an inferior alveolar nerve block, shown in Fig. 1, via NFLJI. This technique targets a nerve within the mandibular ramus, and experiences an estimated 15-35% failure rate even with conventional needle anesthesia [18]. When employing conventional needle anesthesia to deliver this injection, haptic feedback provided by the needle tip may help guide the needle to the correct location; this is not possible when NFLJI is employed. As such, nerve blocks delivered via NFLJI were rarely successful, as a slight deviation in path resulted in dispersion of the anesthetic formulation along the mandibular bone in an incorrect location. To address this issue, the third goal was to identify the best nozzle orientation for the drug to hit the targeted nerve region. The approach was to identify the injection path via a solid model created from clinical CT images (McGill IRB A09-M36-18A). The implementation of ultrasound guidance was considered, but not implemented. These approaches may contribute to an improved clinical technique which will result in successful inferior alveolar nerve block via needle-free liquid jet injection.

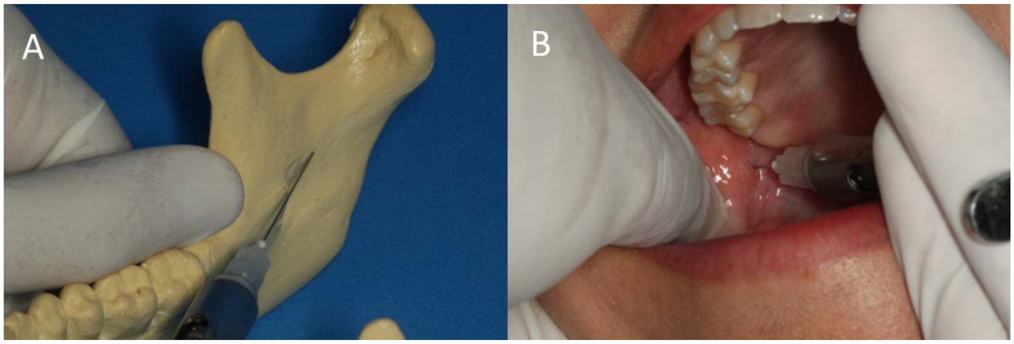

Figure 1: Inferior Alveolar Nerve Block technique for delivery via needle injection demonstrated on a bone model (A) and on a patient (B). Image © 2015, F. S. Rocha, R. P. Carneiro, A. E. H. Magalhães, D. Zanetta-Barbosa, L. M. Furtado, and M. C. P. da Silva. Originally published in [18] under Creative Commons Attribution 3.0 Unported license.

2 LITERATURE REVIEW

2.1 NEEDLE-FREE INJECTION

2.1.1 History of Needle-Free Injection

The first record of needle-free injection technology is a 1936 patent, following which a needle-free device for self-injection of insulin was developed in the 1940s [3]. The first needle-free injection devices were pneumatically powered. In 1947, a needle-free injection device powered by spring loading was introduced [19]. Other driving forces introduced were Lorentz force actuation in 2006 [20], piezoelectric actuation in 2007 [21], and laser-induced jet formation in 2012 [22]. While early jet injectors focused on delivering liquid jets across the dermal barrier, needle-free delivery of powders was first reported in 1987 [23] and needle-free delivery via microneedles was first explored in 1998 [24]. With respect to application, needle-free injection technology was first considered for the purposes of vaccination in the 1940s [13]. These devices were typically pneumatically powered, automated systems which could vaccinate multiple patients without reloading, thereby contributing significantly to mass immunization programs throughout the twentieth century [3]. Widespread use continued until the devices were linked to transmission of Hepatitis B in 1985, eroding trust in the technology [25]. The transfection issue was addressed in many cases by the introduction of a single-use nozzle or cap that would be changed in between patients in the 1990s [3]. Needle-free injection systems were first reported for use in delivering insulin in 1979 [12]. Also in the 1970s, needle-free injection began to see use in the dermatology field [26]. More recently, needle-free injection has been investigated for use in delivering growth hormone therapy since 1993 [13], [27], and for delivery of dental local anesthetic since 1998 [3], [28]. Needle-free liquid jet injection (NFLJI) devices were investigated in the present study. The focus is on pneumatically powered systems, given their applicability for dental anesthesia and their ability to accommodate conventional anesthetic formulations.

2.1.2 Clinical Investigations

In the clinic, the delivery of local anesthetic via NFLJI has been demonstrated to cause decreased levels of injection pain compared to conventional needle injection for hand surgery [5], lumbar puncture [6], small wound suturing [7], and dental local anesthesia [8]. This may be associated with small jet diameter and high flow velocity. The injection duration is significantly shorter than that of a needle injection, and the jet diameter is smaller than that of a hypodermic needle. These features may minimize the injection pain associated with mechanical trauma and distension of the tissue commonly associated with conventional needle injection [11].

Five published clinical trials have investigated the use of NFLJI systems for dental local anesthesia [8], [29]–[32]. Despite recommendation as a promising alternative conventional needle anesthesia [33], the efficacy of this method remains unclear [8], [34] as it did not demonstrate consistently successful dental pulp anesthesia [8], [30], [32]. In some studies, NLFJI was less preferred by patients due to complications including bleeding and discomfort after injection [30], unpleasant taste due to regurgitation of anesthetic [30], [32], and increased pain during treatment due to inefficacious pulp anesthesia [30], [32]. However, only two published studies describe the anesthesia delivery technique utilized, both specifying that injection should be performed by orienting the device perpendicular to the maxilla or mandible [31], [32]. Despite the complications reported associated with injection, no attempt was made to systematically optimize injection protocols in the clinic to try to improve outcomes.

2.1.3 Engineering Investigations

2.1.3.1 Needle Injection

Studies investigating needle insertion have characterized the insertion force [35] [36], the translational frictional force on the needle [37], and the plunger-stopper break force [38]. A few studies have reported preliminary finite element models [39]. Only one study to date has investigated the effect of fluid delivery after needle insertion [40]. The insertion of custom metal punches into porcine adipose tissue have shown that a flat-tipped punch required a higher pressure to penetrate the tissue, and that penetration pressure decreased with increasing punch diameter, as shown in Fig. 2. During fluid injection, fluid was delivered via hypodermic needle (21 gauge or 27 gauge) under X-ray imaging, as shown in Fig. 3. It was observed that the dispersion of the injected fluid occurred through micro-cracks; crack formation could be explained by a hydraulic fracture model [40]. Some studies utilized standard clinical needles [16], [17], while others used custom needle geometries which limits the clinical utility of the collected data [39]–[41]. Other needle insertion studies focused on measurement of tissue fracture toughness in response to the needle insertion, as described in Section 2.2.1. In needle insertion studies, four distinct phases of the force-time profile were described, as shown in Fig. 4 [16]. The first phase is deformation, as the needle tip first meets the surface of the tissue or phantom. Steady state penetration follows, as the energy threshold for material fracture is reached and the needle punctures the tissue or phantom. Third, after the needle has reached its final penetration depth, material relaxation occurs due to the viscoelastic properties of the material. Finally, the force as the needle is extracted involves friction of needle withdrawal and the release of stored strain energy [16].

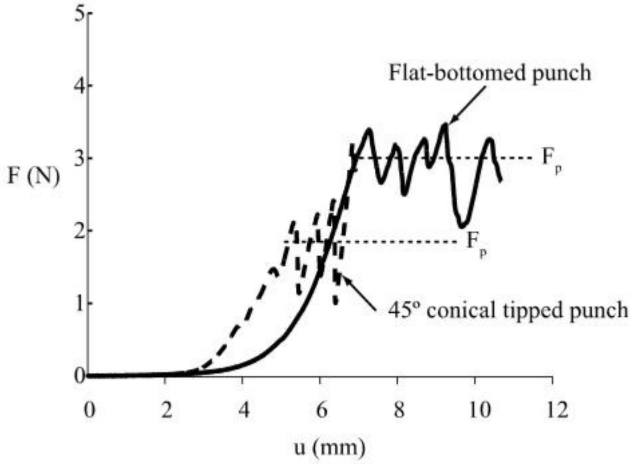

Figure 2: Measured Force vs. Needle Displacement for insertion of 0.6mm punches into porcine adipose tissue at an insertion rate of 0.1 mm/s. Image reproduced with permission from [34].

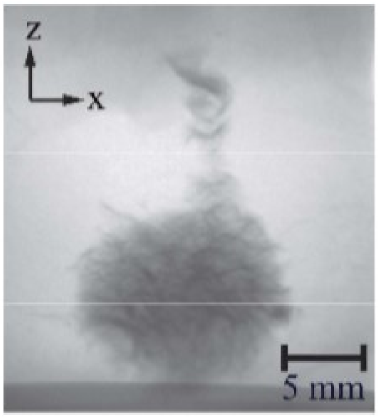

Figure 3: X-ray image of injection of 0.5 mL radioopaque dye into porcine adipose tissue via a 21 gauge hypodermic needle. Image reproduced with permission from [34].

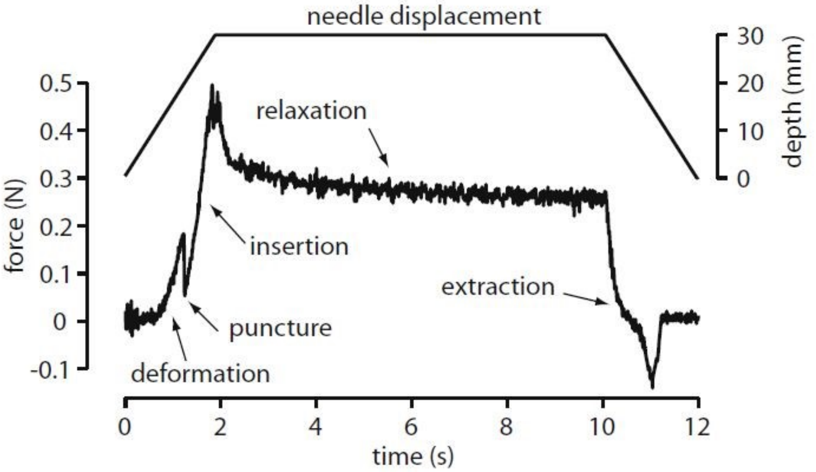

Figure 4: Four phases of needle insertion. Image reproduced with permission from [16].

2.1.3.2 Injection via NFLJI Systems

The effects of various NFLJI injection parameters on jet velocity, impact force, and penetration depth have previously been investigated. The main findings of these investigations were summarized in a 2018 review paper [3]. Increased penetration depth was observed as a result of increased driving force, injection volume, or injected fluid density. Increased stagnation pressure was observed to correlate with increased driving pressure and decreased fluid volume. Finally, increasing the stand-off distance between the NFLJI device nozzle and the injection surface was found to have a negligible effect [3]. Studies employing non-porous soft tissue phantoms have reported wound shapes similar to ‘penny-shaped cracks’ [25], [42] as shown in Fig. 5, which differed significantly from the spherical bolus wound shapes observed in tissue injections [43]. Two studies described regurgitation associated with jet injection, and hypothesized that this was a result of viscoelastic behavior of the tissue or phantom as the jet energy decreases at the end of the injection and residual stress is released [42], [43]. This mechanism is summarized in Fig. 6. The tissue phantoms employed in NFLJI mechanism investigations are summarized in Section 2.3.

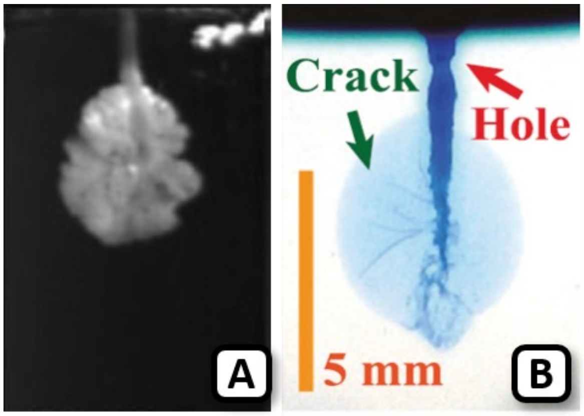

Figure 5: Jet injection wound geometry in non-porous polyacrylamide (A) and gelatin (B) tissue phantoms, described as "penny-shaped cracks" [25] [42]. (A) reproduced with permission from [25]. (B) reproduced with permission from [42].

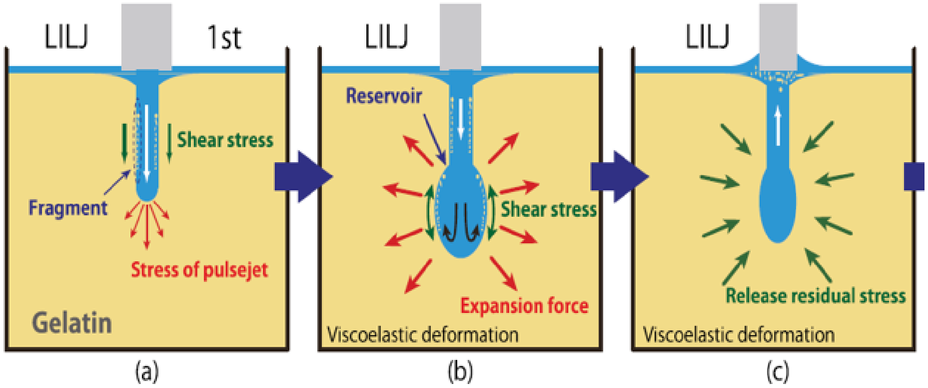

Figure 6: Viscoelastic forces during jet injection, reproduced with permission from [42]. The jet enters, exerting stress at the leading edge and shear stress at the sides (a). As fluid flow continues, the fluid momentum is redirected to recirculation as leading-edge stress is insufficient to continue penetrating. This recirculation causes an expanding force (b). Finally, as jet flow ceases, the viscoelastic properties of gelatin cause a release of residual stress which forces some fluid out of the wound towards the jet nozzle (c).

2.2 SOFT TISSUE MECHANICAL PROPERTIES

The mechanical properties of human oral tissue have been investigated. Structurally, human oral soft tissues comprise a laminar structure as shown in Fig. 7 [44]. The top layers constitute the oral mucosa, the softest portion of the tissue. Beneath the oral mucosa is fatty tissue known as the submucosa, underneath which is a layer of muscle. While the anatomy of the oral mucosa is well understood, little data has been published on the mechanical viscoelastic properties of oral soft tissues. Furthermore, the data available is inconsistently reported and difficult to compare. A meta-analysis of published finite element method studies of oral mucosa found that the reported range of compressive and tensile elastic moduli for oral mucosa were, respectively 0.06-8.089 MPa and 0.91-11.12 MPa. The same study reported the most common choice for linear elastic modulus of oral mucosa tissue to be 1-5 MPa [45]. In an experimental study, it was found that the lingual alveolar, buccal, and buccal alveolar mucosal tissues had young's moduli in tensile testing of 4.79 ± 2.54 MPa, 2.48 ± 0.37 MPa, and 5.74 ± 1.15 MPa respectively [46]. Finally, a study of porcine adipose tissue yielded a strain-rate-dependent young's modulus of 1 kPa-3 MPa [40]. Given the inconsistencies in test methodologies, tissue types, and findings, experimental tests are needed to further characterize porcine oral tissue to facilitate optimal soft tissue phantom design for characterization of dental local anesthetic via NFLJI.

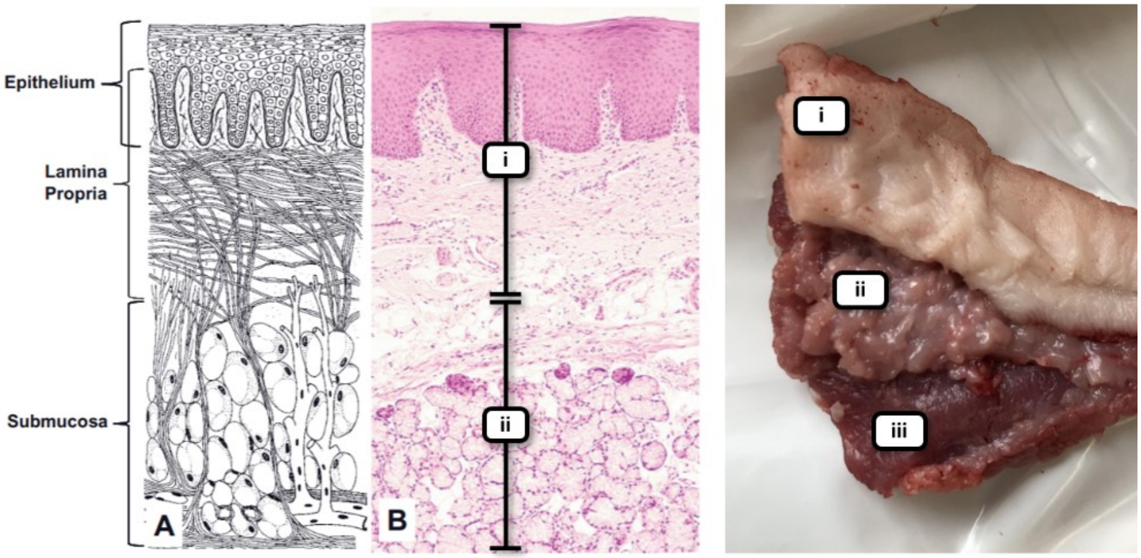

Figure 7: Left: Illustration (A) and histological image (B) showing the layers of oral mucosa tissue. Relevant here is the epithelium and lamina propria, labelled (i) and collectively referred to as the oral mucosa, and the fatty submucosa, labelled (ii). Image reproduced with permission from [47]. Right: Excised porcine oral tissue showing the separable layers of oral mucosa (i), submucosa (ii) and muscle (iii).

2.2.1 Soft Tissue Fracture Toughness

The calculated fracture toughness of a tissue may be used to characterize its response to needle insertion [16], [17], [41] . This method utilizes the difference in work between an initial and a second insertion of a needle into tissue to calculate the fracture toughness, relying on the assumption that only frictional work is produced during the second insertion. By subtracting the work of the second insertion from the that of the first, the work of fracture may be calculated and used to find the fracture toughness J_{IC} as per the relation

$$(F_1 - F_2)du = J_{IC} \cdot a \cdot du, \tag{1}$$

where F_1 is the force of the first insertion, F_2 is the force of the second insertion, u is the needle displacement, and a is the crack width. Experimentally, this is evaluated as

$$J_{IC} = \frac{\int F_1 du - \int F_2 du}{\pi \cdot D_{needle} \cdot u_f} \tag{2}$$

where u is the needle displacement and u_f is the final needle displacement or needle penetration depth. This method has been used to characterize the fracture toughness of porcine and bovine liver, as well as to investigate the effects of various needle insertion parameters in a gelatin soft tissue phantom [16], [17], [35], [41]. It was found that porcine liver has a fracture toughness of 75.8-185.6 J/m^2 in response to various clinical needles [16], while gelatin hydrogel (16.6% mass concentration) has a fracture toughness of 11.8-18.2 J/m^2 in response to a custom hollow needle [17]. Measured fracture toughness varies with cutting tool geometry, as it is a measurement of the tissue's resistance to fracture by that specific tool. The literature also reports a non-linear relationship between insertion speed and measured fracture toughness [16], [17]. Increasing needle diameter was found to decrease fracture toughness over a diameter range of 2-5 mm [41]. Given the variation in experimental parameters and findings, more work is needed to quantify the fracture toughness of porcine tissue, and to investigate the effect of various needle injection parameters.

2.3 SOFT TISSUE PHANTOMS

In NFLJI studies, gelatin hydrogels of various concentrations were commonly employed [45], [48], with a concentration of 5% as the most commonly selected concentration to model soft tissue [39], [42], [49], [50]. Synthetic hydrogels including polyacrylamide [51], acrylamide [52], PVC [53] and PVA-STB [54] have been used, as well as traditional engineering materials silicone rubber [55] and ballistic gel [56]. Only one research group to date has taken advantage of a porous hydrogel phantom, employing a composite hydrogel comprised of phytagel and PVA to mimic porcine brain tissue in a needle insertion study [36]. Despite the infrequent use of a porous tissue phantom, it has been recommended in the literature. Unexpected 'penny-shaped' injection wounds were observed in NFLJI studies utilizing non-porous polyacrylamide or gelatin phantoms, and it was hypothesized that the wound shape would more closely resemble the clinical case if a porous hydrogel phantom were employed [42], [52].

3 METHODOLOGY

3.1 SOFT TISSUE PHANTOM PREPARATION

3.1.1 Gelatin

Gelatin phantoms (5% mass concentration) were prepared as follows. A mass of 52.63 g of type II bovine gelatin (9000-70-8, Sigma-Aldrich) was measured and added to 1000 mL of DI water. The solution was stirred continuously at 65 °C for 60 minutes, then poured into the glass phantom containers. The prepared containers were then refrigerated at 2 °C for 6 hours. To prepare for testing, the phantoms were removed to a room temperature environment and allowed to return to approximately 21 °C. In the present work, all concentrations will be reported in mass fraction concentration unless otherwise specified.

3.1.2 Glycol Chitosan

Glycol chitosan was prepared as described in [1]. Briefly, a 2.5% chitosan solution was prepared by dissolving 1g of chitosan (Xi'an Lyohar Biotech) in 38 mL of 0.2 mol/L acetic acid (64-19-77, Sigma-Aldrich). A gelling agent solution was then prepared by mixing 0.1 M dibasic solution (7558-79-4, Sigma-Aldrich) and 0.1 M monobasic solution (13472-35-0, Sigma-Aldrich) at a volume ratio of 50:3, then adding 1.0283 g of sodium carbonate (497-19-8, Sigma-Aldrich) to 40 mL of the gelling agent solution. To synthesize the porous hydrogel, the gelling agent was added dropwise to the chitosan solution on a vortex mixer in a 3:5 ratio of gelling agent to chitosan solution.

3.1.3 Gelatin Cryogel

Gelatin cryogel phantoms were prepared using the gelatin phantoms prepared as previously described at gelatin concentrations of 5%, 10%, and 20%. The prepared sample was then removed from the glass container and stored at -4 degrees Celsius for 2 hours, then stored at -80 degrees Celsius for eight hours. The frozen sample was then placed in a freeze dryer for 5 days until completely dehydrated. The sample was then rehydrated by immersion in DI water for 12 hours and transferred back into the glass container for testing.

3.1.4 Polyhydroxyethylmethacrylate (pHEMA)

Polyhydroxyethylmethacrylate was prepared according to a protocol adapted from [2]. First, an alginate/acrylamide solution was prepared. Masses of 1.128 g alginate (9005-38-3, Sigma-Aldrich) and 6.76 g acrylamide (A9099, Sigma-Aldrich) were dissolved into 50 mL deionized water underneath the fume hood. The solution was stirred overnight at room temperature until a transparent and homogenous solution was obtained. Next, a calcium sulfate solution was prepared by dispersing 2.07 g of calcium sulfate (255548, Sigma-Aldrich) into 10 mL of deionized water, stirred for 48 hours. Then, a solution of N,N′-Methylenebisacrylamide (MBAA) was prepared by dissolving 200 mg of MBAA (M7279, Sigma-Aldrich) into 10 mL phosphate-buffered saline (PBS). Finally, immediately before synthesis, a solution of ammonium persulfate (APS) was prepared by dissolving 330 mg of APS (A3678, Sigma-Aldrich) into 5 mL of DI water. The alginate and acrylamide solution was then degassed under vacuum for 20 minutes. Two syringes were then prepared. To the first syringe was added 40 mL of the alginate and acrylamide solution, 144 µL of MBAA, and 32 µL of N,N,N′,N′-Tetramethylethylenediamine (T7024, Sigma-Aldrich). The second syringe was prepared by adding 0.764 mL of calcium sulfate solution and 0.904 mL of APS solution. The two syringes were quickly mixed, and the resulting solution poured into a glass phantom container. The container was sealed with parafilm to prevent oxygen exposure and left to crosslink at room temperature overnight.

3.2 TEST BENCH DESIGN

A schematic of the experimental test bench is provided in Fig. 8. The test bench utilized for fracture toughness and force profile measurements comprised a custom jet or needle mount fixed to a linear traverse (Velmex, USA); a strain gauge force transducer (GSO500, Transducer Techniques, USA); and custom modular phantom platform, a tissue phantom in a custom 40 mm square glass container with height 40 mm, 100 mm or 140 mm; a high-speed camera head (Photron USA Inc., USA) fixed to two linear traverses (Velmex, USA); a camera processing unit (Photron USA Inc., USA); and a data acquisition system (Model, National Instruments Corp., USA). The strain gauge transducer and camera traverses were installed on a laser table (Thorlabs, USA). Perpendicular and angled NFLJI test configurations are demonstrated in Figures 9 and 10, respectively. For measuring the force profile of a needle injection, a syringe pump (New Era Pump Systems Inc., USA) was connected to the needle mount via a T connector (Thermo Fisher Scientific, USA) as shown in Fig. 11.

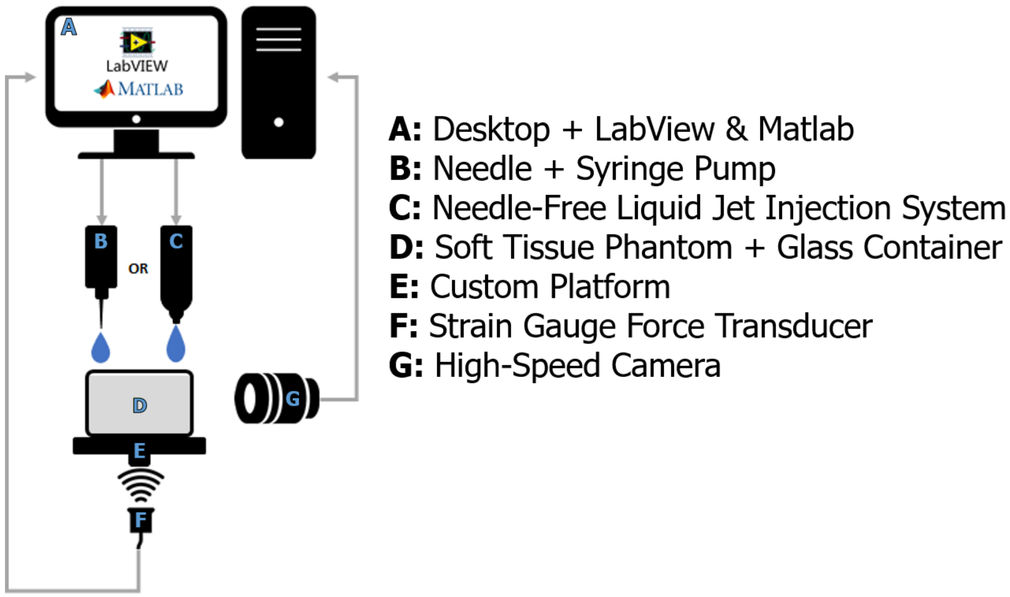

Figure 8: Schematic indicating the key components of the experimental test bench and their interactions. A LabView (National Instruments Corp., USA) script on a dedicated desktop computer (A) controlled fluid delivery via a needle and syringe pump (B) or a NFLJI system (C) into a soft tissue phantom (D). The phantom was supported by a 3D-printed platform (E) rigidly affixed to a strain gauge force transducer (F) which recorded the injection forces. The penetration behavior of the injected fluid was captured by a high-speed camera (G). The force and camera data were collected by the desktop (A) and analyzed in Matlab (The Mathworks Inc, USA).

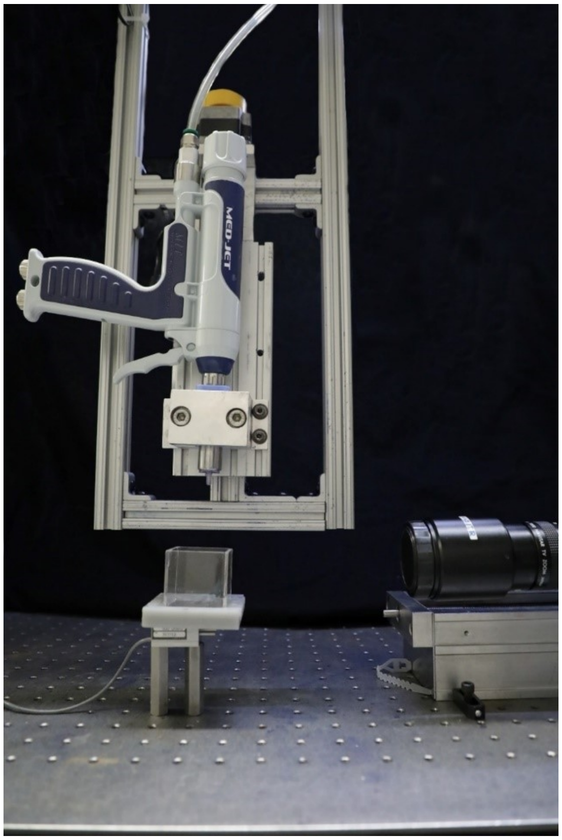

Figure 9: Experimental test bench with NFLJI system (Med-Jet, MIT Canada Inc., Canada) installed.

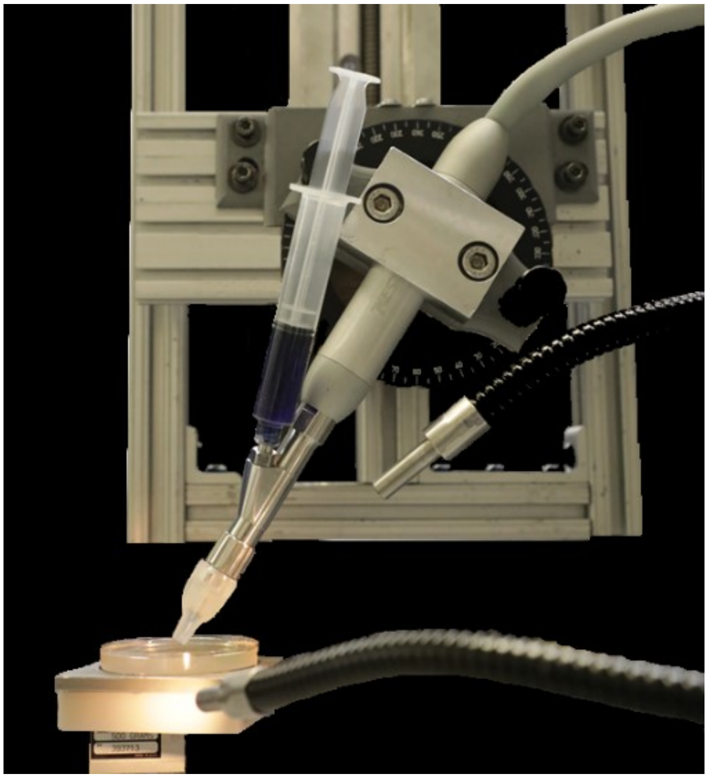

Figure 10: Experimental test bench configuration for assessing the impact of nozzle angulation from 0 to 75 degrees on outcomes of the NFLJI system (Meso-Jet, MIT Canada Inc, Canada).

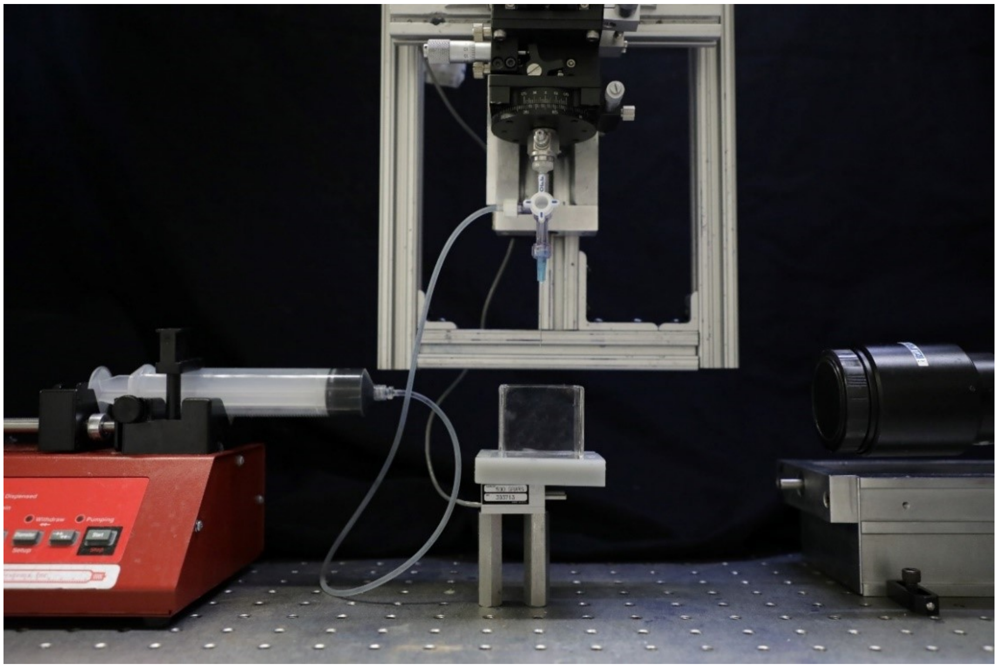

Figure 11: Experimental test bench with needle injection system installed. The same configuration was employed for needle insertion tests, with the syringe pump disconnected.

3.2.1 Design Evolution

The test bench initially comprised a linear traverse, custom needle mount, and PCB force sensor. The bench was then modified as follows: the PCB force sensor lacked sufficient low-force resolution and was exchanged for a more accurate strain gauge transducer; the needle mount was modified to accommodate the NFLJI device; the data acquisition system was modified for automated control of the NFLJI device; and the container platform was redesigned to resist off-axis moments. The linear traverse and jet or needle mount were redesigned to decouple them from the laser table, as the motor and jet vibrations were affecting the force transducer measurement. Finally, additional test bench components were created via additive manufacturing to accommodate angulation of the nozzle, in order to investigate oblique injection. A NFLJI device mount was created to allow nozzle angulation of 0-90 degrees, and a new container platform was introduced to accommodate a larger tissue phantom for oblique injection.

3.3 FORCE TIME HISTORY MEASUREMENT

3.3.1 Needle Insertion

The linear traverse first moved the needle to a start position immediately above the surface of the phantom, then performed the first insertion at the desired needle travel speed. The needle paused at the bottom of the insertion, and was then withdrawn at the same needle travel speed. The needle paused for three seconds, then performed the second insertion and withdrawal at the defined needle travel speed. Force data was recorded by LabView (National Instruments Corp., USA) at a sampling rate of 10,000 Hz.

3.3.1.1 Work of Needle Insertion Calculation

In this case, only the first insertion of the needle was considered. The needle insertion work was calculated as

$$W_{insertion} = \int F \cdot dx \tag{3}$$

where $W_{insertion}$ is the work of needle insertion, F is the measured force data, and dx is the incremental needle travel at each sampling interval.

3.3.1.2 Needle Insertion Fracture Toughness Calculation

The Fracture Toughness measurement was performed as described in [16]. The work of the two subsequent injections was calculated as previously described. Then, the fracture toughness associated with insertion was calculated as described in Section 2.2.1 [16]. Figure 12 shows the force time history of two consecutive insertions into the gelatin (5%) sample, and highlights the integrated area beneath the difference curve of the insertion force signals, which corresponds to the work associated with material fracture.

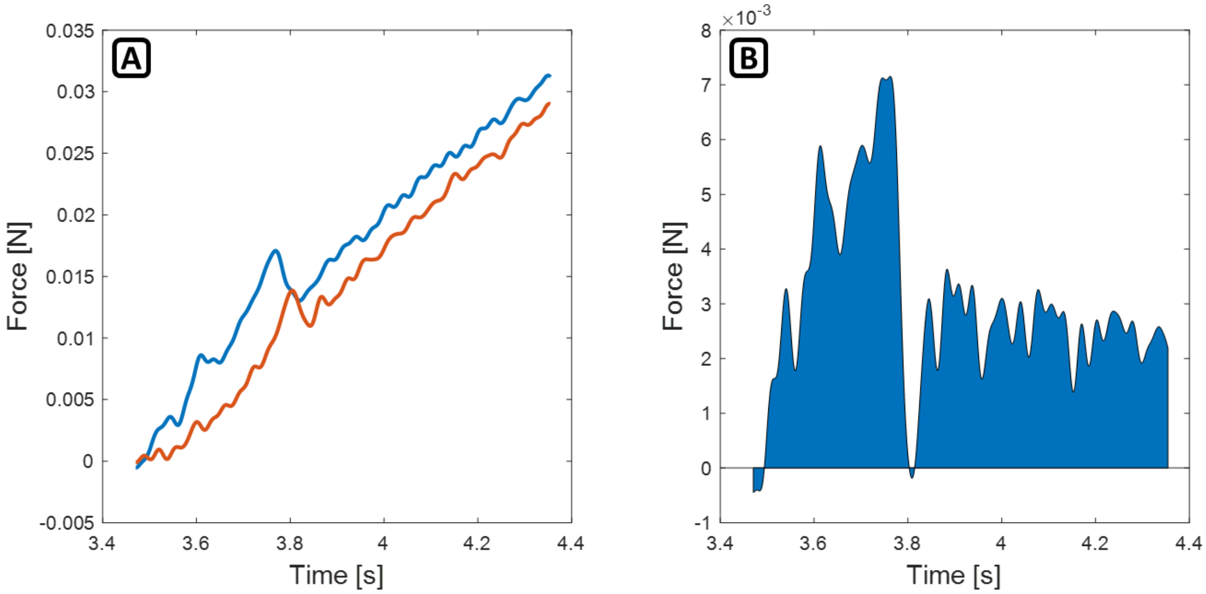

Figure 12: (A) Force time history of first (blue) and second (orange) consecutive insertions into the gelatin (5%) tissue phantom. (B) Difference curve demonstrating the remaining signal after subtraction of the force signals, and highlighting the integrated area beneath the curve, which represents the insertion work associated with fracture of the phantom material.

3.3.2 NFLJI

The NFLJI measurement was performed as follows: The jet and high-speed camera were triggered simultaneously, and the desired liquid volume was injected into the phantom. The supply pressure was set manually prior to injection. Force transducer signals and high-speed camera data were recorded using LabView (National Instruments Corp., USA).

3.3.2.1 NFLJI Work of Injection Calculation

The work of injection associated with NFLJI was characterized by first plotting the measured force signal against the jet penetration depth for the duration of the injection. As the penetration depth data was not strictly increasing due to the oscillatory nature of jet penetration, a manual eight-point approximation of the curve was then used for integration. The work associated with injection was then approximated as the surface under the fitted curve.

3.3.3 Needle Injection

The needle injection measurement was performed as follows: the high-speed camera and linear traverse were triggered simultaneously. The linear traverse moved the needle tip close to the surface of the phantom, then performed the insertion at the desired needle travel speed. The needle paused at the end of the insertion, then the syringe pump delivered the defined amount of injection fluid at the pre-programmed flow rate. The needle was then withdrawn from the phantom. Force transducer and high-speed camera data were recorded by LabView (National Instruments Corp., USA).

3.3.3.1 Work of Needle Injection Calculation

The work associated with needle injection was characterized in two phases: the insertion phase, and the fluid delivery phase. The work of needle injection was calculated according to the formula

$$W_{injection} = W_{insertion} + W_{fluid\ delivery} \tag{4}$$

where $W_{injection}$ was calculated directly from experimental results of the needle insertion phase as described in Section 3.3.1.1, and $W_{fluid\ delivery}$ was the analytically-derived work associated with delivering fluid through the needle. The losses associated with flow between the syringe pump and the needle were neglected, as these losses would not be present in a clinical injection. The analytically derived values of $W_{fluid\ delivery}$ were obtained for each volumetric flow rate (0.9 mL/minute and 7.2 mL/minute) and injection volume (0.3 mL and 1 mL) experimentally assessed. First, the state of the fluid flow in the needle was verified via calculation of the Reynold's number via the equation

$$Re = \frac{\rho U D}{\mu} \tag{5}$$

where the associated values for each variable are reported in Table 1.

Table 1: Calculation variables in analytical derivation of the work associated with major and minor losses in a needle injection via 25-gauge needle.

Symbol	Description
ρ	Density of water at 20 °C
$\boldsymbol{\overline{U}}$	Average velocity of fluid flow
D	Needle Internal Diameter
μ	Viscosity of water at 20° Celsius

The average velocity of fluid flow, $\overline{U}$, was calculated from the volumetric flow rate as

$$\overline{U} = \frac{Q}{A_{pipe}} \tag{6}$$

where Q is the volumetric flow rate of fluid delivery and A_{pipe} is the internal area of the needle. The Reynold's number calculated above was found to be 73.177 for a volumetric flow rate of 0.9 mL/minute and 585.41 for a volumetric flow rate of 7.2 mL/minute. As such, the flow in the needle was laminar. Therefore, the work associated with fluid delivery was calculated according to [57] as the fluid dynamic head modified by *K*, the minor loss coefficient associated with minor loss due to pipe exit. This yielded the equation

$$W_{fluid\ delivery} = V \cdot K \cdot \frac{1}{2}\rho\overline{U}^2 \tag{7}$$

where V is the injection volume. In this case, K was considered the minor loss of an abrupt expansion with secondary pipe area significantly larger than the first. As such, $\frac{A_1}{A_2} = 0$ and therefore $K = 1$. The calculated minor losses and energy losses for each volumetric flow rate and injection volume are shown in Table 2.

Table 2: Analytically derived minor losses and associated energy associated with nozzle exit in needle injection via 25-gauge needle.

Q $\left[\frac{mL}{min}\right]$	Injection Volume [mL]	$W_{fluid\ delivery}$ [J]
0.9	0.3	$1.195\text{x}10^{-5}$
0.9	1	$3.984\ \text{x}10^{-5}$
7.2	0.3	$7.649\ \text{x}10^{-4}$
7.2	1	$2.550\ \text{x}10^{-3}$

The above analytically derived values for the work associated with delivery of fluid in needle injection were combined with the experimental values of work of needle insertion to derive the total work of needle injection.

3.3.4 Impact Hammer

An impact hammer (Model, PCB, USA) was used to evaluate the natural mode shapes of the test bench components. Briefly, each configuration of container platform and container was assembled, and struck with the impact hammer to collect the frequency spectrum of the response. This was performed with an empty container, and with each of the evaluated tissue phantoms. The impact hammer frequency response was compared with the NFLJI force time history data to identify the natural frequencies of the test bench in the spectral analysis process.

3.4 PORCINE SOFT TISSUE SAMPLE PREPARATION

Porcine soft tissue was used to define the desired phantom material properties. Fresh porcine oral tissue (Boucherie des Tours, Canada) was excised and separated manually into the visible layers of oral mucosa (comprising the epithelium and lamina propria), submucosal fatty tissue, and muscle. The tissue samples were then trimmed to 10 mm discs using a scalpel in preparation for immediate rheological measurement.

3.5 RHEOMETRY

Tissue and gelatin material properties were measured via torsional rheometer (Discovery II, TA Instrument, USA). For tissue samples, a custom solvent ring was affixed to the rheometer base plate and filled with PBS (Sigma-Aldrich). A 10 mm circular sample of excised tissue was then immersed in the PBS for 5 minutes prior to measurement. For gelatin and pHEMA samples, the hydrogel was synthesized in 10 mm discs via a customized mold and placed directly on the clear rheometer base plate. The storage moduli and complex viscosities of samples were determined via a time sweep at a strain of 0.1% and frequency of 1 Hz for 120 seconds.

3.6 POROSITY MEASUREMENT

Fresh porcine soft tissue samples (Boucherie des Tours, Canada) were separated as previously described into oral mucosa, submucosa, and muscle and trimmed to form 10 mm discs. These were then progressively dehydrated in increasing concentrations of ethanol: 15 minutes each in 10, 30, 70, and 90%. These dehydrated samples were then placed in a supercritical dryer (EM CPD030, Leica Microsystems, Canada) for 45 minutes. Then, the dried sampled were sputter-coated with 100 nm of platinum (EM ACE600, Leica Microsystems, Canada). Finally, a scanning electron microscope (Quanta FEG 450, FEI, Japan) at power 5000 W was used to image the surfaces of the samples. Thresholding via Dragonfly (Object Research Systems, Canada) was then used to calculate the void fraction of the samples.

In measuring the porosity of pHEMA, a 40 mm cubic sample was prepared as per the established protocol and imaged via computerized tomography (CT) scan at a resolution of 2 μm. Then, CT reconstruction was performed in Dragonfly (Object Research Systems, Canada) and thresholding applied. The void volume was finally calculated as a percentage of the total reconstructed volume.

3.7 SEGMENTATION OF ANATOMICAL COMPUTERIZED TOMOGRAPHY IMAGES

Segmentation was performed via Dragonfly (The Objects, Canada, 2019). Briefly, the anatomical features of the mandible, foramen, and mandibular nerve were identified in MRI data obtained from the McGill Dental Clinic (McGill IRB A09-M36-18A). Then, window levelling was applied to clearly visualize the area and a region of interest constructed for each of the mandible, the nerve, the surrounding soft tissue, and the space between soft tissue and mandible. Finally, the angle between the plane of the desired injection path and the lower occlusal plane of the central incisors was measured.

4 FINDINGS

4.1 SOFT TISSUE PHANTOM DESIGN

To facilitate design of an appropriate soft tissue phantom, the relevant material properties of soft tissue were characterized via rheometry. The complex viscosity and storage modulus of the excised porcine oral tissue layers were recorded as described in Section 3.5. This tissue source was selected for optimal applicability to the clinical test case of dental local anesthesia. It was found, as shown in Fig. 13, that porcine oral mucosa, submucosa, and muscle exhibit storage moduli of 309±18.9 Pa, 1115±81.1 Pa, and 2434±262.7 Pa, respectively. The complex viscosity of each layer was 54±3.0 Pa·s for mucosa, 180±12.3 Pa·s for submucosa, and 399±43.6 Pa·s for muscle. The porosity structure of the soft tissue was characterized via scanning electron microscopy (SEM) as shown in Fig. 14, and it was found via image segmentation in Dragonfly (Object Research Systems, Canada) that porcine oral submucosa exhibited a porosity of 43%, and porcine oral muscle exhibited 37%. The porosity of oral mucosa could not be determined, as the surface of the tissue was smooth and the internal pore structure could not be imaged. Phantom design then proceeded with the identification of candidate materials which could potentially attain these stiffness and viscosity characteristics. The first candidate, gelatin (type II bovine), was commonly utilized in the literature [39], [42], [48]–[50], [58]. Concentrations of gelatin from 2% to 10% were evaluated, and the best match determined to be a concentration of 5%. At this concentration, the storage modulus was found to be 1156 Pa and the complex viscosity to be 184 Pa·s as shown in Fig. 13. A representative time sweep test result for the 5% gelatin phantom is presented in Fig. 15. Given the acceptability of these values, and the advantageous optical clarity of the material, gelatin was selected as a soft tissue phantom to be employed for the bulk of the investigation.

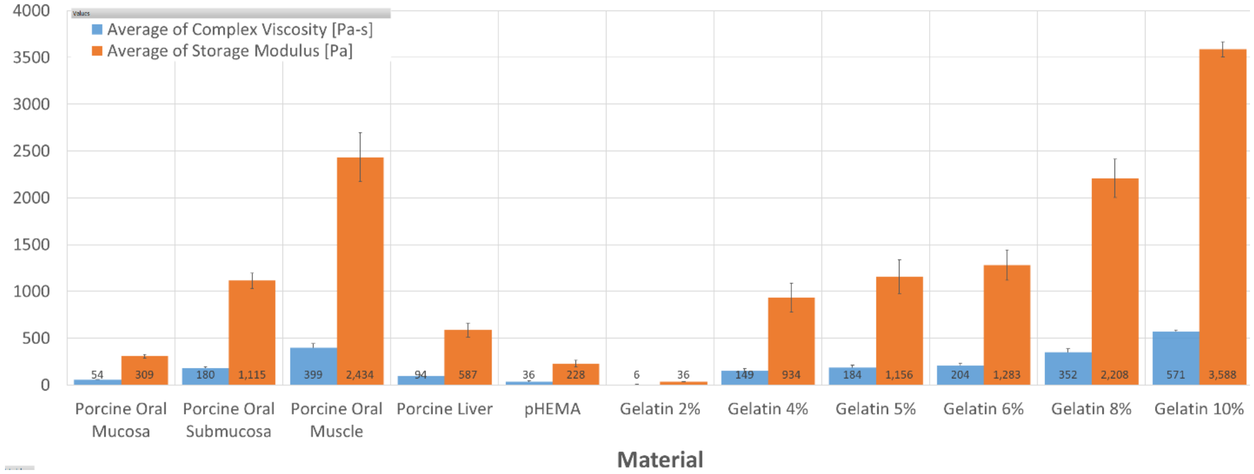

Figure 13: Storage Modulus (orange) and Complex Viscosity (blue) measured via rheometry of porcine oral tissue layers, porcine liver tissue, and key candidate tissue phantom materials pHEMA and gelatin at various concentrations. Values shown are the mean and standard error of the mean across all trials.

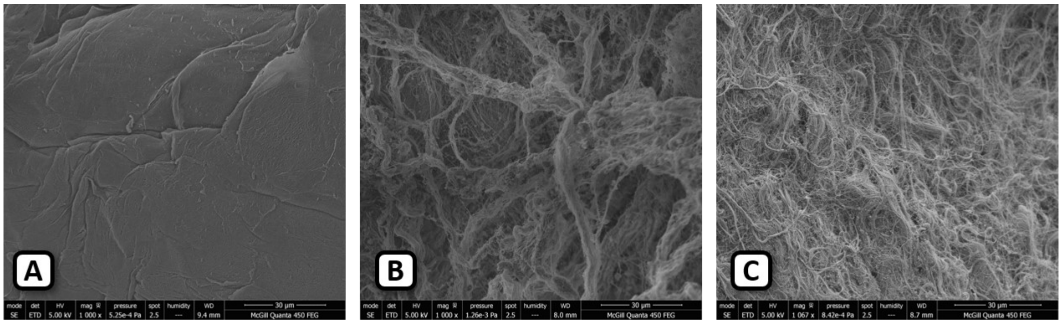

Figure 14: Scanning electron microscopy images of excised porcine oral mucosa (A), submucosa (B) and muscle (C).

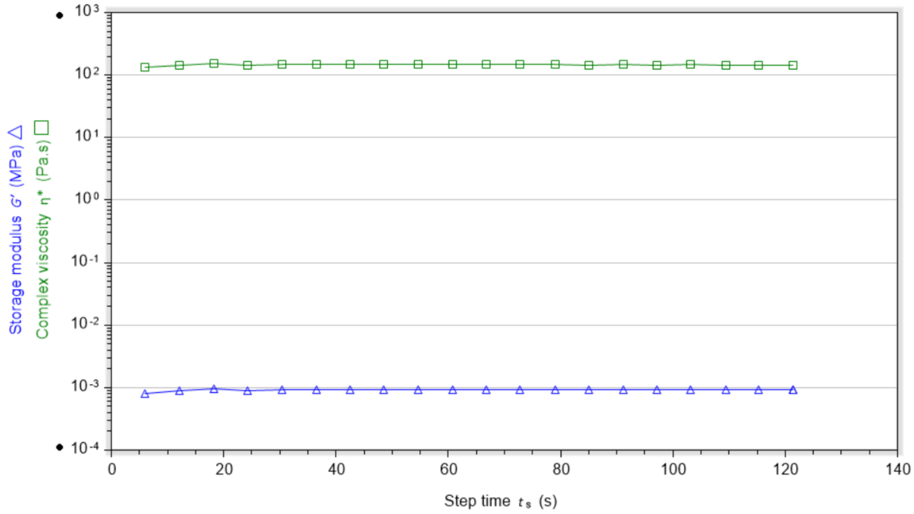

Figure 15: Representative time sweep test result for a 10 mm sample of gelatin with concentration 5% by mass.

Since it was indicated in the literature that porosity of the phantom may affect injection results, a series of porous phantom candidate materials were then identified based on their promising stiffness characteristics. These included glycol chitosan, pHEMA, and gelatin cryogel. Glycol chitosan was quickly eliminated as it was difficult to manufacture a phantom of the dimensions required for injection testing. Gelatin cryogel, another promising alternative, was rejected as the porosity structure obtained via cryogelation resulted in an unstable phantom with excessively large and inconsistent pores. Assessment of the use of pHEMA proved successful, and the storage modulus of 228±34.2 Pa and complex viscosity of 36±5.6 Pa·s recorded were a satisfactory match for the stiffness and viscosity of porcine oral mucosa. Moreover, SEM imaging as shown in Fig. 16 and segmentation as shown in Fig. 17 revealed a pore size of 20-30 microns and an overall porosity of 25%. The measured pore size values are within the appropriate range for soft tissue [59]. The injection wound morphology observed in the pHEMA phantom was more similar to that observed in porcine liver tissue than the gelatin phantom, as shown in Fig. 18. As shown in Fig. 19, the force time history signal obtained from NFLJI delivery into the pHEMA phantom lacked the oscillatory behavior observed in the gelatin phantom.

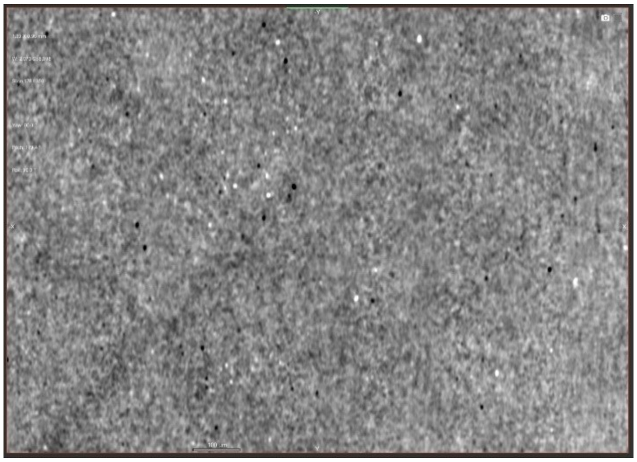

Figure 16: Computerized Tomography (CT) scan image of pHEMA obtained at a resolution of 2µm.

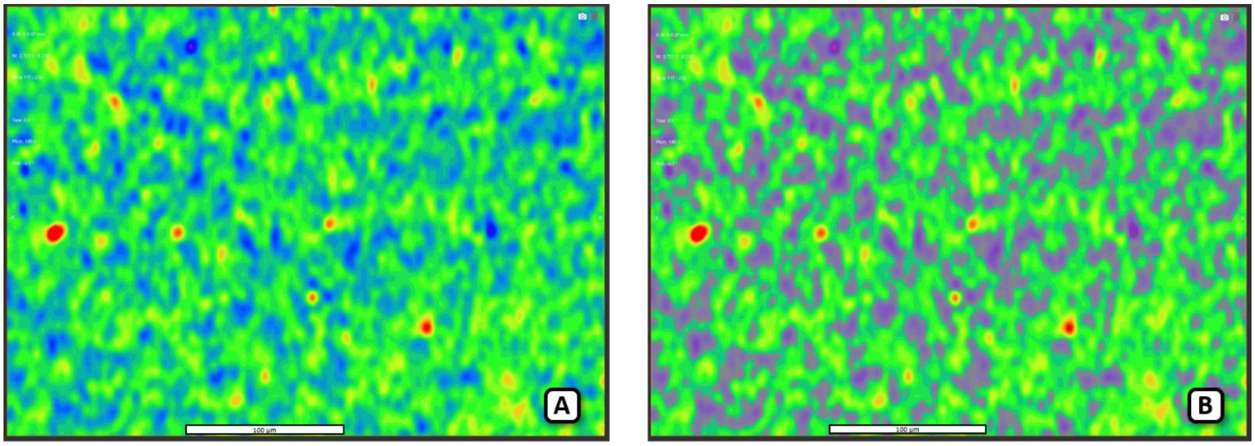

Figure 17: (A) Window-levelling applied to pHEMA CT scan image. (B) Region of Interest (purple) denoting the void volume in calculating the approximate porosity and pore size of pHEMA.

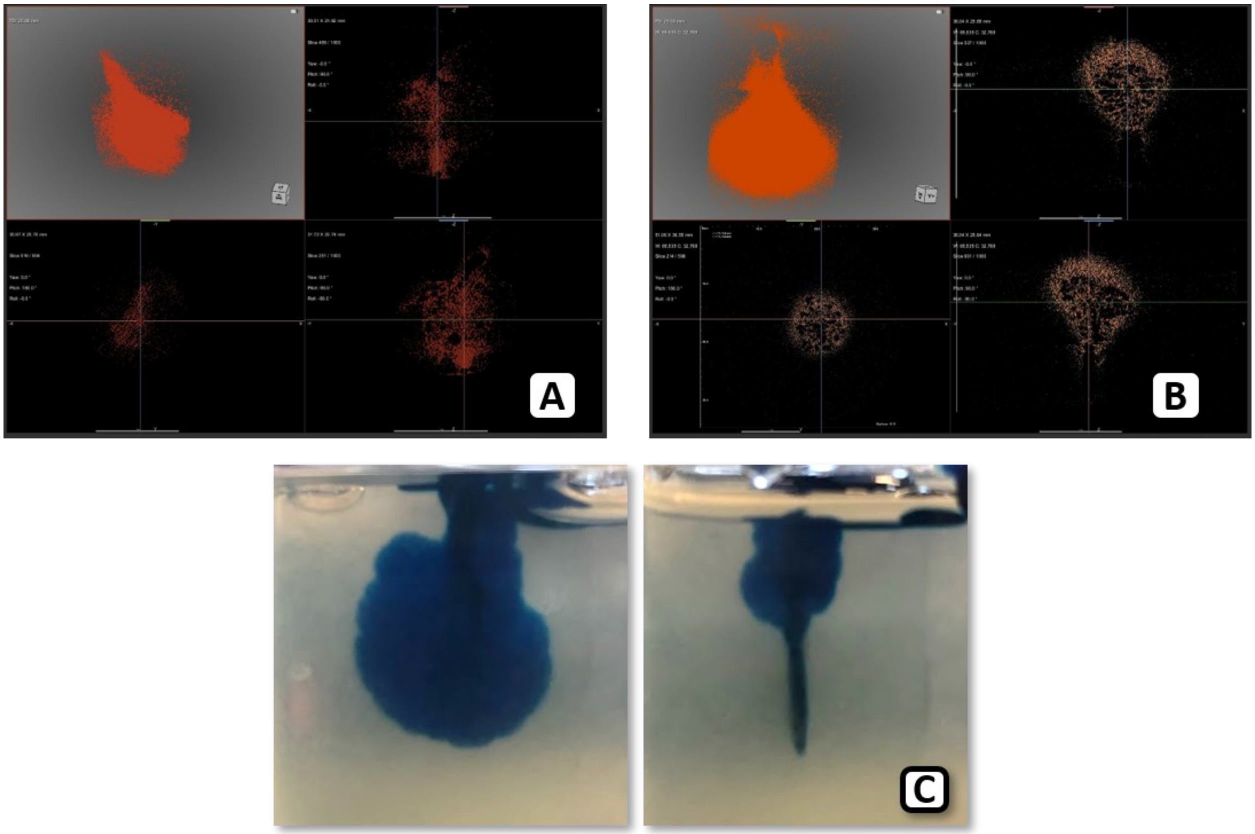

Figure 18: (A) CT reconstruction of NFLJI into porcine liver tissue. (B) CT reconstruction of NFLJI into pHEMA tissue phantom. (C) NFLJI into gelatin (5%) tissue phantom.

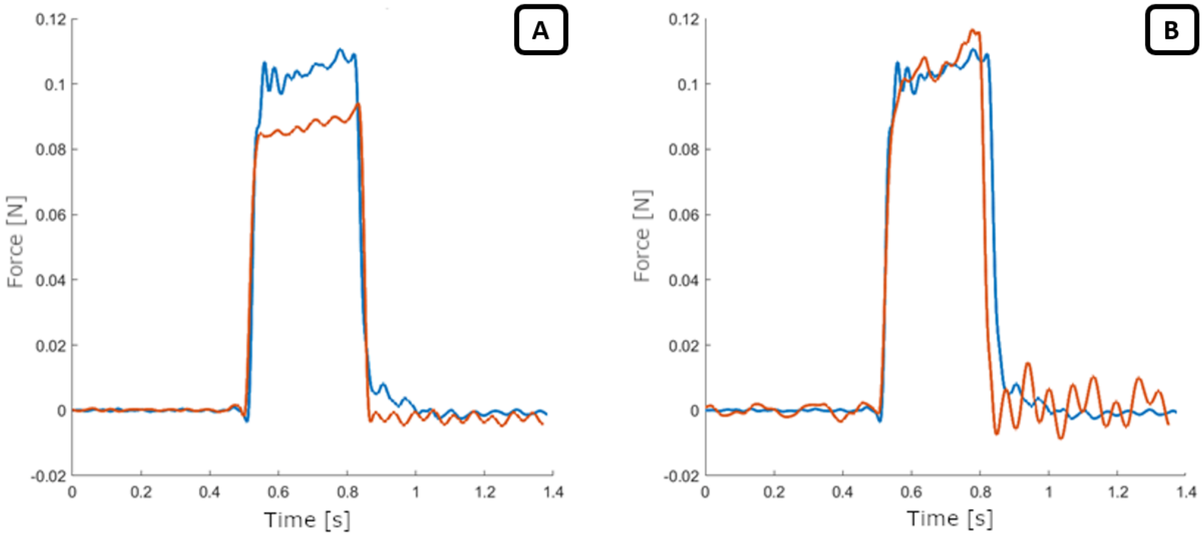

Figure 19: (A) Sample force time history of NFLJI with pneumatic supply pressure 413.7 kPa / 60 psi and injection volume of 0.3 mL into porcine liver tissue (blue) and the gelatin (5%) phantom (orange). (B) Sample force time history of NFLJI with pneumatic supply pressure 413.7 kPa / 60 psi and injection volume of 0.3 mL into porcine liver tissue (blue) and the pHEMA phantom (orange).

4.2 *In Vitro* COMPARISON OF TRANSDERMAL DRUG DELIVERY VIA NEEDLE INJECTION AND NFLJI SYSTEM

4.2.1 Needle Insertion Dynamics

As shown in Fig. 20, the four phases of needle insertion as reported in the literature are visible in the sample force time history for two consecutive insertions of a 21-gauge flat-tipped needle into the gelatin (5%) phantom at a speed of 5 mm/s. Deformation occurred until the first peak at approximately 4.5 seconds, followed by penetration until the second peak at approximately 69 seconds. The subsequent decrease in applied force corresponded to the relaxation phase, and finally the extraction phase corresponding with the distinct negative slope at 10 seconds. The force time history of the second insertion lacked the initial peak corresponding to the end of the deformation phase, and displayed a lower peak force, since the “wound” had already been created and therefore the primary force acting on the needle was friction. The detailed dataset of insertion force signals can be found in Section 8.1.

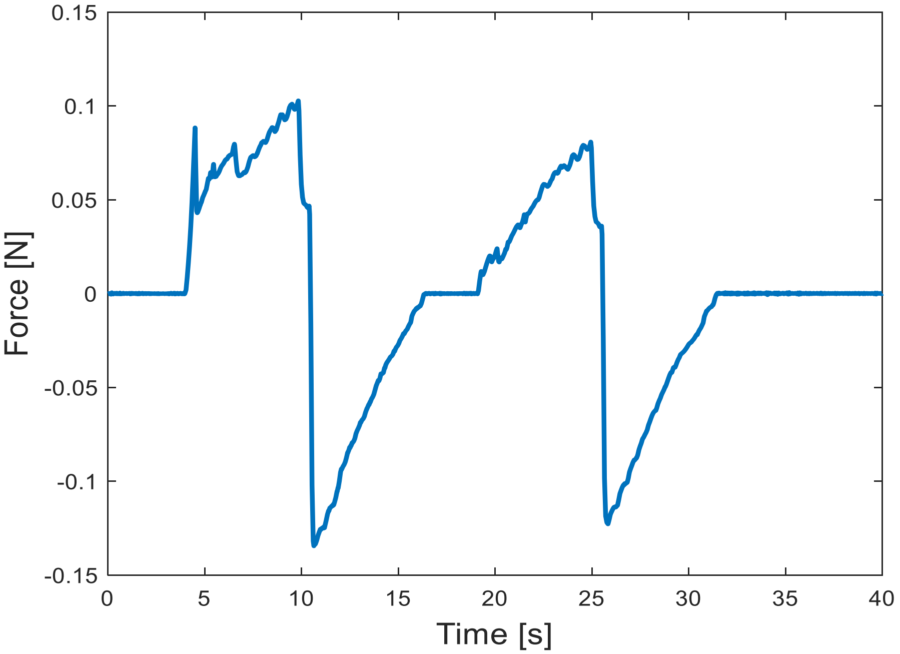

Figure 20: Force time history of two consecutive insertions of a 21 gauge flat-tip needle inserted into 5% gelatin at an insertion speed of 5 mm/s. Four distinct phases are visible: deformation, steady-state penetration, relaxation, and extraction.

The effect of various needle insertion parameters was then investigated. A range of clinically relevant needle gauges were selected, and the force time history for two consecutive insertions into the gelatin (5%) phantom at an insertion speed of 5 mm/s were collected. It was found, as shown in the sample signals in Fig. 21, that increasing needle gauge (and therefore a decreasing needle outer diameter) resulted in a decrease in amplitude of the force signal during insertion. This was indicated in the fracture toughness data reported in Fig. 22, as there was a trend of decreasing fracture toughness as needle gauge increases. This result is reasonable, as increasing needle gauge corresponds to smaller needle diameter, and therefore the force applied to the phantom occurs over a smaller area and the resistance to fracture of the phantom material is therefore reduced.

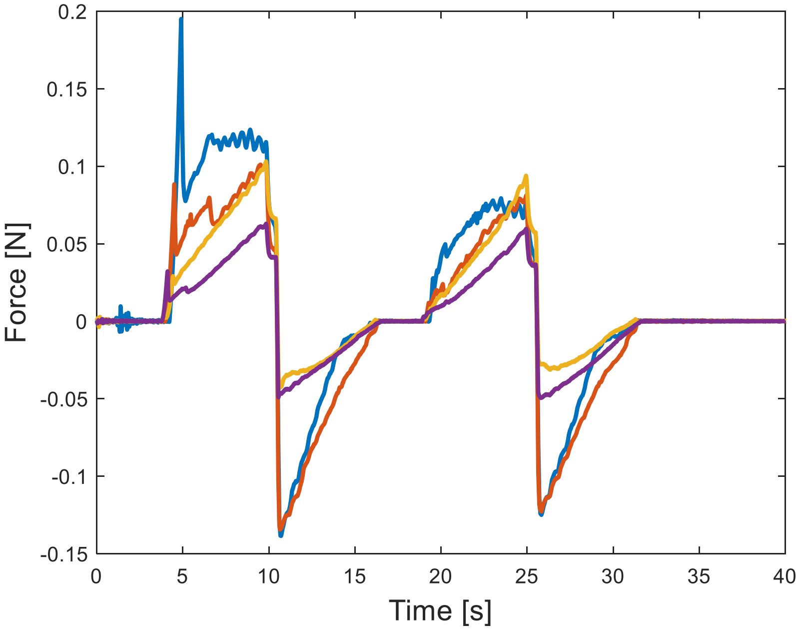

Figure 21: Force time history of two consecutive needle insertions of flat-tip needles into a gelatin (5%) phantom at an insertion speed of 5 mm/s with sizes 18-gauge (blue), 21-gauge (red), 25-gauge (yellow), and 27-gauge (violet).

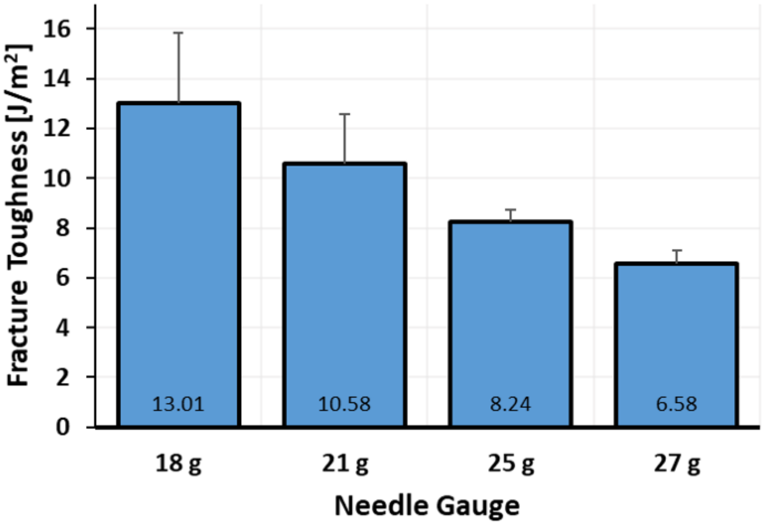

Figure 22: Fracture toughness calculated from force data for insertion of a 18-27 gauge flat-tip needles into the gelatin (5%) phantom at an insertion speed of 5 mm/s. Values shown are the mean and standard error of the mean across all trials.

The effect of needle insertion speed was then investigated, as shown in the sample signals in Fig. 23 below. A 21g flat-tip needle was inserted into the gelatin (5%) phantom at clinically relevant insertion speeds ranging 2-37.5 mm/s. Increasing insertion speed was found to have an overall non-linear effect on the amplitude of the force signal, as the amplitude increased with insertion speed 2-30 mm/s, but decreased from 30-37.5 mm/s. This effect was further demonstrated in the fracture toughness trends displayed in Fig. 24. Increasing insertion speed did not exhibit a clear effect on the fracture toughness value, suggesting a non-linear relationship.

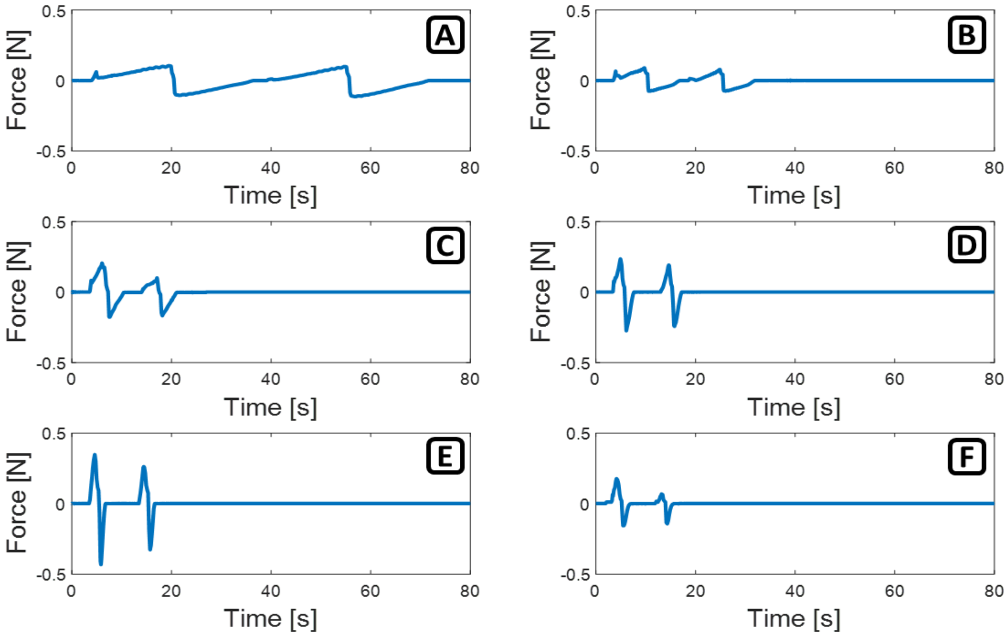

Figure 23: Force time history of two consecutive insertions of a 21 gauge flat-tip needle into the gelatin (5%) phantom at insertion speeds of 2 mm/s (A), 5 mm/s (B), 10 mm/s (C), 20 mm/s (D), 30 mm/s (E), and 37.5 mm/s (F).

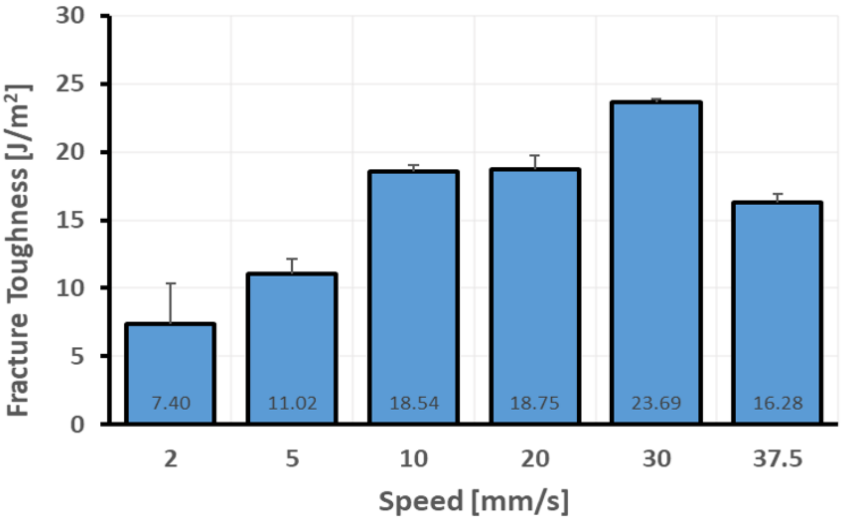

Figure 24: Fracture Toughness calculated from force temporal data for insertion of a 21 gauge flat-tip needle into the gelatin (5%) phantom at insertion speeds of 2-37.5 mm/s. Values shown are the mean and standard error of the mean across all trials.

The final needle insertion parameter for investigation was the effect of needle tip geometry. The force time history and fracture toughness of needle insertions of flat-tipped and clinical bevel-tip needles were compared. As shown in the sample signals in Fig. 25, insertion into the gelatin (5%) phantom at 5 mm/s produced a greater force amplitude when using a flat-tip needle. Additionally, the deformation phase was largely absent when inserting a bevel-tip needle, as the geometry easily penetrated the gelatin phantom with minimal deformation. These findings were echoed in the fracture toughness result, as shown in Fig. 26. Insertion of bevel-tip needles revealed a lower fracture toughness than flat-tipped needles of the same gauge.

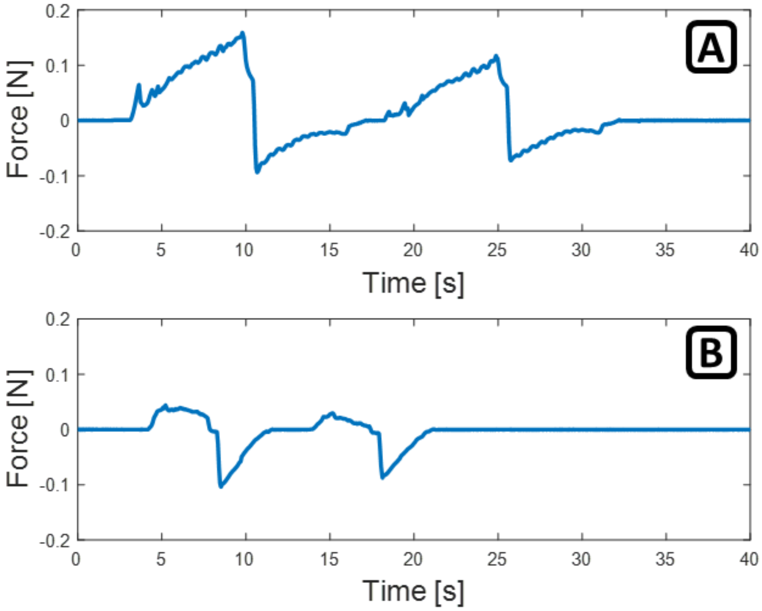

Figure 25: Force time histories of two consecutive insertions of 18 gauge needles with flat (A) or beveled (B) tip geometries into the gelatin (5%) phantom at an insertion speed of 5 mm/s.

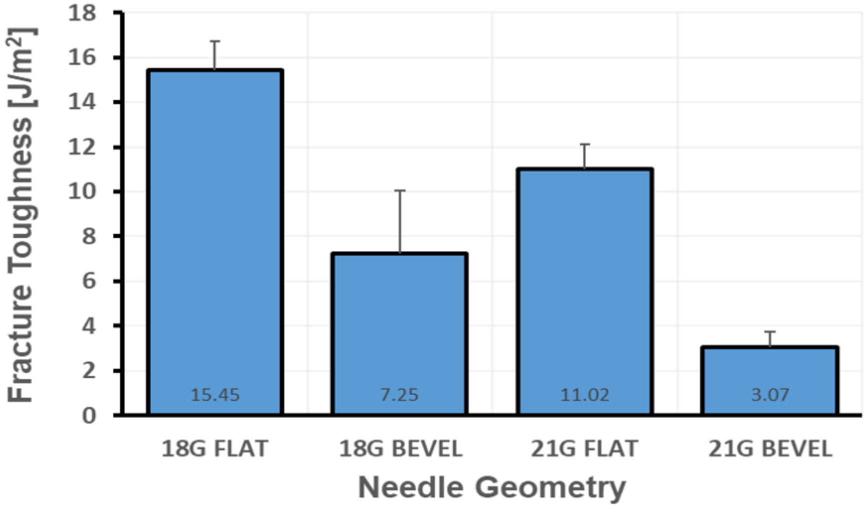

Figure 26: Fracture Toughness calculated from force data for insertion of 18 and 21 gauge flat (blue) bevel (orange) tipped needles into the gelatin (5%) phantom at an insertion speed of 5 mm/s. Values shown are the mean and standard error of the mean across all trials.

4.2.2 Needle Injection Dynamics

The parameters of needle injection investigated were injection volume and volumetric flow rate of fluid delivery via the syringe pump. The selected values were chosen for clinical relevance: it is recommended during clinical injection to deliver a fluid at a flow rate of approximately 0.9 mL per minute [60]. However, consultation revealed that clinicians often dispense at a significantly higher rate. Thus, 7.2 mL per minute was chosen as an additional test flow rate to simulate a typical injection. The injection volumes were chosen to represent typical clinical doses in dental anesthesia. As shown in the sample signals in Fig. 27, the most obvious effect of changes to these parameters was the injection length. Notably, the extraction phase was less significant than in previous needle insertion results when delivering an injection volume of 1 mL. It is hypothesized that this was due to a lubrication effect from the dispensed fluid, decreasing the frictional force on the needle as it was withdrawn. The impulse of each insertion, calculated as the area beneath the force-time curve, is shown in Fig. 28. It was found that increasing flow rate resulted in decreased impulse associated with injection, likely due to the significant decrease in injection duration. Similarly, increasing injection volume resulted in increased impulse.

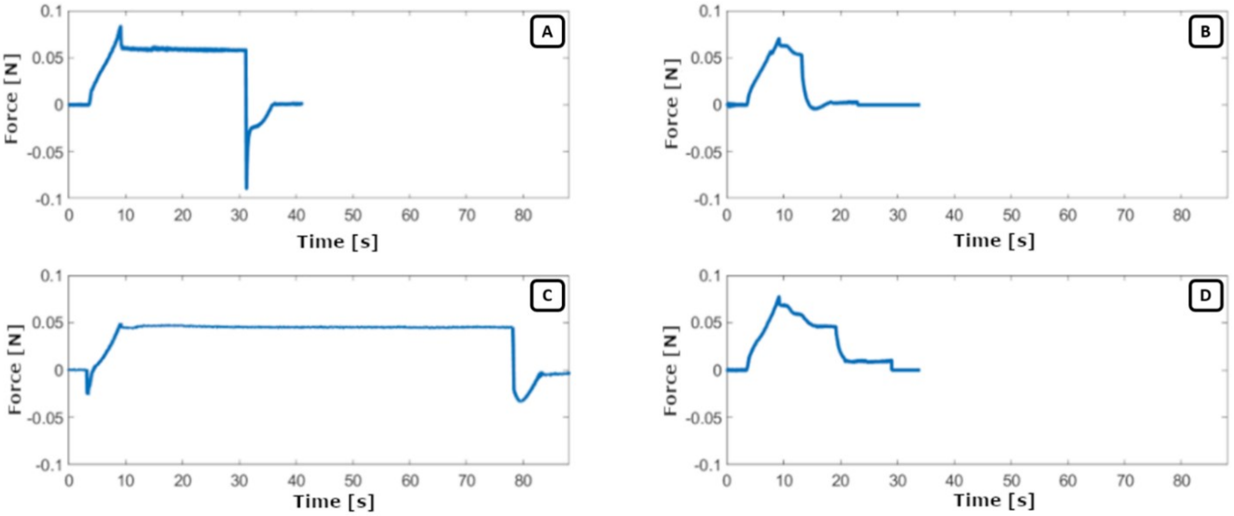

Figure 27: Force time history of needle injection via 25 gauge bevel-tipped needle into the gelatin (5%) phantom at an insertion speed of 5 mm/s with (A) injection volume of 0.3 mL and volumetric flow rate of 0.9 mL/min; (B) injection volume of 0.3 mL and volumetric flow rate of 7.2 mL/min; (C) injection volume of 1 mL and volumetric flow rate of 0.9 mL/min; and (D) injection volume of 1 mL and volumetric flow rate of 7.2 mL/min.

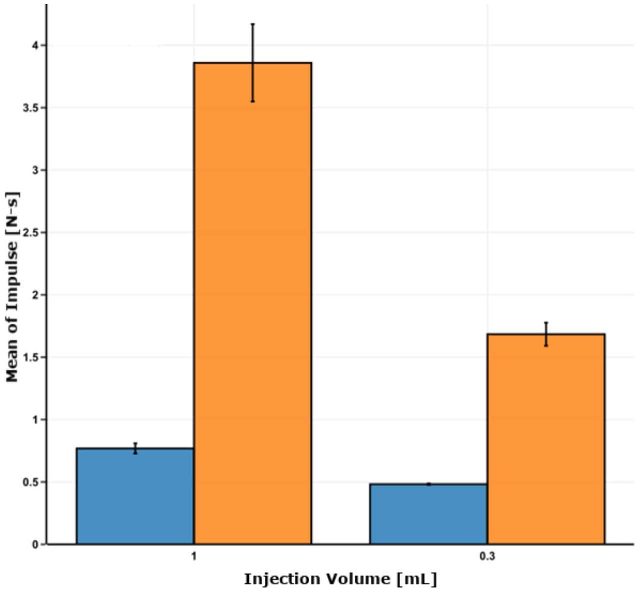

Figure 28: Impulse calculated from force data of needle injection via 21 gauge bevel-tipped needle into the gelatin (5%) phantom at an insertion speed of 5 mm/s with volumetric flow rate of 0.9 mL/min (orange) and 7.2 mL/min (blue). Values shown are the mean and standard error of the mean across all trials.

The work of each needle injection was quantified as described in Section 3.3.3.1. As shown in Fig. 29, it was found that work of injection increased with volumetric flow rate. At a fixed volumetric flow rate, the relationship between injection volume and work of injection was non-linear. At a volumetric flow rate of 0.9 mL/min, increasing injection volume corresponded with a decrease in work of injection, while the reverse trend was seen at a volumetric flow rate of 7.2 mL/min. This may be associated with the fact that, as shown in Fig. 30, the analytically derived $W_{fluid\ delivery}$ was negligible at the 0.9 mL/min volumetric flow rate yet experienced a significant increase with flow rate. Additionally, $W_{insertion}$ was greater than $W_{fluid\ delivery}$ for most configurations, but at an injection volume of 1 mL and volumetric flow rate of 7.2 mL/min, $W_{fluid\ delivery}$ surpassed $W_{insertion}$ as the increase in volume and flow rate of fluid resulted in significantly more work associated with fluid delivery as outlined in equation 7. As the needle insertion phase of each injection performed was identical, $W_{insertion}$ varied very little across injections.

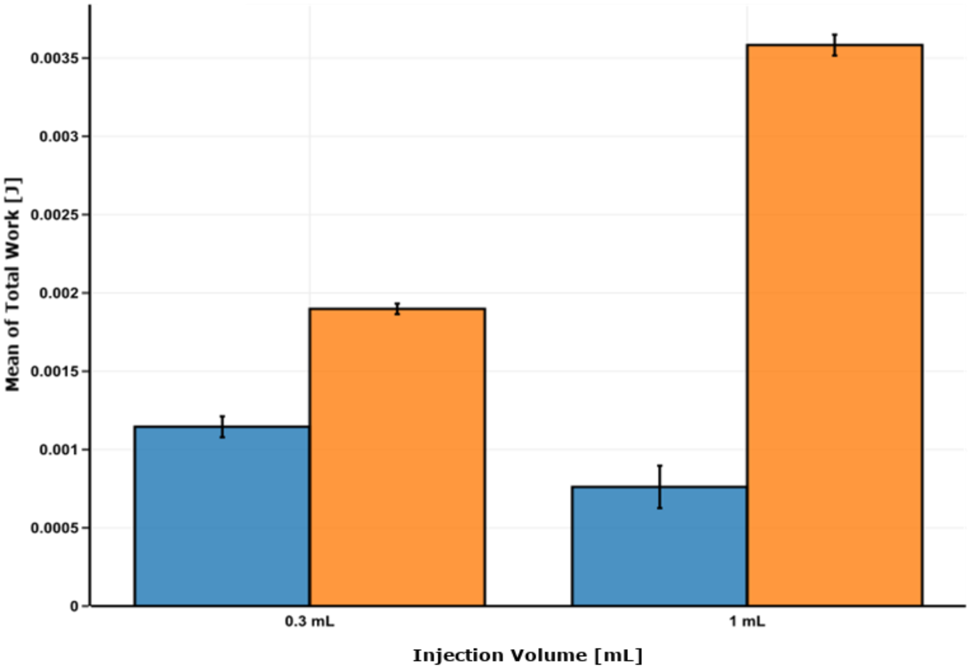

Figure 29: Work of Injection calculated for needle injection via 25-gauge bevel-tip needle into gelatin (5%) phantom at injection volumes of 0.3 mL and 1 mL and volumetric flow rates of 0.9 mL/min (blue) and 7.2 mL/min (orange). Values shown are the mean and standard error of the mean across all trials.

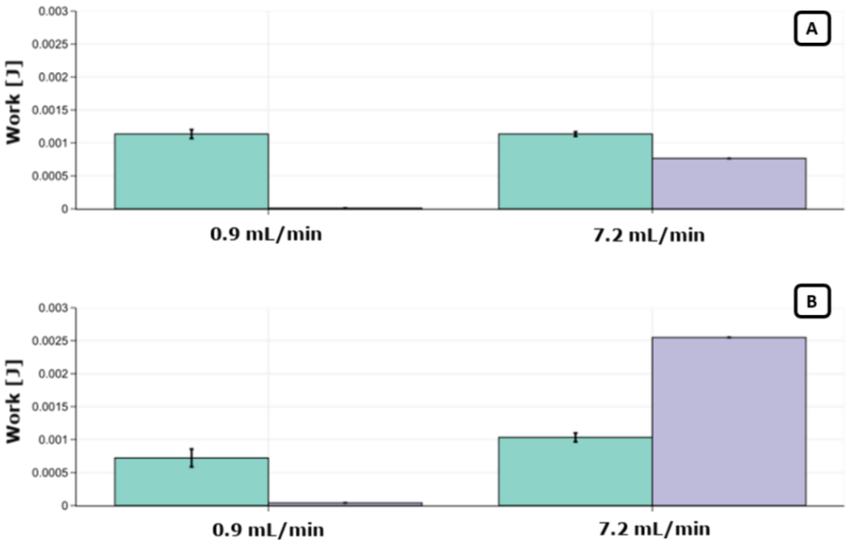

Figure 30: Components of the work of needle injection, $W_{insertion}$ (teal) and $W_{fluid\ delivery}$ (mauve) via 25-gauge bevel-tip needle at injection volumes of 0.3 mL (A) and 1 mL (B). The Work of Insertion is directly calculated, while the Work of Fluid Delivery is derived analytically as described in Section 3.3.3.1. Values shown are the mean and standard error of the mean across all trials.

4.2.3 NFLJI Dynamics

Jet injection investigations in the gelatin (5%) phantom revealed a similar wound shape to that described in the literature in a non-porous tissue phantom, as shown in Fig. 31. The thin, “penny-shaped” crack morphology was hypothesized in the literature to be an artifact of gelatin mechanical properties, as it is more brittle than soft tissue [25]. For this reason, a subsequent investigation of jet injection in a porous phantom, pHEMA, was performed.

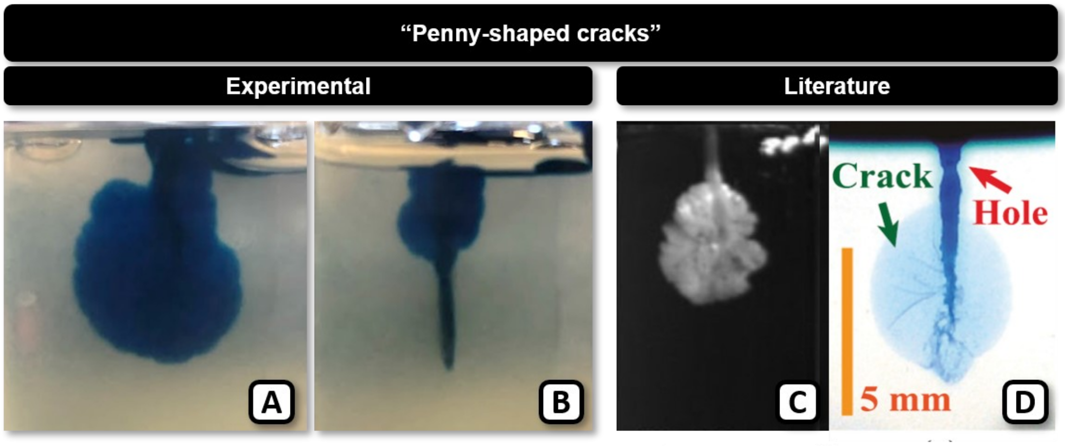

Figure 31: (A) and (B) are orthogonal views of a typical jet injection into the gelatin (5%) phantom. The same behaviour, described in [25] as "penny-shaped cracks" occurs in the literature investigations using similarly non-porous phantoms of (C) polyacrylamide [25] and (D) gelatin [42] . (C) reproduced with permission from [25]. (D) reproduced with permission from [42].

Before proceeding with analysis of jet injection force data, the test bench frequency spectrum response was assessed. Impact hammer measurement of the frequency response of the system with a gelatin (5%) and pHEMA phantom was performed as shown in Fig. 32 to elucidate any natural frequencies of the test apparatus.

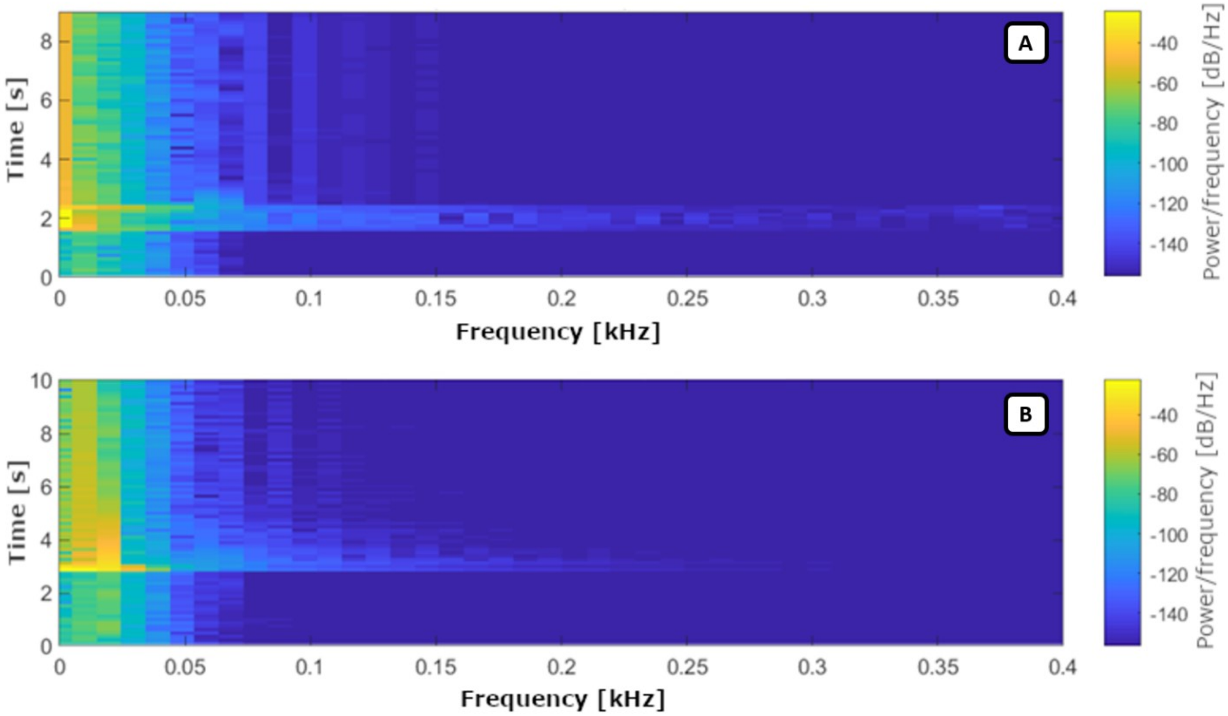

Figure 32: Frequency content of sample Jet Injection (A) and Impact Hammer (B) force time history data.

Separation of the force signals low- and high- frequency components via low-pass filter at 1 Hz and high-pass filter at 1 Hz, as shown in Fig. 33, revealed an intransient frequency component at approximately 68 Hz in all signals which was not obvious in the full spectrum shown in Fig. 32. The low-frequency component of the force signal was retained for investigation of the force time history in tissue, as the injection time history and force amplitude were optimally preserved. The high-frequency component spectrum was then compared with the impact hammer results and high-speed video data for each signal. Each impact hammer dataset exhibited a strong frequency band at a value of approximately 20 Hz which lasted up to three seconds after impact, as shown in Figure

33(d), indicating the natural frequency value of each system configuration. The high-frequency spectrum associated with jet injection, as shown in Fig. 34(c), shows greater high-frequency in the NFLJI data which is notably absent from the impact hammer data. Some of these frequency bands correspond with the oscillation frequency of the gelatin surface measured from high-speed video of NFLJI delivery. For the injection parameters of 620.5 kPa pneumatic supply pressure and volume of 1 mL, the mean surface oscillation frequency observed was 145.8±13.8 Hz. It is therefore likely that the additional high-frequency oscillations were generated as waves propagated through the phantom material and were reflected off of the sides of the glass container.

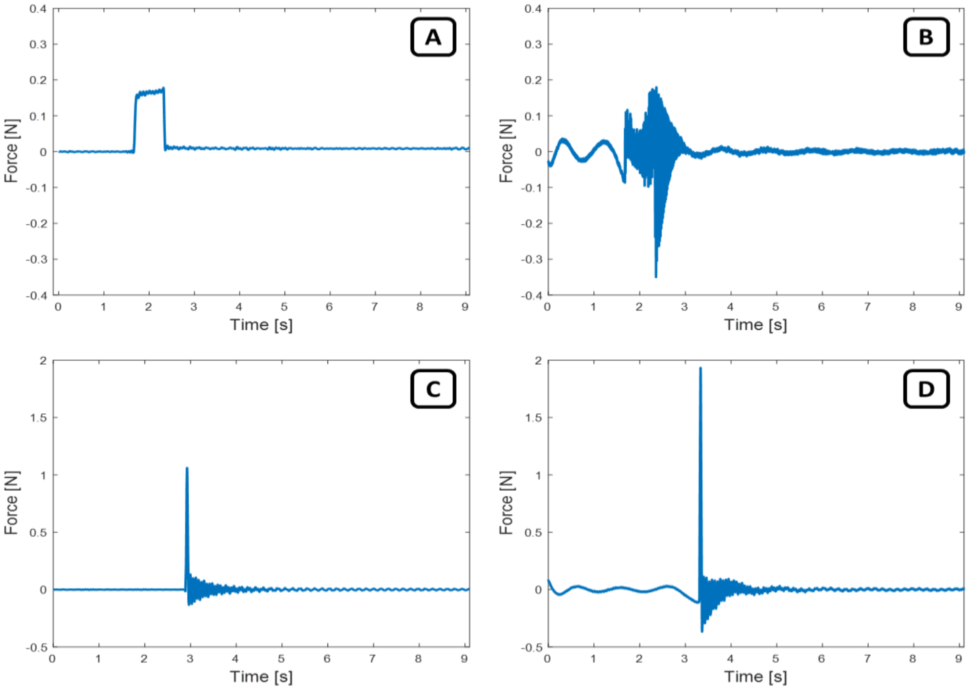

Figure 33: Sample force signals of NFLJI delivery with injection volume of 1 mL and pneumatic supply pressure of 620.5 kPa into the gelatin (5%) phantom with low-pass filter at 1 Hz (A) and highpass filter at 1 Hz (B). Sample force signals of impact hammer striking the gelatin (5%) phantom with low-pass filter at 1 Hz (C) and high-pass filter at 1 Hz (D).

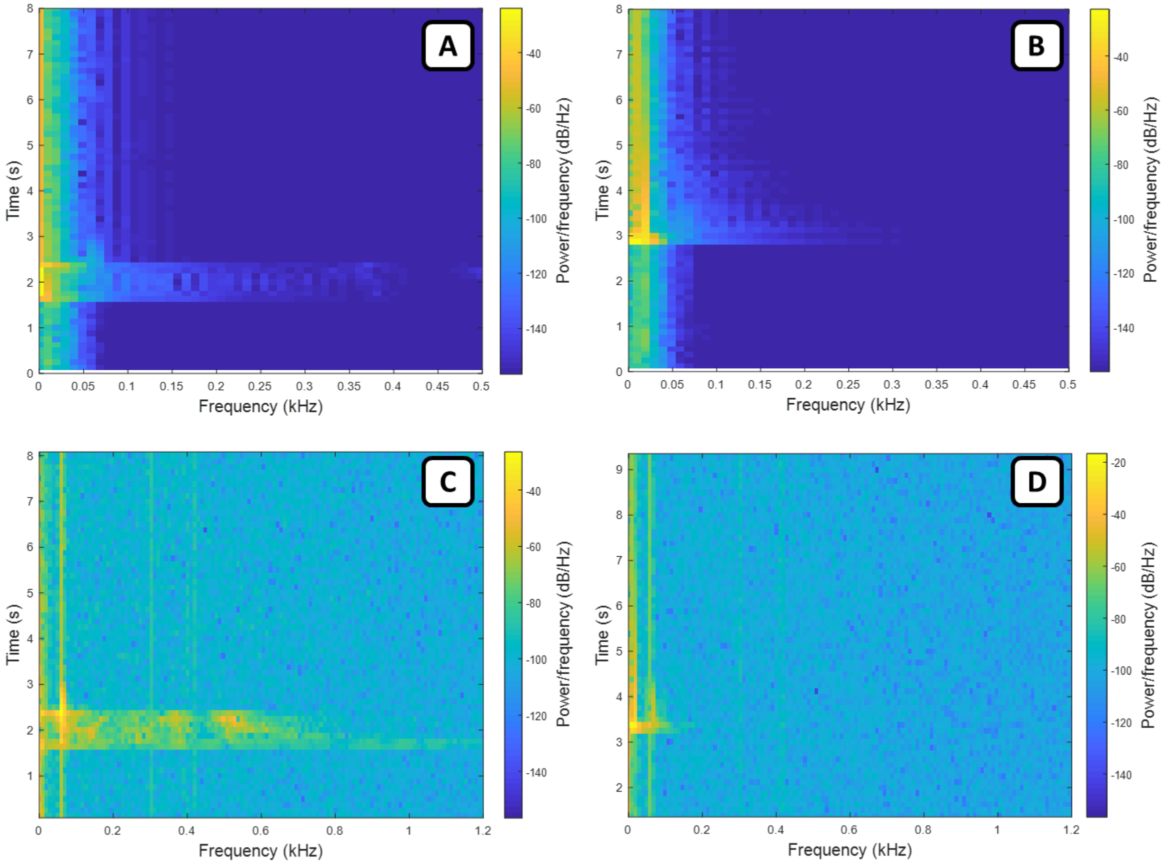

Figure 34: (A) Spectrogram of NFLJI force time history with low-pass filter applied at 1 Hz. (B) Spectrogram of impact hammer strike force time history with low-pass filter applied at 1 Hz. (C) Spectrogram of NFLJI force time history with high-pass filter applied at 1 Hz. (D) Spectrogram of impact hammer strike force time history with high-pass filter applied at 1 Hz .

Measurement of the force time history of jet injection focused on the effect of jet injection volume and pneumatic supply pressure to the NFLJI device. Injection volume was selected to represent a range of clinically relevant values for jet injection as utilized in the clinical pilot study. Similarly, pneumatic supply pressure was chosen to represent a clinically relevant range for delivery of dental anesthetic during clinical investigation. As shown in the sample signals of force data for jet injection into the gelatin (5%) phantom in Fig. 35, increasing injection volume did not have a significant effect on the observed amplitude of the force signal. Increasing pneumatic supply pressure, however, corresponded to an increase in the amplitude of the measured force during injection. This corresponded to the effects of NFLJI driving force described in the literature [3]. These effects are summarized in Fig. 36.

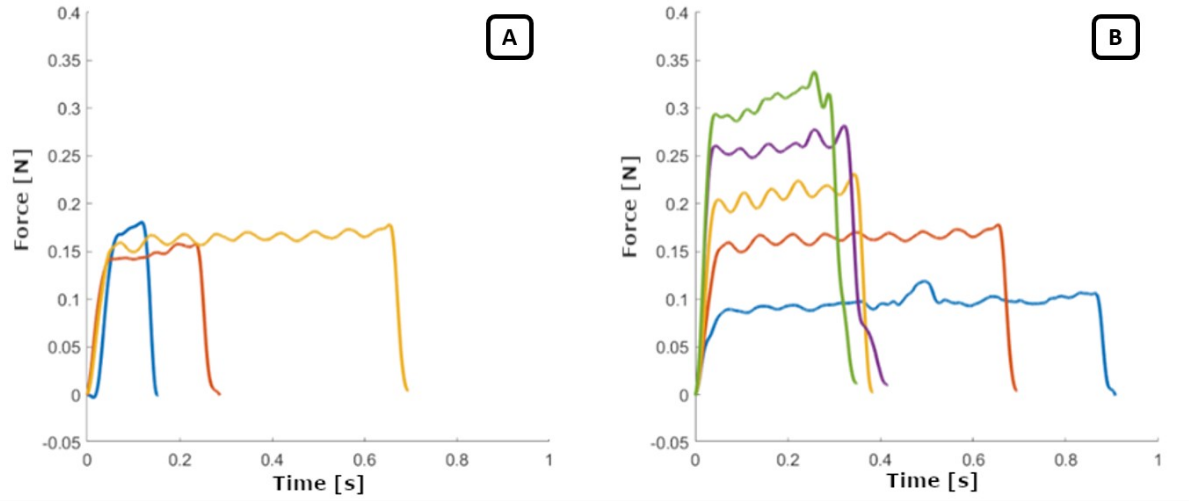

Figure 35: (A) Force time history signals of delivery via NFLJI into the gelatin (5%) phantom at pneumatic supply pressure of 620.5 kPa and injection volumes of 0.1 mL (blue), 0.3 mL (red) and 1 mL (yellow). (B) Sample force time history signals of delivery via NFLJI into the gelatin (5%) phantom at injection volume of 1 mL and pneumatic supply pressure of 413.7 kPa (blue), 620.5 kPa (red), 827.4 kPa (yellow), 1034.2 kPa (violet) and 1241.1 kPa (green). The detailed injection dataset may be found in Section 8.3.1.

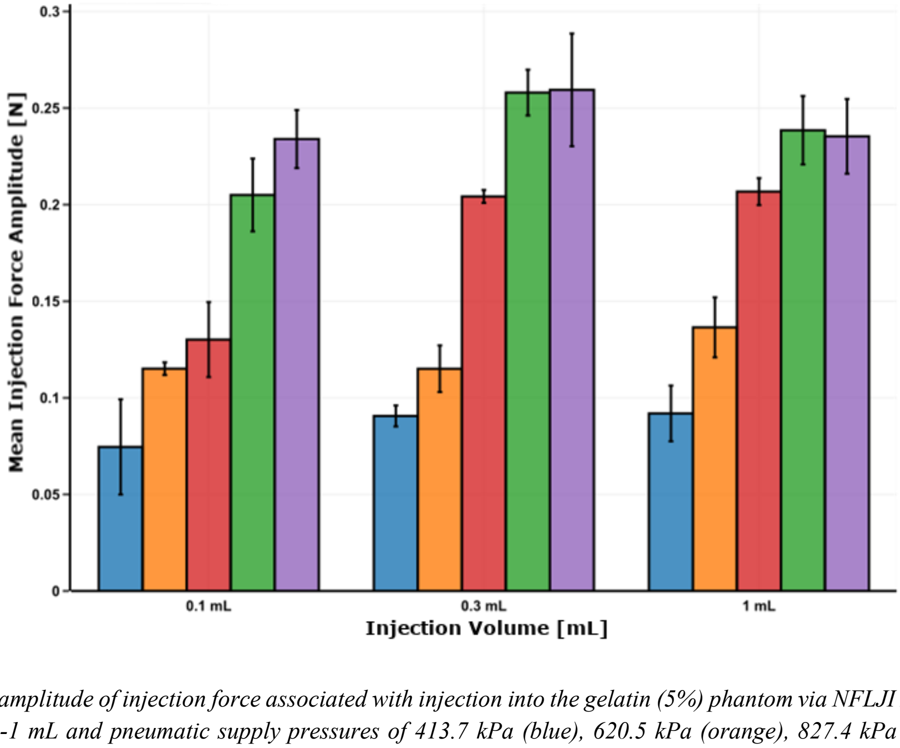

Figure 36: Mean amplitude of injection force associated with injection into the gelatin (5%) phantom via NFLJI system at injection volumes from 0.1-1 mL and pneumatic supply pressures of 413.7 kPa (blue), 620.5 kPa (orange), 827.4 kPa (red), 1034.2 kPa (green) and 1241.1 kPa (violet). Values shown are the mean and standard error of the mean across all trials.

As shown in Fig. 37, increasing injection volume corresponded with greater injection duration. The observed relationship between pneumatic supply pressure and injection duration was non-linear.

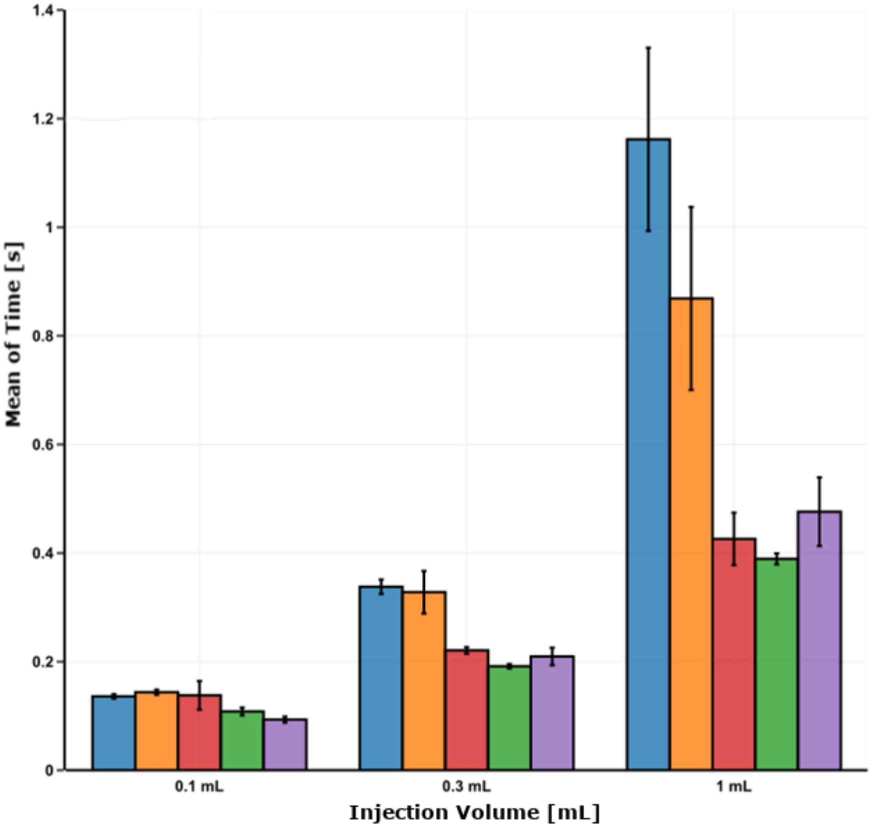

Figure 37: Duration of Injection forNFLJI delivery into the gelatin (5%) phantom at injection volumes 0.1-1 mL and pneumatic supply pressures 413.7 kPa (blue), 620.5 kPa (orange), 827.4 kPa (red), 1034.2 kPa (green) and 1241.1 kPa (violet). Values shown are the mean and standard error of the mean across all trials.

The impulse associated with each jet injection was then calculated and is shown in Fig. 38. It was found that increasing injection volume corresponded strongly with increased impulse. For the 0.1 mL and 0.3 mL injection volumes, increasing pneumatic supply pressure was found to increase the calculated impulse associated with injection, but this trend did not hold at the 1 mL injection volume. A non-linear relationship between impulse and pneumatic supply pressure was observed.

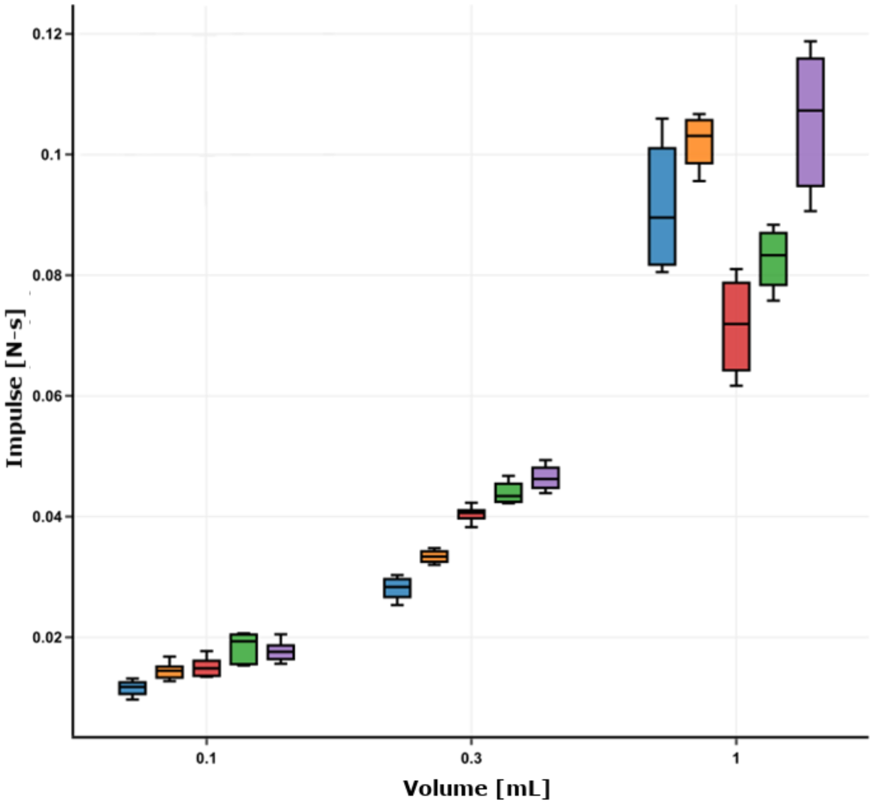

Figure 38: Calculated Impulse of Injection for NFLJI delivery into the gelatin (5%) phantom at injection volumes of 0.1-1 mL and pneumatic supply pressures of 13.7 kPa (blue), 620.5 kPa (orange), 827.4 kPa (red), 1034.2 kPa (green) and 1241.1 kPa (violet). Values shown are the mean and standard error of the mean across all trials.

The average velocity of the jet was then approximated as per the equation

$$v_{average} = \frac{I}{\rho V} \tag{8}$$

where $v_{average}$ is the average velocity of the jet, I is the jet linear momentum (or impulse), ρ is the fluid density, and V is the injection volume. It was found, as shown in Fig. 39, that increasing injection volume tended to correlate with decreased jet average velocity. Pneumatic supply pressure correlated with increasing jet average velocity at injection volumes of 0.1 mL and 0.3 mL, but at a volume of 1 mL the relationship was non-linear.

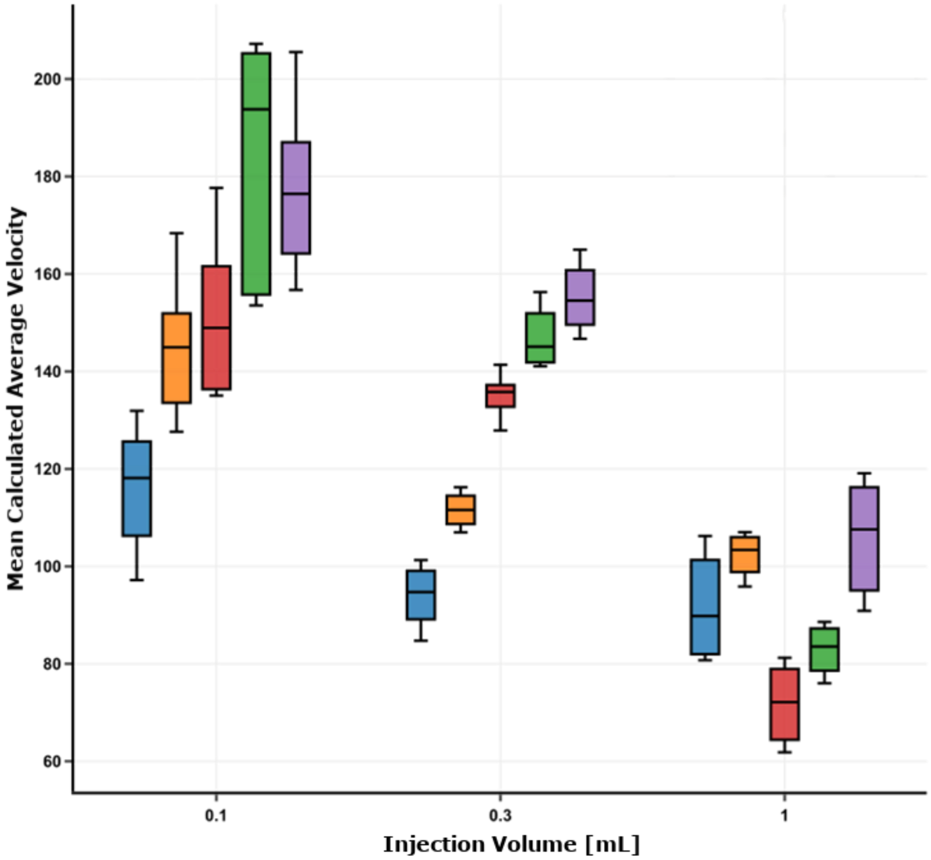

Figure 39: Average jet flow velocity vs. Injection volume for injection via NFLJI into the gelatin (5%) phantom at pneumatic supply pressure of 413.7 kPa (blue), 620.5 kPa (orange), 827.4 kPa (red), 1034.2 kPa (green) and 1241.1 kPa (violet). Values shown are the mean and standard error of the mean across all trials.

The time history of penetration depth of the jet during injection was collected via high-speed camera as shown in the sample signals in Fig. 40, below. It was found, as shown in Fig. 41, that increasing pneumatic supply pressure corresponded with increased penetration depth, while the relationship between injection volume and penetration depth was non-linear. The maximum mean penetration depth, 82.5 ±5.7 mm, occurred at a pneumatic supply pressure of 1241.1 kPa and an injection volume of 0.3 mL. At constant pneumatic supply pressure, an injection volume of 0.3 mL tended to penetrate the phantom more deeply.

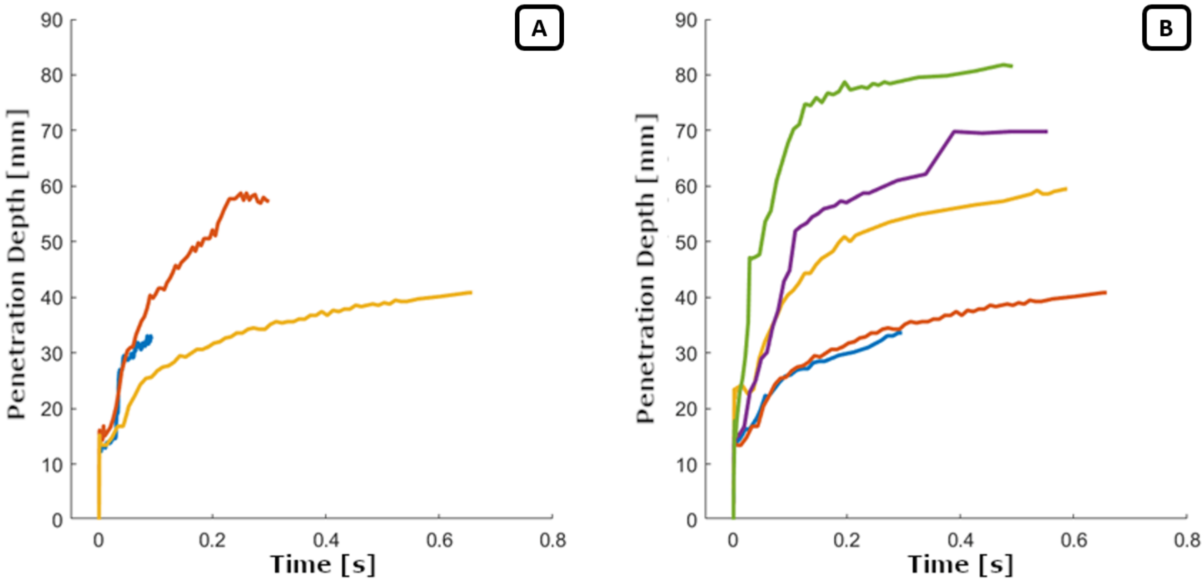

Figure 40: (A) Sample penetration depth time history signals of NFLJI delivery into the gelatin (5%) phantom at pneumatic supply pressure 620.5 kPa and injection volumes of 0.1 mL (blue), 0.3 mL (red) and 1 mL (yellow). (B) Sample penetration depth time history signals of NFLJI delivery into the gelatin (5%) phantom at injection volume 1 mL and pneumatic supply pressure of 413.7 kPa (blue), 620.5 kPa (red), 827.4 kPa (yellow), 1034.2 kPa (violet) and 1241.1 kPa (green). Detailed penetration depth datasets may be found in Section 8.3.2.

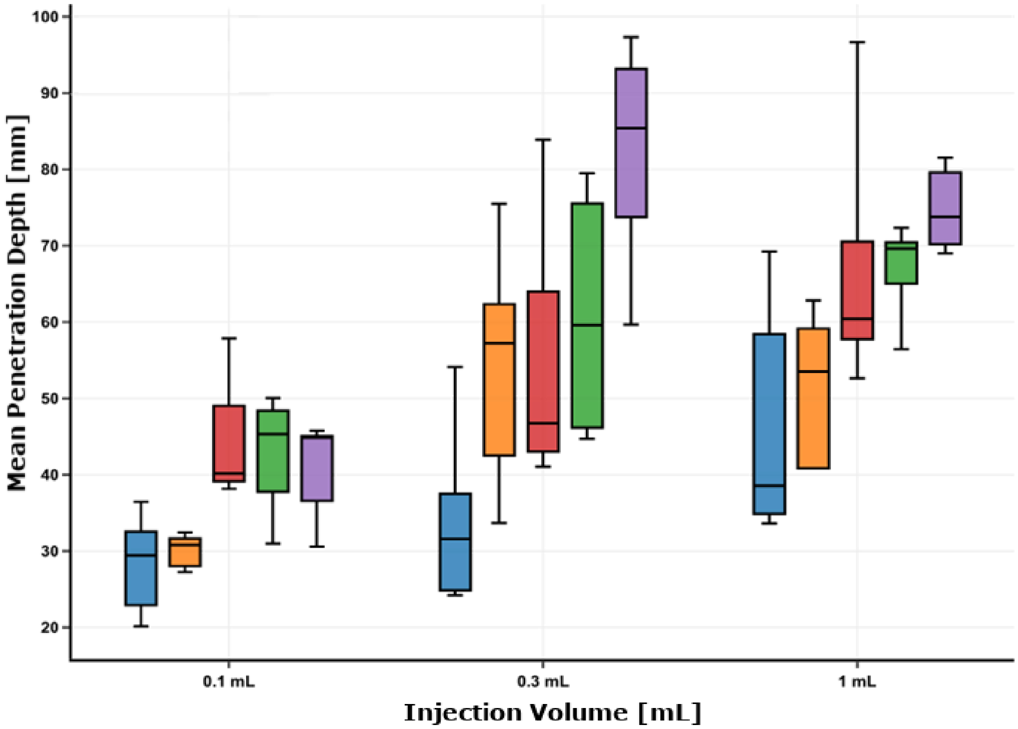

Figure 41: Mean jet penetration depth for NFLJI delivery into the gelatin (5%) phantom at injection volumes of 0.1-1 mL and pneumatic supply pressures of 413.7 kPa (blue), 620.5 kPa (orange) 827.4 kPa (red), 1034.2 kPa (green) and 1241.1 kPa (violet). Values shown are the mean and standard error of the mean across all trials.

The work of injection was then calculated as described in Section 3.3.2.1. First, the injection force signal was plotted against the penetration depth for the duration of the injection as demonstrated by the sample signals in Fig. 42. As the penetration depth data is not strictly increasing due to the oscillatory nature of jet penetration, a manual eight-point approximation of the curve was then performed to permit integration as demonstrated in Fig. 43. The work associated with injection was then approximated as the integral under this fitted curve. The resulting work associated with each set of injection parameters is shown in Fig. 44. It was found that increasing pneumatic supply pressure correlated with increased work of injection. Increasing injection volume resulted in increased work of injection at volumes of 0.1 mL and 0.3 mL, but the increasing trend did not hold as the injection volume increased to 1 mL.

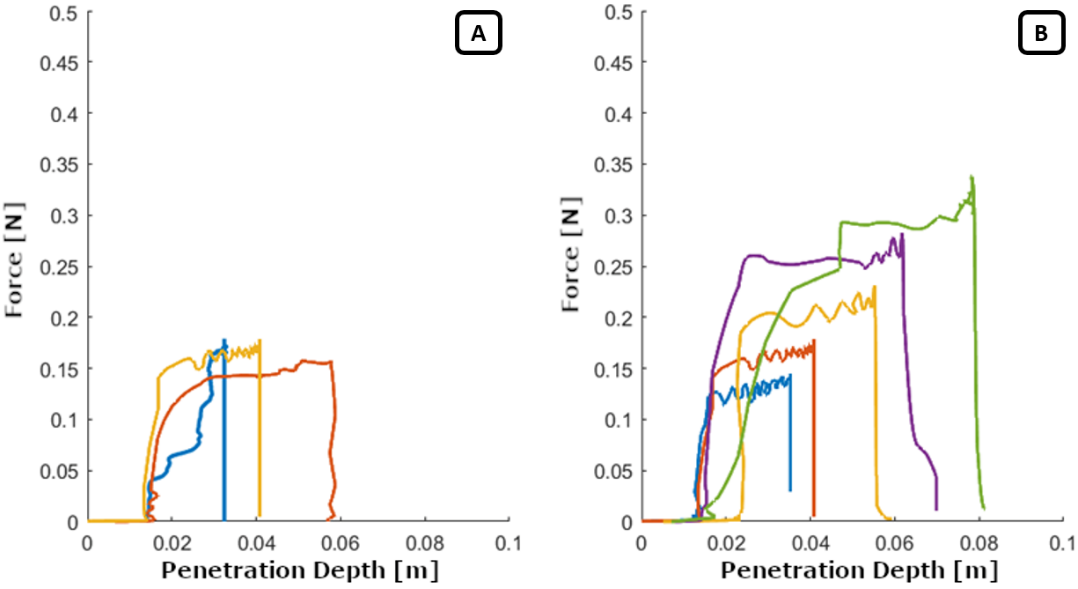

Figure 42: (A) Sample force vs. penetration depth signals for NFLJI delivery into the gelatin (5%) phantom at pneumatic supply pressure 620.5 kPa and injection volumes of 0.1 mL (blue), 0.3 mL (red) and 1 mL (yellow). (B) (A) Sample force vs. penetration depth signals for NFLJI delivery into the gelatin (5%) phantom at injection volume 1 mL and pneumatic supply pressure of 413.7 kPa (blue), 620.5 kPa (red), 827.4 kPa (yellow), 1034.2 kPa (violet) and 1241.1 kPa (green). The detailed dataset may be found in Section 8.3.3.

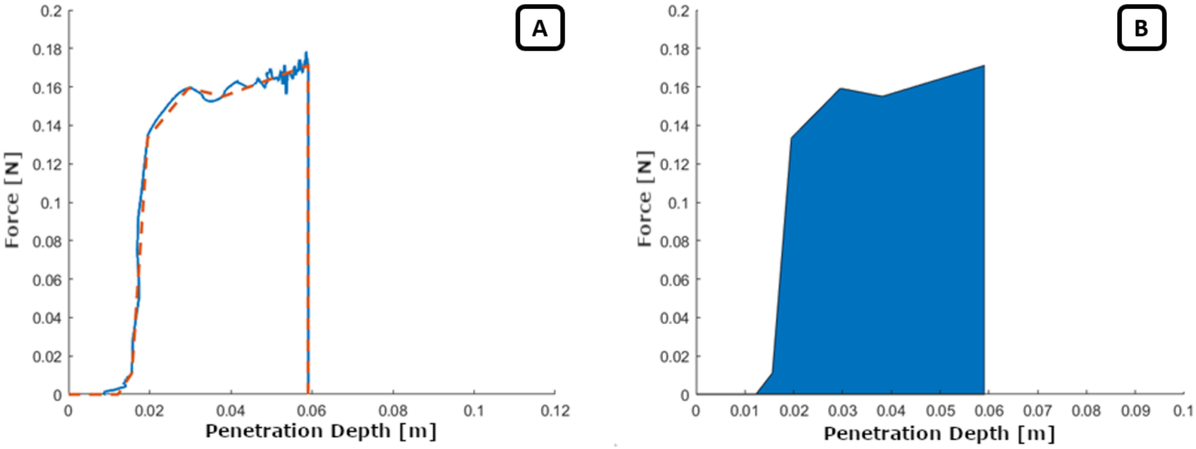

Figure 43: (A) Sample Approximation demonstrating the eight-point manual approximation (dashed line) of the force vs. penetration depth signal (solid line). (B) Sample approximated area under the force vs. penetration depth curve in preparation for calculation of the Work of Injection.

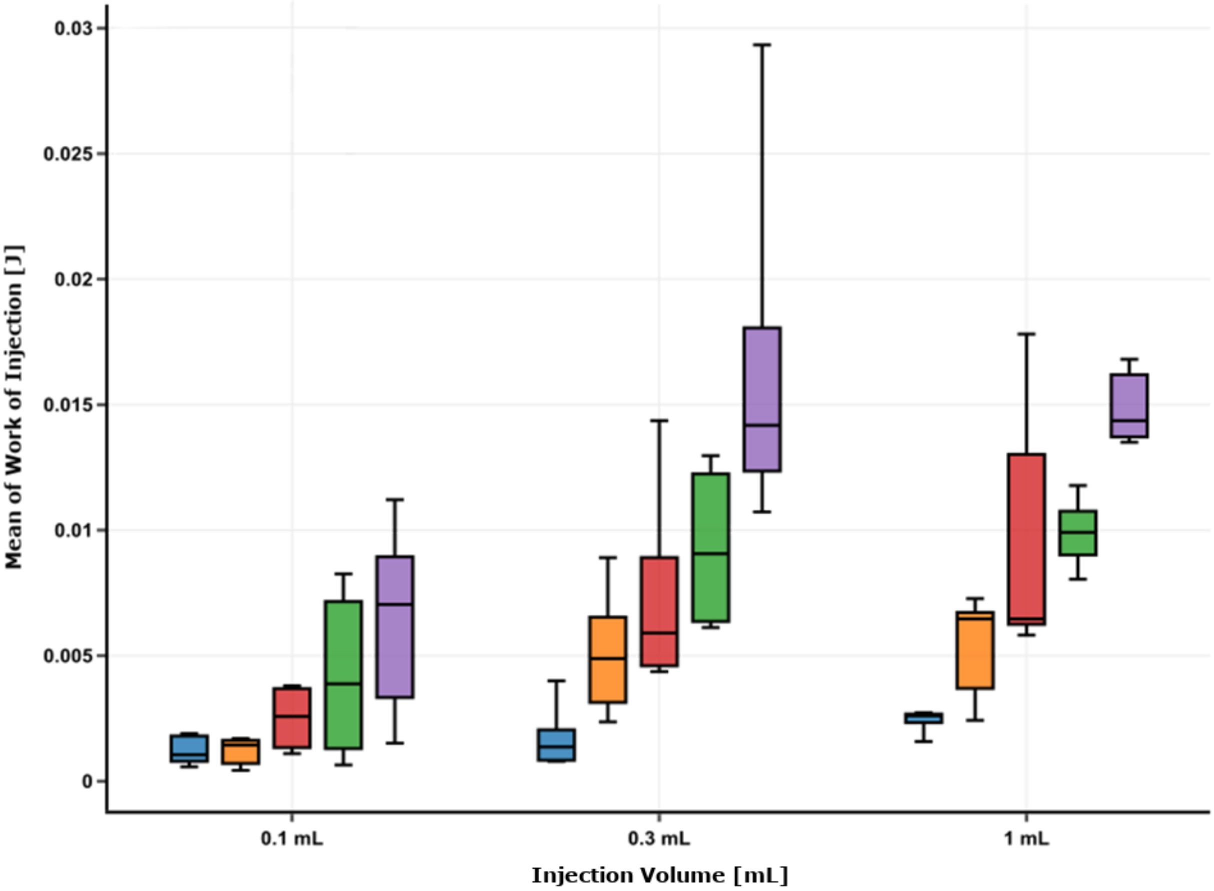

Figure 44: Work of Injection for NFLJI delivery into the gelatin (5%) phantom at injection volumes of 0.1-1 mL and pneumatic supply pressures of 413.7 kPa (blue), 620.5 kPa (orange), 827.4 kPa (red), 1034.2 kPa (green) and 1241.1 kPa (violet). Values shown are the mean and standard error of the mean across all trials.

4.2.4 Comparison between NFLJI and Needle Injection Dynamics

The effects of fluid delivery into the gelatin (5%) phantom via both needle and jet injection were compared. For the purposes of comparison, the most clinically relevant parameters were selected for each injection. For both needle and jet injection, an injection volume of 1 mL was chosen. A pneumatic supply pressure of 620.5 kPa was chosen for jet injection, and a volumetric flow rate of 7.2 mL/min selected for needle injection. These parameter sets represent the best *in vitro* approximation of the use of each delivery method in the clinical pilot studies for dental local anesthesia. Orthogonal views of the wound morphology of each injection method are provided in Fig. 45.

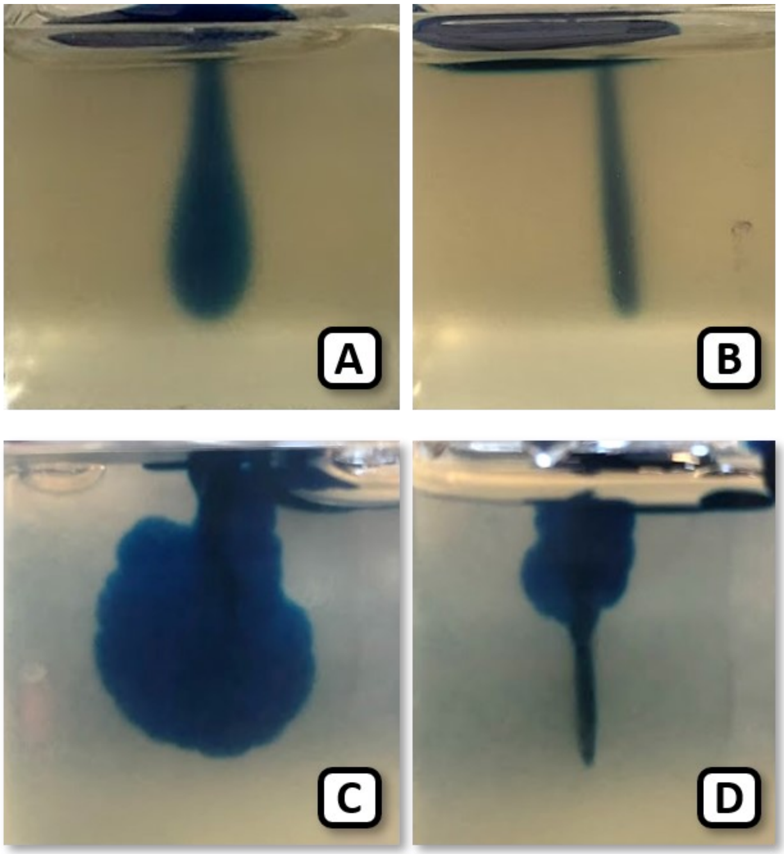

Figure 45: Comparison of morphology of 1 mL needle and jet injections performed in the gelatin (5%) phantom. (A) and (B) Orthogonal views of needle injection at a volumetric flow rate of 7.2 mL/minute. (C) and (D) orthogonal views of a jet injection with pneumatic supply pressure 620.5 kPa.

In comparing the force time history of jet and needle injection as demonstrated by the sample signals shown in Fig. 46, it was clear that the duration of needle injection was significantly greater. This may contribute to pain sensation as described previously [11]. However, the amplitude of the force signal during the injection was found to be higher when jet injection was employed.

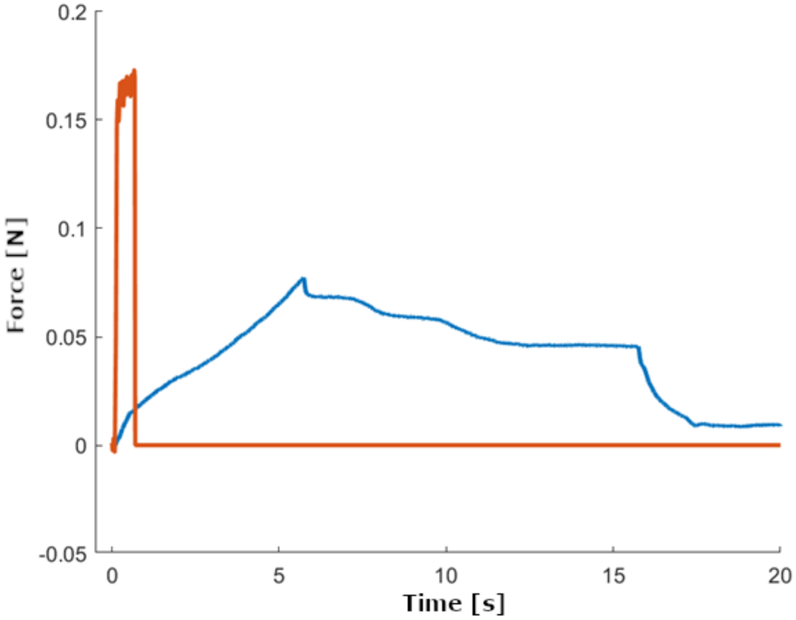

Figure 46: Sample force time history of 1 mL injection via needle (blue) and NFLJI (orange) into the gelatin (5%) phantom. The injection parameters were selected for clinical relevance: for needle injection, a volumetric flow rate of 7.2 mL/minute, and for jet injection, a pneumatic supply pessure of 90 psi or 620.5 kPa.

A shown in Fig. 47, the impulse associated with jet injection was significantly less than that of needle injection, despite the elevated injection force, which may indicate less damage to the tissue.

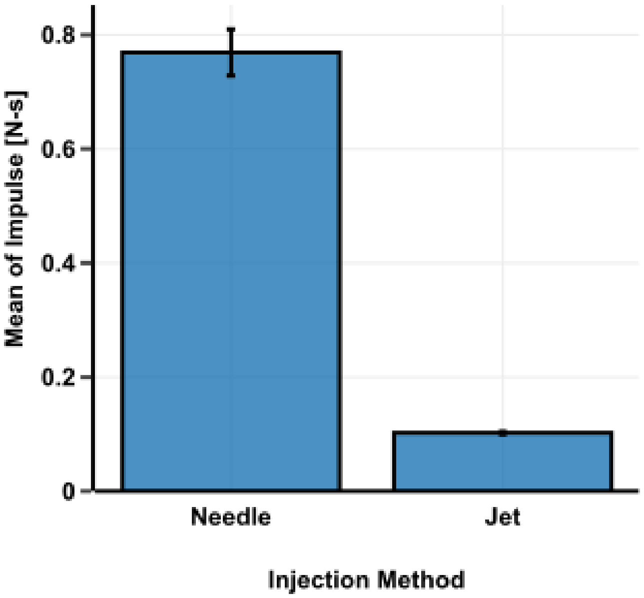

Figure 47: Impulse of injection associated with injection of 1 mL via needle injection (volumetric flow rate = 7.2 mL/minute) and NFLJI (pneumatic supply pressure = 620.5 kPa). Values shown are the mean and standard error of the mean across all trials.

It was found that injection via NFLJI system was associated with greater energy than needle injection, as shown in Fig. 48, at the selected clinical evaluation parameters. In considering all investigated parameter configurations, as shown in Fig. 49, the work of injection associated with injection via NFLJI was greater than that of needle injection for most configurations. The work of injection associated with NFLJI and needle injections was equivalent only at an injection volume of 0.3 mL, with needle volumetric flow rate of 7.2 mL/min and a NFLJI pneumatic supply pressure of 413.7 kPa. The work of injection associated with needle injection was greater than that of injection via NFLJI only at an injection volume of 1 mL with needle volumetric flow rate of 7.2 mL/min and NFLJI pneumatic supply pressure of 413.7 kPa.

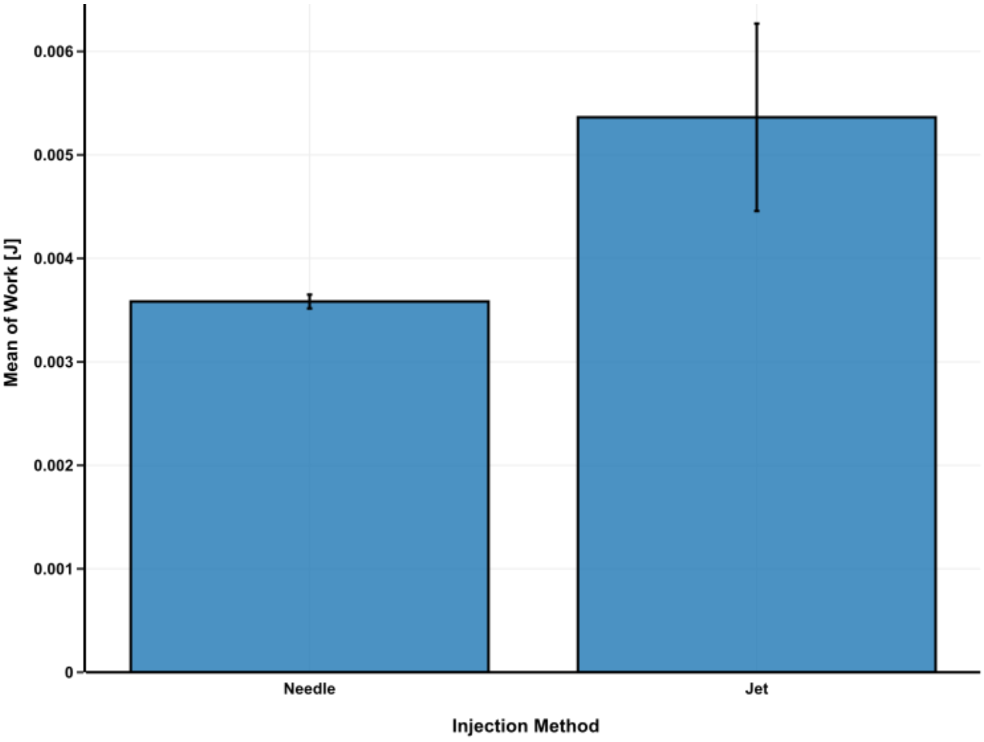

Figure 48: Comparison of the calculated work of a 1 mL injection via NFLJI (pneumatic supply pressure = 620.5 kPa) and needle injection (volumetric flow rate = 7.2 mL/min, 25-gauge bevel-tip needle) into the gelatin (5%) phantom. Values shown are the mean and standard error of the mean across all trials.

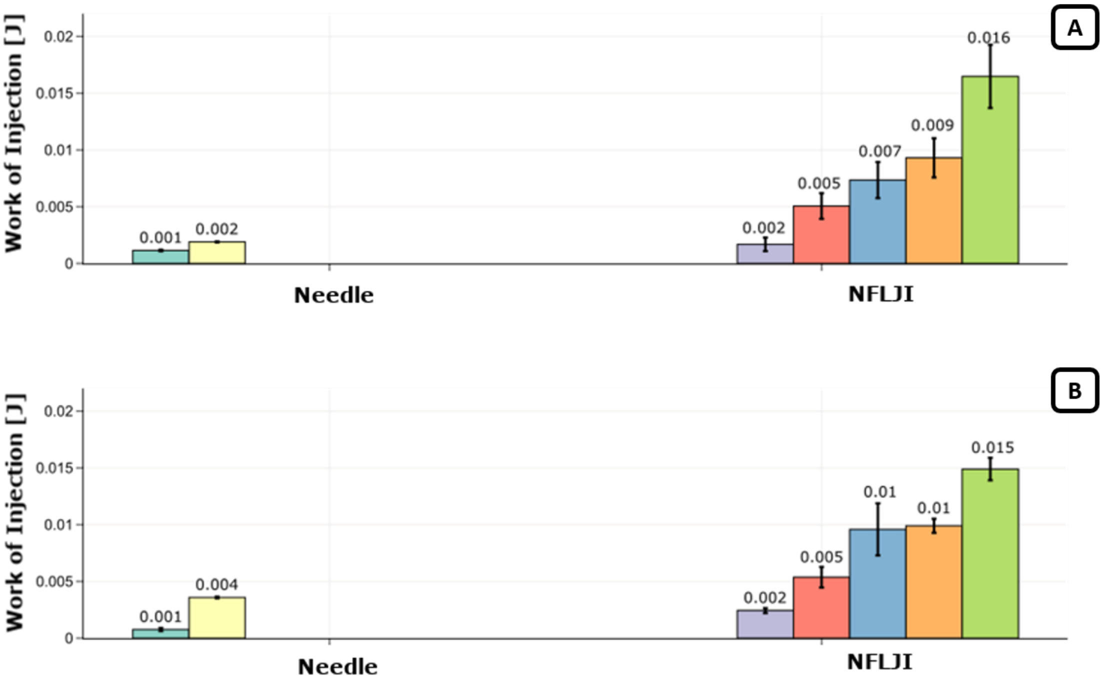

Figure 49: (A) Work of Injection for a 0.3 mL injection delivered via needle at volumetric flow rates of 0.9 mL/min and 7.2 mL/min, and NFLJI at NFLJI pneumatic supply pressures of 413.7 kPa, 620.5 kPa, 827.4 kPa, 1034.2 kPa, and 1241.1 kPa. (B) Work of Injection for a 1 mL injection delivered via needle at volumetric flow rates of 0.9 mL/min and 7.2 mL/min, and NFLJI at NFLJI

pneumatic supply pressures of 413.7 kPa, 620.5 kPa, 827.4 kPa, 1034.2 kPa, and 1241.1 kPa. Values shown are the mean and standard error of the mean across all trials.

Finally, regurgitation of injected fluid was observed in the clinical pilot studies, resulting in a bitter taste and negative overall experience for the patient. To investigate this, regurgitation of fluid delivered via both NFLJI and needle injection was compared as shown in Figures 40 and 51. It was found that both methods result in fluid regurgitation, the extent of which increases as the injection volume increases. For NFLJI injection, it was found that the effect of increasing pneumatic supply pressure on regurgitation volume was unclear. For some NFLJI injections, the regurgitation calculated was negative, indicating that the mass of the phantom increased by more than the expected mass of the injected fluid. It is hypothesized that this is due to slight inconsistencies in the volume of fluid delivered by the system. Given the prevalence of this effect at the smallest injection volume of 0.1 mL, and the range of 0-30% overshoot in final mass, it is not unreasonable that the NFLJI system delivered an extra 0.03 mL with the injection.

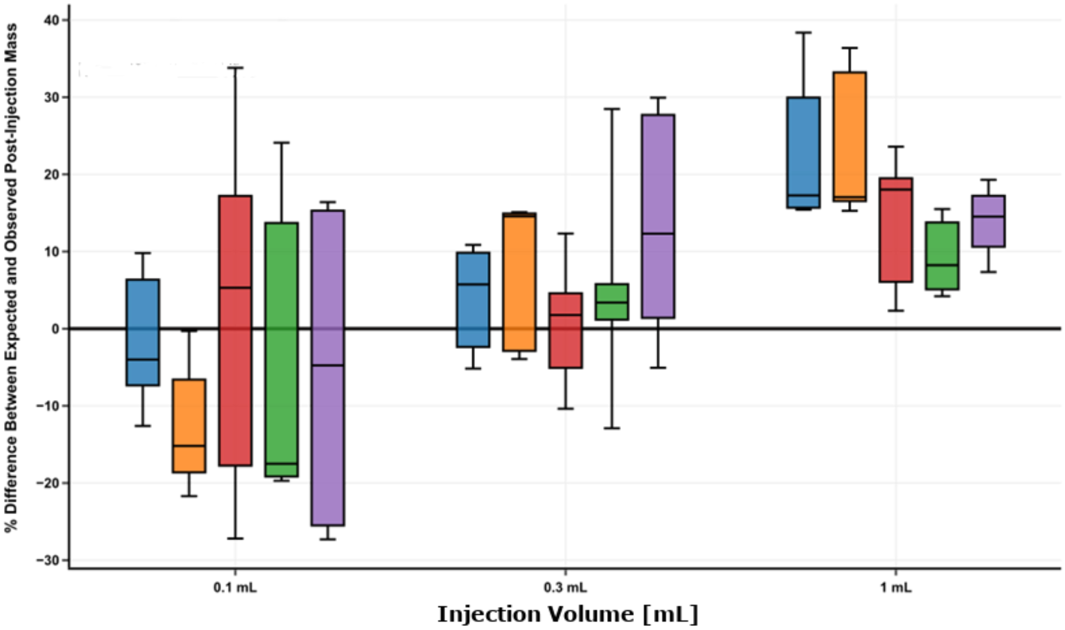

Figure 50: Percentage difference from expected post-injection mass for jet injections performed at injection volumes of 0.1-1 mL and pneumatic supply pressures of 417.3 kPa (blue), 620.5 kPa (orange), 827.4 kPa (red), 1034.2 kPa (green) and 1241.1 kPa (violet). Values shown are the mean and standard error of the mean across all trials.

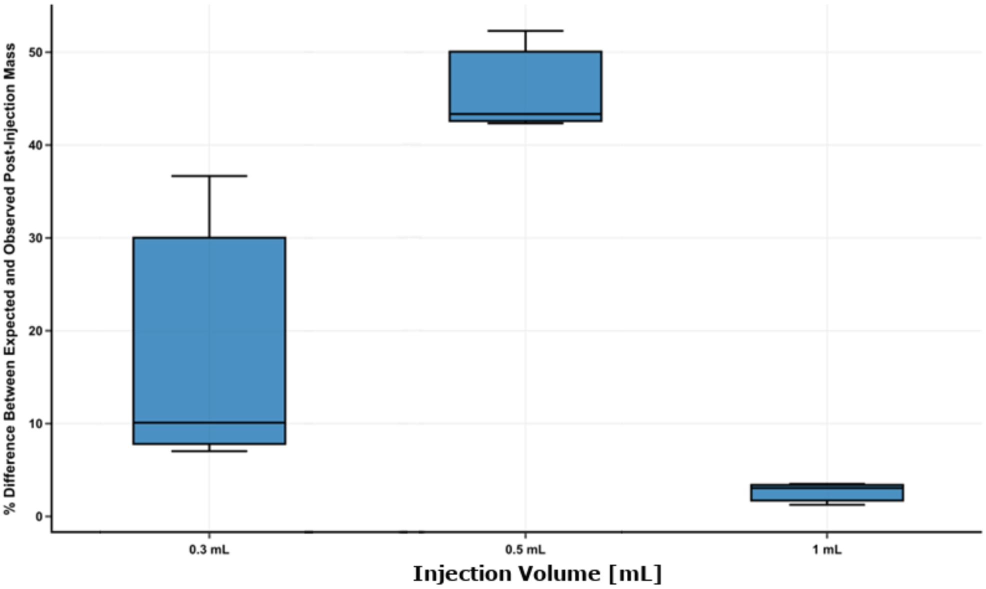

Figure 51: Percentage difference from expected post-injection mass for needle injections performed at a volumetric flow rate of 1.8 mL/minute. Values shown are the mean and standard error of the mean across all trials.

4.2.4.1 Comparison of NFLJI and Needle Injection in pHEMA phantom

The morphology of an injected fluid volume of 0.3 mL via needle injection and NFLJI were compared via CT scan of a completed injection. The wound morphology was found to be quite similar as shown in Fig. 52. Notably, the needle injection morphology lacked the tapered upper portion observed in the jet injection, as the bolus of fluid was delivered directly at depth via the needle insertion.

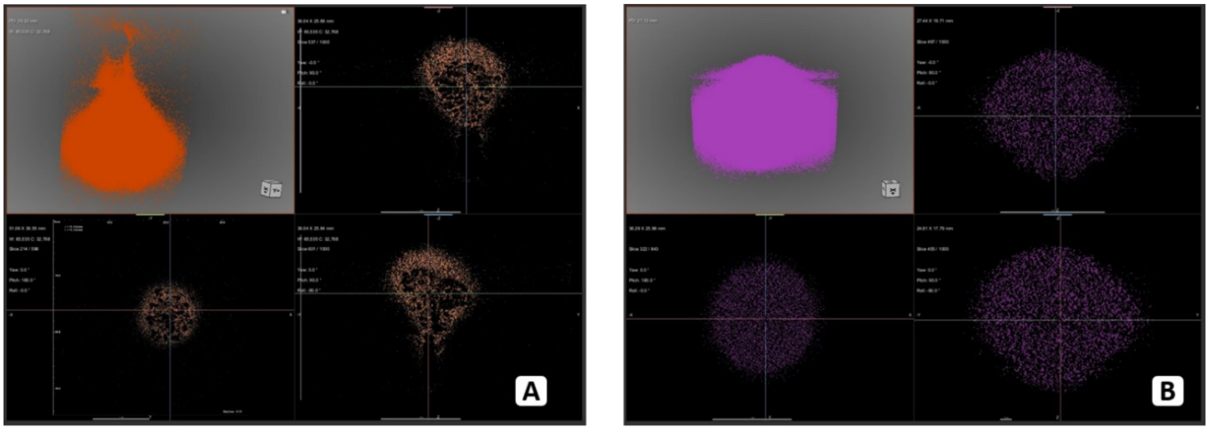

Figure 52: (A) Reconstruction of CT data for jet injection of 0.3 mL of Omnipaque (Supplier) at a pneumatic supply pressure of 90 psi into the pHEMA phantom. (B) Reconstruction of CT data for needle injection of 0.3 mL of Omnipaque (Supplier) by hand into the pHEMA phantom.

4.3 OPTIMIZED CLINICAL APPLICATION FOR DENTAL LOCAL ANESTHESIA PILOT STUDY IN HUMANS

Clinical pilot testing was ongoing at the McGill Dental Clinic until closure due to COVID-19 on March 13, 2020. Issues with performing an inferior alveolar nerve block via jet injection were encountered, related to the lack of haptic feedback available during needle injection to help guide the injection path. To address this issue, first, segmentation of the mandible and surrounding space was performed from a computerized tomography (CT) dataset obtained from the McGill Dental Clinic (McGill IRB A09-M36-18A) to more accurately define the injection path. Segmentation of CT images was performed as described in Section 3.7. The resulting path construction, demonstrated in Fig. 53, resulted in a re-designed NFLJI nozzle which incorporated a 15 degree angle relative to the lower occlusal plane of the central incisors to better achieve the desired path within the geometric constraints of a patient's mouth. The prototype nozzle design prepared by Medical International Technologies (MIT Canada) Inc. is shown in Fig. 54. Testing was halted by COVID-19 related restrictions, but will resume once restrictions are lifted. An invention disclosure (D2020-0140) was filed with the McGill Office of Innovation and Partnerships in conjunction with Medical International Technologies Canada Inc. Also considered to improve success rates of the inferior alveolar nerve block as implementing ultrasound guidance in the dental local anesthesia setting. An appropriate ultrasound probe was researched and ordered; however, due to restrictions associated with COVID-19, the feasibility of this approach was not untested.

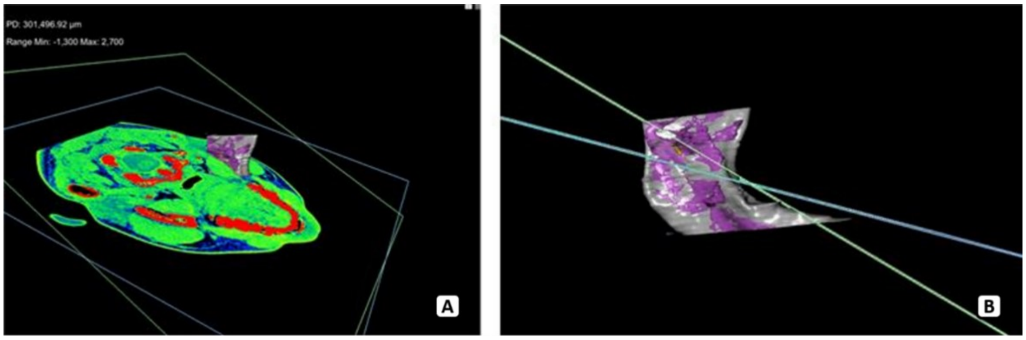

Figure 53: (A) CT image reconstruction comprising a single cross-sectional image of the skull, and a partial 3-dimensional reconstructino of the manidble. (B) 3D reconstruction of the left mandibular bone showing the plane of the rear molars (blue) and plane representing the required angulation to reach the inferior alveolar injection site (green).

Figure 54: Re-designed NFLJI nozzle prototype prepared by Medical International Technologies (MIT Canada) Inc. This nozzle targets an injection angle of 15 degrees relative to the lower occlusal plane of the central incisors.

5 DISCUSSION

The motivation of this work was to contribute to the knowledge base supporting NFLJI and potentially drive adoption of the technology by assisting in the creation of evidence-based clinical practice guidelines. The clinical application targeted was delivery of dental local anesthetic. This was pursued by first constructing an appropriate soft tissue phantom for the clinical use case by characterizing the mechanical properties and porosity structure of porcine oral tissue, and then comparing these properties to a variety of candidate hydrogels. The hydrogels were evaluated based on their mechanical properties, porosity structure, and the morphology and force response of injected fluid as compared to tissue. Then, using the identified gelatin soft tissue phantoms and a customized force balance test apparatus, the underlying mechanism of each drug delivery method was investigated. First, needle insertion was addressed and the effects of needle gauge, tip geometry, and needle insertion speed were evaluated by measuring the fracture toughness as previously described [16], [17]. Then, fluid delivery was introduced and the mechanism of needle injection was characterized by measuring the injection forces and regurgitation of delivered fluid. The second method of fluid delivery, NFLJI, was then assessed using the same test apparatus. The injection forces and penetration behavior of the jet were characterized, as well as the regurgitation effects of injected fluid. Finally, the characterizations of needle and jet injection were directly compared. The direct comparison and standardized test methods in this study provides a rigorous comparison of drug delivery via needle injection and NFLJI, an outcome which is overlooked in the literature despite its clinical relevance. This standardization was provided in large part by the strain gauge-based test apparatus, which may have lent greater accuracy than the piezoelectric (PCB) force sensors commonly reported in the literature. Given the magnitude of the forces associated with injection, with a range well under 1 N, a PCB force sensor which provides reliable results and a reasonable time constant is a challenge. For this reason, a strain gauge force sensor is the more reliable choice and was utilized in this work with some success. The present work also focused on parameter selection for optimal applicability to clinical use, a major strength lent by the interdisciplinary nature of the research team.

It was found that the measured storage moduli and complex viscosities of porcine oral tissue were lower than some found in the literature, although comparison was difficult as many of the tests in the literature focused on tensile or compressive modulus [40], [45], [46]. The porosity values identified for porcine oral submucosa and muscle were similarly lower than that which is estimated by the literature. The porosity structure of porcine oral mucosa could not be imaged, as only smooth portions of the surface of the tissue were visible. Future investigations should further refine the SEM protocol or include an SEM imaging system which can perform three-dimensional analysis.

Gelatin was an appropriate match for the elastic and viscoelastic properties of soft tissue. This was supported by the literature, as gelatin was a common choice [39], [42], [45], [48]–[50]. However, some potential artifacts of the use of a gelatin phantom were identified. Primarily, the morphology of the injection wound and regurgitation behavior of the injected fluid differed significantly from those observed in tissue. This result was predicted in the literature, as it was indicated that porosity of the phantom may provide improved fidelity to injection behavior in tissue [42]. For this reason, preliminary testing was performed for a porous soft tissue phantom. The selected material, pHEMA, was not employed in previous needle or jet injection studies but provided excellent results. The modulus and complex viscosity are an similar to that of porcine oral mucosa, and the 20-30 μm pore size is on the scale reported in soft tissues [59]. The injection morphology observed in pHEMA phantoms was much closer to that observed in liver tissue and differed from the ‘penny-shaped cracks' reported in a non-porous gelatin phantom. As such, it is recommended that pHEMA be further investigated as a soft tissue phantom and employed in future investigations relating to the present work.

Characterization of needle insertion revealed an injection force time history which reproduces the four distinct phases of needle insertion described in the literature [16]. The observed trends of decreased fracture toughness and magnitude of insertion forces with increasing needle gauge and decreasing magnitude of insertion forces and fracture toughness with a beveled tip geometry were in agreement with the literature [40]. Moreover, these results are intuitive as a smaller area of force application, due either to beveled tip or decreased needle diameter, decreases the area over which force is applied. This increases stress on the material surface at the insertion site and therefore facilitates material rupture. These results may be of interest to clinicians, as the forces produced during injection may affect the pain sensation experienced by the patient. The relationship between needle insertion speed and insertion forces or fracture toughness was unclear. Further investigations could address the effects of this parameter *in silico*, as it is likely a more complex relationship must be elucidated.

It was found that increasing needle flow rate decreased the calculated impulse with little effect of the magnitude of injection forces. This change in impulse is therefore largely tied to the injection duration, which is decreased as the flow rate increases. Interestingly, it was found that while the relationship between work of needle injection and injection volume is linear, that of work and volumetric flow rate is not. This is likely because analytically calculated $W_{fluid\ delivery}$ increases significantly as the volumetric flow rate increases, surpassing $W_{insertion}$ at a volumetric flow rate of 7.2 mL/min and an injection volume of 1 mL. This result may once more interest clinicians, as the injection forces and energy delivered to the tissue during fluid delivery may contribute to both pain sensation and the dispersion of delivered therapeutic agents. These result may reflect on the established clinical guideline for fluid delivery, which emphasizes a flow rate of 0.9 mL/minute [60]. It may, therefore, be optimal to select a different volumetric flow rate for various volumes of injection to balance minimizing the energy delivered to the tissue with the duration of injection. Finally, it was found that the lowest regurgitation of fluid occurred at the highest injection volumes. This may be due to the increased linear momentum and energy of a larger volume of fluid, which may more effectively fracture the phantom material to allow injected fluid to remain inside.

In investigating NFLJI, it was found that, as expected, injection forces produced were very in short duration. While a clear linearly increasing trend was observed in the effect of increasing injection volume with respect to calculated impulse, the relationship between injection volume and jet penetration depth was less obvious. While increasing the pneumatic supply pressure correlated with increasing jet penetration depth, this was only true of the relationship between pneumatic supply pressure and calculated impulse at injection volumes of 0.1 mL and 0.3 mL. At an injection volume of 1 mL, the correlation appears to be non-linear. This trend, while difficult to capture *in vitro*, could be investigated *in silico* via an appropriate finite element model. If pneumatic supply pressure is understood as the driving force of the NFLJI system, then the pneumatic supply pressure aligns with the literature, while the unclear injection volume trend does not; it was reported that increasing injection volume corresponds with increased jet penetration depth [3]. The surprising finding that penetration depth tended to be greater at an injection volume of 0.3 mL indicates an underlying mechanism in the relationship between injection volume and penetration depth that could be investigated *in silico*. In quantifying the work of injection via NFLJI, it was found that increasing pneumatic supply pressure corresponded with increasing work; however, the relationship between injection volume and work was non-linear. This is potentially of great interest to clinicians as, coupled with the penetration depth data, there could be developed an optimal strategy to reach the targeted injection location or anatomical structure while delivering minimal potentially damaging energy to the tissue. It was additionally found that increasing injection volume corresponded with increased regurgitation of fluid, a result which counters that seen in needle injection. This may have occurred because the greater impulse delivered by a higher volume elicited a greater viscoelastic response in the gelatin phantom. Further investigations should address regurgitation in a porous phantom for confirmation, as the fluid dispersion and viscoelastic response is expected to change. Also notable was the vibration produced following injection, a phenomenon not substantially addressed in the literature. These vibrations following injection may to some extent be an artifact of the homogenous and viscoelastic soft tissue phantom, as they were less pronounced in NFLJI injections performed in pHEMA phantoms. The oscillatory effects may also be amplified by the relatively small container size, so future experiments could consider increasing the container size to prevent oscillation due to the reverberation of waves generated in the phantom following injection. Future work should confirm the significance of vibrational effects in porous phantoms and tissue, as these may affect the tissue and they are not observed in needle injections. Additionally, future investigations should employ porous soft tissue phantoms wherever possible, as the morphology of the wound formed exhibits greater similarity to that observed in tissue. These investigations should also attempt to record the temporal development of wound morphology, as the present work performs three-dimensional reconstruction only after injection is complete. Combination of force and three-dimensional morphological data would provide an improved understanding of the stress enacted on the tissue, a crucial parameter in investigating wound formation and healing.

In comparing fluid delivery between needle injection and NFLJI, it was found that the injection forces produced were of similar magnitudes. The key differences lay in the duration of injection, which was significantly less in fluid delivery via NFLJI, and work of injection. The injection duration finding directly correlates with the decreased impulse calculated from NFLJI delivery compared to needle injection. This may contribute to the reported decrease in injection pain, as a temporal aspect has been reported [11]. Also potentially relevant to injection pain, it was found that at relevant clinical injection parameters, needle injection is associated with less energy delivered to the tissue than an equivalent injection via NFLJI. This could indicate lesser damage to the tissue. However, given the clinical evidence that NFLJI systems have been associated with decreased injection pain, this result could indicate that the temporal aspect of pain sensation is more dominant than the energy delivered. Moreover, the difference in energy when considering injection via NFLJI at low pneumatic supply pressures is small, indicating that a clinically equivalent injection may be achieved via NFLJI more quickly and with little additional energy delivered and potential tissue damage. This suggests a potential for selecting a method of transdermal drug delivery to optimally manage procedure time, injection pain for the patient, and injection outcomes based on the required injection volume and target anatomical structure. The penetration depth and work of injection data presented here may aid in this clinical decision-making. It was found that injection via NFLJI produced vibrational effects which are not seen in needle injection, and which warrant further investigation. While some of the oscillation observed in the NFLJI injection forces and high-speed video were likely associated with the gelatin phantom as previously described, there will remain a vibrational effect on the tissue which has not been investigated to date and should be addressed in future work. In assessing the wound geometry of each method, a large difference was not observed. Further work should address the dispersion of fluid within the tissue over time.

Promising solutions were proposed to address difficulties reaching the inferior alveolar nerve block. An angled injector provided a potential immediate improvement to the outcome of the clinical pilot testing. This solution may find potentially valuable commercial applications.

6 CONCLUSIONS

The objective of the present work was to contribute to the knowledge base surrounding drug delivery via NFLJI, and in doing so enable the optimization of the technology to the field of dental local anesthesia. This required investigation of the mechanisms of both NFLJI and the conventional drug delivery technique, needle injection. A suitable soft tissue phantom was first developed. It was found that type-II bovine gelatin (5%) provided a reasonable facsimile for the storage modulus and viscosity of porcine oral tissue, and this phantom material was selected for use in the present investigation. The wound morphology created in the gelatin phantom, however, was found to differ from that developed in tissue. As such, a pHEMA phantom was investigated and found to adequately mimic the mechanical properties and porous characteristics of porcine oral mucosa, and to facilitate a wound morphology with greater similarity to that of injection into tissue. The favourable mechanical properties and porosity structure of the pHEMA phantom make it a promising choice for future work, and it should be utilized in future investigations. The mechanisms of needle insertion and needle injection were then characterized. The effects of insertion speed and needle geometry upon the insertion forces, work, and fracture toughness of needle insertion assessed. It was found that increasing needle gauge corresponded with decreased insertion forces and fracture toughness, while a beveled tip geometry decreased insertion forces and fracture toughness. The relationship between insertion speed and insertion force amplitude was found to be non-linear. With respect to needle injection, the effects of injection volume and volumetric flow rate of fluid delivery were then investigated. It was found that increased injection volume corresponded with greater injection force amplitude and calculated impulse of injection, while the relationship between injection volume and work of injection was non-linear. Increased injection volume was found to correlate with a decrease in impulse of injection, due to the decreased injection duration, and an increase in work of injection owing largely to the increased work associated with fluid delivery. Injection volume was associated with no significant change in the magnitude of injection forces developed. Finally, the effects of pneumatic supply pressure and injection volume on the injection forces and work of jet injection were evaluated. Increased injection volume resulted in increased injection force amplitude, impulse, and work of injection. Increased pneumatic supply pressure to the NFLJI system was found to increase the impulse, work, and injection force amplitude at injection volumes of 0.1 mL and 0.3 mL, but the effect at 1 mL was non-linear. Increasing pneumatic supply pressure was also found to correlate with increasing penetration depth of the jet into the soft tissue phantom. Regurgitation of fluid following NFLJI was found to be the highest at low injection volumes in the gelatin phantom. In comparing needle injection and NFLJI as methods of fluid delivery into the soft tissue phantom, it was found that the injection force amplitudes were comparable; however, the injection duration of NFLJI delivery was significantly shorter than that of needle injection. It was also found that NFLJI produced vibrational effects in the tissue, absent in needle injection, which should be further explored in future work. In comparing the energy delivered to the phantom, characterized as the work of injection via each method, it was found that the energy was comparable at an injection volume of 0.3 mL, with needle volumetric flow rate of 7.2 mL and NFLJI pneumatic supply pressure of 413.7 kPa. At the clinical benchmark values of volumetric flow rate of 7.2 mL/minute for needle injection and a NFLJI pneumatic supply pressure of 620.5 kPa, it was found that a 1 mL injection volume was delivered with lesser energy via needle injection. At most configurations investigated, the work of injection, and therefore energy delivered to the tissue, was greater when injection was performed with a NFLJI system. This increase in energy may indicate greater potential damage to the tissue; however, the difference was not large in magnitude for low NFLJI pneumatic supply pressures. Thus, physicians may still potentially take advantage of the shorter duration of injection that NFLJI systems provide. These results may contribute to evidence-based clinical decision-making, allowing clinicians to select their injection parameters based on the desired penetration depth while exposing the patient to minimal injection pain and inflicting minimal damage to patient tissue. The finding that NFLJI delivers the same volume of fluid with greater energy delivered to patient tissue at clinically relevant injection parameters may provide some insight into the pain mechanism of NFLJI as compares to needle injection. Since it was reported that injection via NFLJI was associated with decreased injection pain, this could indicate that pain sensation is dominated by the temporal aspect, as injection via NFLJI is much shorter in duration than via needle. The present investigation, by directly comparing the dynamics of injection via needle and NFLJI, may assist clinicians in selecting the optimal method of drug delivery to achieve the best clinical outcome with minimal patient discomfort.

7 REFERENCES

[1] N. Latifi, M. Asgari, H. Vali, and L. Mongeau, "A tissue-mimetic nano-fibrillar hybrid injectable hydrogel for potential soft tissue engineering applications," *Sci. Rep.*, vol. 8, no. 1, Art. no. 1, Jan. 2018, doi: 10.1038/s41598-017-18523-3.

[2] J. Yang, R. Bai, and Z. Suo, "Topological Adhesion of Wet Materials," *Adv. Mater.*, vol. 30, no. 25, p. 1800671, 2018, doi: https://doi.org/10.1002/adma.201800671.

[3] A. Mohizin and J. K. Kim, "Current engineering and clinical aspects of needle-free injectors: A review," *J. Mech. Sci. Technol.*, vol. 32, no. 12, pp. 5737–5747, Dec. 2018, doi: 10.1007/s12206-018-1121-9.

[4] O. A. Shergold and N. A. Fleck, "Mechanisms of deep penetration of soft solids, with application to the injection and wounding of skin," *Proc. R. Soc. Lond. Ser. Math. Phys. Eng. Sci.*, vol. 460, no. 2050, pp. 3037–3058, Oct. 2004, doi: 10.1098/rspa.2004.1315.

[5] B. E. Earp, S. J. Stanbury, A. N. Mora, and P. E. Blazar, "Needle-Free Jet Lidocaine Administration for Preinjection Anesthesia in Trigger Finger Injection: A Randomized Controlled Trial," *J. Hand Surg.*, vol. 42, no. 8, pp. 618–622, Aug. 2017, doi: 10.1016/j.jhsa.2017.05.001.

[6] M. Hajimaghsoudi, E. Vahidi, M. Momeni, A. Arabinejhad, and M. Saeedi, "Comparison of local anesthetic effect of lidocaine by jet injection vs needle infiltration in lumbar puncture," *Am. J. Emerg. Med.*, vol. 34, no. 7, pp. 1225–1229, Jul. 2016, doi: 10.1016/j.ajem.2016.03.030.

[7] B. Saghi, M. Momeni, M. Saeedi, and M. Ghane, "Efficacy of the jet injector in local anaesthesia for small wound sutures: a randomised clinical trial compared with the needle infiltration technique," *Emerg. Med. J. EMJ*, vol. 32, no. 6, pp. 478–480, Jun. 2015, doi: 10.1136/emermed-2013-203135.

[8] C. S. Makade, P. R. Shenoi, and M. K. Gunwal, "Comparison of acceptance, preference and efficacy between pressure anesthesia and classical needle infiltration anesthesia for dental restorative procedures in adult patients," *J. Conserv. Dent. JCD*, vol. 17, no. 2, pp. 169–174, Mar. 2014, doi: 10.4103/0972-0707.128063.

[9] M. Majstorović and J. Veerkamp, "Relationship between needle phobia and dental anxiety," *J. Dent. Child. Chic. Ill*, vol. 71, pp. 201–5, Sep. 2004.

[10] A. Taddioa, S. Thivakar, A. Jamald, C. Parikha, and S. Smarta, *Contents lists available at SciVerse ScienceDirect*. .

[11] N. P. Fuller, R. A. Menke, and W. J. Meyers, "Perception of pain to three different intraoral penetrations of needles," *J. Am. Dent. Assoc. 1939*, vol. 99, no. 5, pp. 822–824, Nov. 1979, doi: 10.14219/jada.archive.1979.0384.

[12] S. L. Patwekar, S. G. Gattani, and M. M. Pande, "Needle free injection system: A review," *Int J Pharm Pharm Sci*, vol. 5, no. 4, pp. 14–19, 2013.

[13] E. L. Giudice and J. D. Campbell, "Needle-free vaccine delivery," *Adv. Drug Deliv. Rev.*, vol. 58, no. 1, pp. 68–89, Apr. 2006, doi: 10.1016/j.addr.2005.12.003.

[14] J. R. Shapiro *et al.*, "Needle-free delivery of influenza vaccine using the Med-Jet® H4 is efficient and elicits the same humoral and cellular responses as standard IM injection: A randomized trial," *Vaccine*, vol. 37, no. 10, pp. 1332–1339, 28 2019, doi: 10.1016/j.vaccine.2019.01.039.

[15] D. L. B. Pharm.D and F. Pass, "Delivery of Insulin by Jet Injection: Recent Observations," *Diabetes Technol. Ther.*, vol. 3, no. 2, pp. 225–232, Jun. 2001, doi: 10.1089/15209150130020959.

[16] T. Azar and V. Hayward, "Estimation of the Fracture Toughness of Soft Tissue from Needle Insertion," in *Biomedical Simulation*, 2008, pp. 166–175.

[17] N. S. Yen, G.-J. Lan, and C.-L. Lin, "Fracture Toughness Characterization and Mixed-Mode Fracture Finite Element Modeling for Accurate Biopsy Needle Cutting Force Prediction," Apr. 2018, p. V001T08A003-V001T08A003, doi: 10.1115/DMD2018-6834.

[18] F. S. Rocha, R. P. Carneiro, A. E. H. Magalhães, D. Zanetta-Barbosa, L. M. Furtado, and M. C. P. da Silva, "Modified Jorgensen and Hayden Approach to Intraoral Mandibular Anesthesia," *Textb. Adv. Oral Maxillofac. Surg. Vol. 2*, Apr. 2015, doi: 10.5772/59163.

[19] A. B. Baker and J. E. Sanders, "Fluid mechanics analysis of a spring-loaded jet injector," *IEEE Trans. Biomed. Eng.*, vol. 46, no. 2, pp. 235–242, Feb. 1999, doi: 10.1109/10.740886.

[20] B. D. Hemond, D. M. Wendell, N. C. Hogan, A. J. Taberner, and I. W. Hunter, "A Lorentz-Force Actuated Autoloading Needle-free Injector," in *2006 International Conference of the IEEE Engineering in Medicine and Biology Society*, Aug. 2006, pp. 679–682, doi: 10.1109/IEMBS.2006.259918.

[21] J. C. Stachowiak, M. G. von Muhlen, T. H. Li, L. Jalilian, S. H. Parekh, and D. A. Fletcher, "Piezoelectric control of needle-free transdermal drug delivery," *J. Control. Release Off. J. Control. Release Soc.*, vol. 124, no. 1–2, pp. 88–97, Dec. 2007, doi: 10.1016/j.jconrel.2007.08.017.

[22] M. Park, H. Jang, F. V. Sirotkin, and J. J. Yoh, "Er:YAG laser pulse for small-dose splashback-free microjet transdermal drug delivery," *Opt. Lett.*, vol. 37, no. 18, pp. 3894–3896, Sep. 2012, doi: 10.1364/OL.37.003894.

[23] R. M. Klein, E. D. Wolf, R. Wu, and J. C. Sanford, "High-velocity microprojectiles for delivering nucleic acids into living cells. 1987," *Biotechnol. Read. Mass*, vol. 24, pp. 384–386, 1992.

[24] Y.-C. Kim, J.-H. Park, and M. R. Prausnitz, "Microneedles for drug and vaccine delivery," *Adv. Drug Deliv. Rev.*, vol. 64, no. 14, pp. 1547–1568, Nov. 2012, doi: 10.1016/j.addr.2012.04.005.

[25] A. Mohizin, K. R. Roy, D. Lee, S. K. Lee, and J. Kim, "Computational fluid dynamics of impinging microjet for a needle-free skin scar treatment system," *Comput Biol Med.*, 2018, doi: 10.1016/j.compbiomed.2018.08.005.

[26] D. Barolet and A. Benohanian, "Current trends in needle-free jet injection: an update," *Clin. Cosmet. Investig. Dermatol.*, vol. 11, pp. 231–238, 2018, doi: 10.2147/CCID.S162724.

[27] Y. Igarashi, "Clinical Evaluation of the Needle-free Injection System VISION® for Growth Hormone Therapy in Children," *Clin. Pediatr. Endocrinol.*, vol. 15, no. 3, pp. 117–122, 2006, doi: 10.1297/cpe.15.117.

[28] G. M. Duckworth, H. R. Millward, C. D. Potter, G. Hewson, T. L. Burkoth, and B. J. Bellhouse, "Oral PowderJect: a novel system for administering local anaesthetic to the oral mucosa," *Br. Dent. J.*, vol. 185, no. 10, pp. 536–539, Nov. 1998, doi: 10.1038/sj.bdj.4809857.

[29] N. N. Dabarakis, V. Alexander, A. T. Tsirlis, N. A. Parissis, and M. Nikolaos, "Needle-less local anesthesia: clinical evaluation of the effectiveness of the jet anesthesia Injex in local anesthesia in dentistry," *Quintessence Int. Berl. Ger. 1985*, vol. 38, no. 10, pp. E572-576, Dec. 2007.

[30] K. N. Arapostathis, N. N. Dabarakis, T. Coolidge, A. Tsirlis, and N. Kotsanos, "Comparison of acceptance, preference, and efficacy between jet injection INJEX and local infiltration anesthesia in 6 to 11 year old dental patients," *Anesth. Prog.*, vol. 57, no. 1, pp. 3–12, 2010, doi: 10.2344/0003-3006-57.1.3.

[31] A. C. A. de Oliveira *et al.*, "Assessment of anesthetic properties and pain during needleless jet injection anesthesia: a randomized clinical trial," *J. Appl. Oral Sci.*, vol. 27, Jan. 2019, doi: 10.1590/1678-7757-2018-0195.

[32] O. H *et al.*, "Is the jet injection effective for teeth extraction?," *J. Stomatol. Oral Maxillofac. Surg.*, vol. 121, no. 1, pp. 19–24, May 2019, doi: 10.1016/j.jormas.2019.05.001.

[33] L. Geenen, L. A. M. Marks, and L. C. Martens, "[Clinical evaluation of the INJEX system, a local anesthesia system without needles: a comfort evaluation study]," *Rev. Belge Med. Dent.*, vol. 59, no. 3, pp. 149–155, 2004.

[34] J. A. Cooper, L. M. Bromley, A. P. Baranowski, and S. G. Barker, "Evaluation of a needle-free injection system for local anaesthesia prior to venous cannulation," *Anaesthesia*, vol. 55, no. 3, pp. 247–250, Mar. 2000, doi: 10.1046/j.1365-2044.2000.01210.x.

[35] B. Maurin *et al.*, "In vivo study of forces during needle insertions," vol. 14, Apr. 2004, doi: 10.1142/9789812702678_0056.

[36] A. Leibinger *et al.*, "Soft Tissue Phantoms for Realistic Needle Insertion: A Comparative Study," *Ann. Biomed. Eng.*, vol. 44, no. 8, pp. 2442–2452, 2016, doi: 10.1007/s10439-015-1523-0.

[37] A. Asadian, R. V. Patel, and M. R. Kermani, "Dynamics of Translational Friction in Needle–Tissue Interaction During Needle Insertion," *Ann. Biomed. Eng.*, vol. 42, no. 1, pp. 73–85, Jan. 2014, doi: 10.1007/s10439-013-0892-5.

[38] T. Prasetyono and P. Adhistana, "Laboratory Study on Injection Force Measurement on Syringe and Needle Combinations," *Malays. J. Med. Sci.*, vol. 26, pp. 66–76, May 2019, doi: 10.21315/mjms2019.26.2.8.

[39] M. Oldfield, D. Dini, G. Giordano, and F. Rodriguez Y Baena, "Detailed finite element modelling of deep needle insertions into a soft tissue phantom using a cohesive approach," *Comput. Methods Biomech. Biomed. Engin.*, vol. 16, no. 5, pp. 530–543, 2013, doi: 10.1080/10255842.2011.628448.

[40] K. Comley and N. Fleck, "Deep penetration and liquid injection into adipose tissue," *J. Mech. Mater. Struct.*, vol. 6, no. 1, pp. 127–140, Jun. 2011, doi: 10.2140/jomms.2011.6.127.

[41] C. Gokgol, C. Basdogan, and D. Canadinc, "Estimation of fracture toughness of liver tissue: Experiments and validation," *Med. Eng. Phys.*, vol. 34, no. 7, pp. 882–91, Sep. 2012, doi: 10.1016/j.medengphy.2011.09.030.

[42] T. Kato *et al.*, "Mechanics of the injected pulsejet into gelatin gel and evaluation of the effect by puncture and crack generation and growth," *J. Appl. Phys.*, vol. 116, no. 7, p. 074901, Aug. 2014, doi: 10.1063/1.4893175.

[43] A. Kiyama *et al.*, "Visualization of penetration of a high-speed focused microjet into gel and animal skin," *J. Vis.*, vol. 22, no. 3, pp. 449–457, Jun. 2019, doi: 10.1007/s12650-019-00547-8.

[44] C. Squier and K. A. Brogden, "The Functions of Oral Mucosa," in *Human Oral Mucosa*, John Wiley & Sons, Ltd, 2013, pp. 1–7.

[45] J. Chen, R. Ahmad, W. Li, M. Swain, and Q. Li, "Biomechanics of oral mucosa," *J. R. Soc. Interface*, vol. 12, no. 109, p. 20150325, Aug. 2015, doi: 10.1098/rsif.2015.0325.

[46] S. Goktas, J. J. Dmytryk, and P. S. McFetridge, "Biomechanical behavior of oral soft tissues," *J. Periodontol.*, vol. 82, no. 8, pp. 1178–1186, Aug. 2011, doi: 10.1902/jop.2011.100573.

[47] C. Squier and K. A. Brogden, "The Organization of Oral Mucosa," in *Human Oral Mucosa*, John Wiley & Sons, Ltd, 2013, pp. 9–17.

[48] T. Seto, H. Yamamoto, K. Takayama, A. Nakagawa, and T. Tominaga, "Characteristics of an actuator-driven pulsed water jet generator to dissecting soft tissue," *Rev. Sci. Instrum.*, vol. 82, no. 5, p. 055105, May 2011, doi: 10.1063/1.3587069.

[49] Y. Tagawa, N. Oudalov, A. El Ghalbzouri, C. Sun, and D. Lohse, "Needle-free injection into skin and soft matter with highly focused microjets," *Lab. Chip*, vol. 13, no. 7, pp. 1357–1363, 2013, doi: 10.1039/C2LC41204G.

[50] P. Rohilla and J. O. Marston, "In-vitro studies of jet injections," *Int. J. Pharm.*, vol. 568, p. 118503, Sep. 2019, doi: 10.1016/j.ijpharm.2019.118503.

[51] J. Schramm-Baxter and S. Mitragotri, "Needle-free jet injections: dependence of jet penetration and dispersion in the skin on jet power," *J. Controlled Release*, vol. 97, no. 3, pp. 527–535, Jul. 2004, doi: 10.1016/j.jconrel.2004.04.006.

[52] J. Schramm-Baxter, J. Katrencik, and S. Mitragotri, "Jet injection into polyacrylamide gels: investigation of jet injection mechanics," *J. Biomech.*, vol. 37, no. 8, pp. 1181–1188, Aug. 2004, doi: 10.1016/j.jbiomech.2003.12.006.

[53] Y. He *et al.*, "Characterizing mechanical and medical imaging properties of polyvinyl chloride-based tissue-mimicking materials," *J. Appl. Clin. Med. Phys.*, vol. 20, no. 7, pp. 176–183, 2019, doi: 10.1002/acm2.12661.

[54] R. F. Donnelly, D. I. J. Morrow, P. A. McCarron, M. J. Garland, and A. D. Woolfson, "Influence of solution viscosity and injection protocol on distribution patterns of jet injectors: Application to photodynamic tumour targeting," *J. Photochem. Photobiol. B*, vol. 89, no. 2, pp. 98–109, Dec. 2007, doi: 10.1016/j.jphotobiol.2007.09.009.

[55] O. A. Shergold, N. A. Fleck, and T. S. King, "The penetration of a soft solid by a liquid jet, with application to the administration of a needle-free injection," *J. Biomech.*, vol. 39, no. 14, pp. 2593–2602, Jan. 2006, doi: 10.1016/j.jbiomech.2005.08.028.

[56] T. M. Grant, K. D. Stockwell, J. B. Morrison, and D. D. Mann, "Effect of injection pressure and fluid volume and density on the jet dispersion pattern of needle-free injection devices," *Biosyst. Eng.*, vol. 138, pp. 59–64, Oct. 2015, doi: 10.1016/j.biosystemseng.2015.04.010.

[57] P. J. Pritchard, *Fox and McDonald's Introduction to Fluid Mechanics, 8th Edition*. John Wiley & Sons, 2010.

[58] R. Chen, D. Zhang, and Y. Wu, "Study on the influence of standoff distance on substrate damage under an abrasive water jet process by molecular dynamics simulation," *Friction*, vol. 6, no. 2, pp. 195–207, Jun. 2018, doi: 10.1007/s40544-017-0168-4.

[59] C. C. Xu, R. W. Chan, D. G. Weinberger, G. Efune, and K. S. Pawlowski, "A bovine acellular scaffold for vocal fold reconstruction in a rat model," *J. Biomed. Mater. Res. A*, vol. 92, no. 1, pp. 18–32, Jan. 2010, doi: 10.1002/jbm.a.32279.

[60] S. Malamed, *Handbook of Local Anesthesia*, 7th ed. Mosby, 2019.

8 DETAILED INJECTION DATASETS

8.1 NEEDLE INSERTION

8.1.1 Effect of Needle Gauge

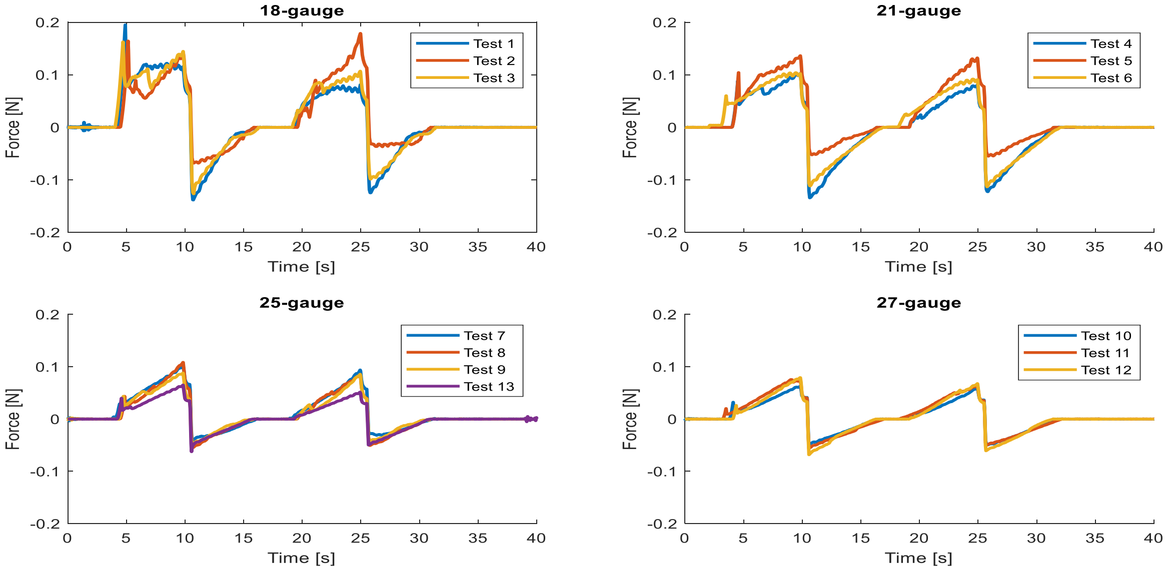

Figure 55: Time history of measured force (in Newtons) for needle insertion of a flat-tipped needle into the gelatin (5%) phantom at an insertion speed of 5 mm/s with varied needle gauge.

8.1.2 Effect of Needle Geometry

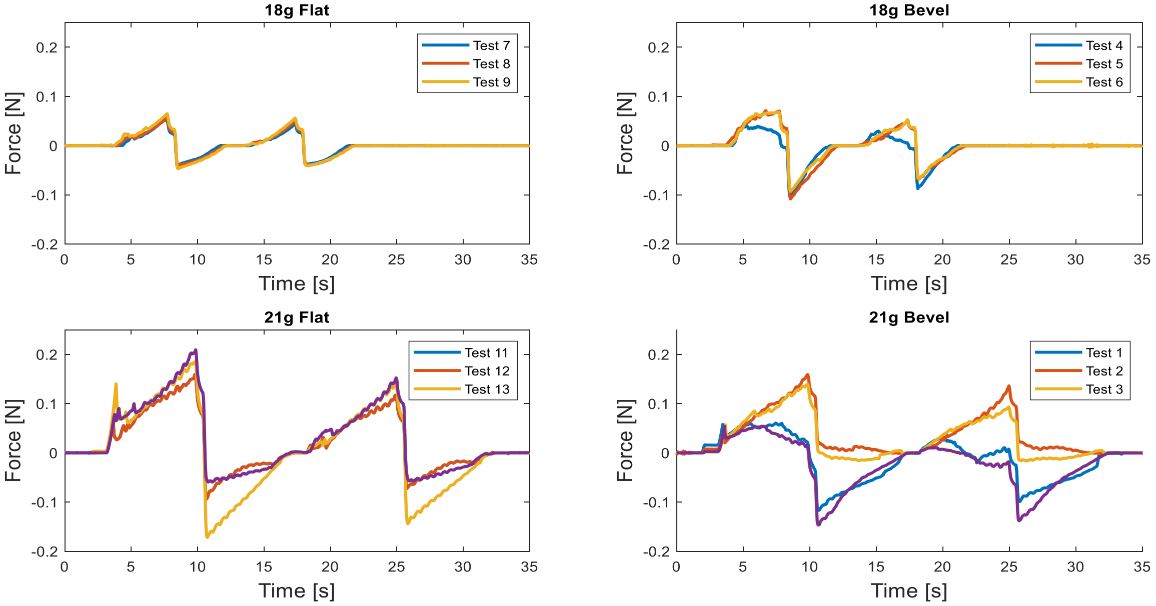

Figure 56: Time history of measured force (in Newtons) for needle insertion into the gelatin (5%) phantom at an insertion speed of 5 mm/s with varied needle gauge and tip geometry.

8.1.3 Effect of Needle Insertion Speed:

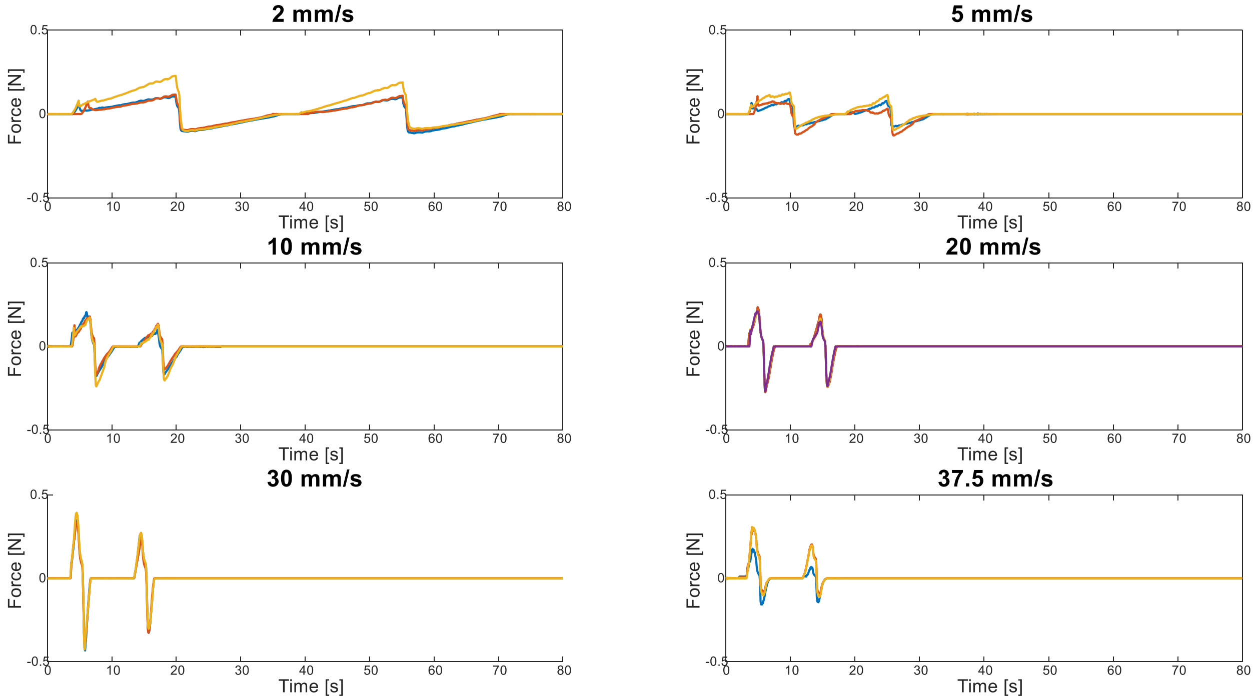

Figure 57: Time history of measured force (in Newtons) for needle insertion into the gelatin (5%) phantom at insertion speeds of 2-37. 5 mm/s with 21-gauge flat-tipped needle.

8.2 NEEDLE INJECTION

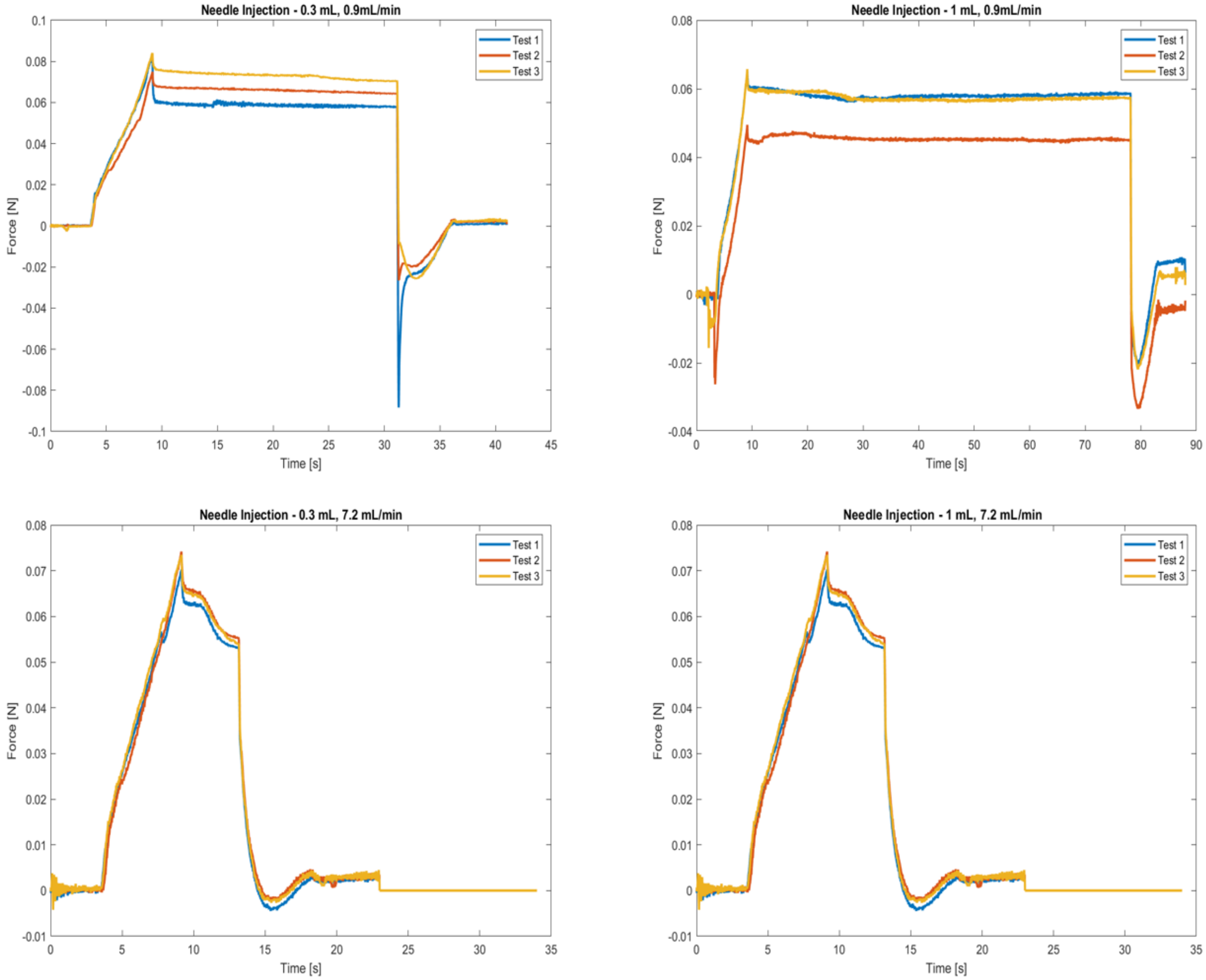

Figure 58: Time history of measured force (in Newtons) for each needle injection performed.

8.3 INJECTION VIA NFLJI

8.3.1 Force Time History

Supply Pressure = 60 psi, Injection Volume = 0.1 mL

Test 1 **Test 2** **Test 3** **Test 5** **Test 6** **Test 7**

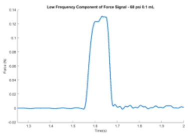

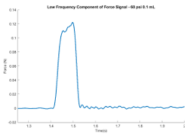

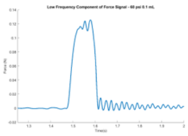

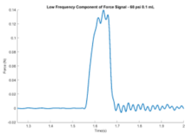

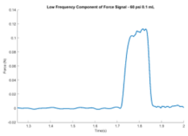

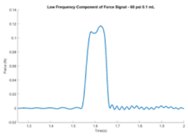

Supply Pressure = 90 psi, Injection Volume = 0.1 mL

Test 1 **Test 2** **Test 3** **Test 4** **Test 5**

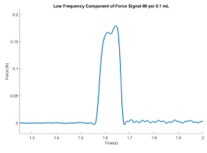

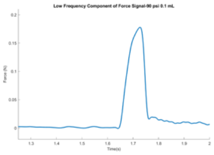

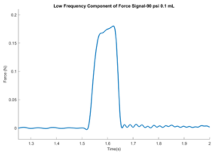

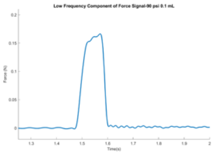

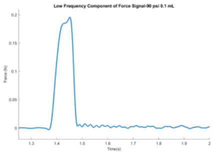

Supply Pressure = 120 psi, Injection Volume = 0.1 mL

Test 1 **Test 2** **Test 3** **Test 4** **Test 5** **Test 6**

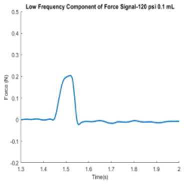

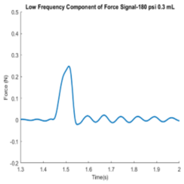

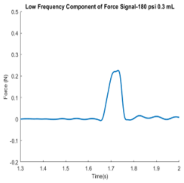

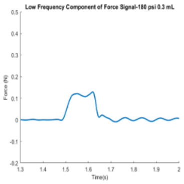

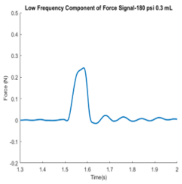

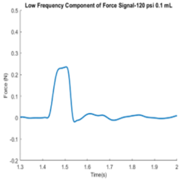

Supply Pressure = 150 psi, Injection Volume = 0.1 mL

Test 1 **Test 2** **Test 3** **Test 4** **Test 5**

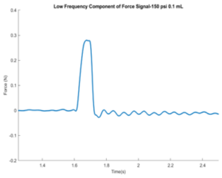

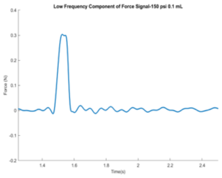

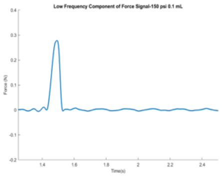

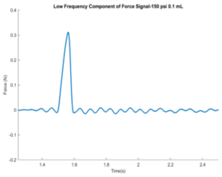

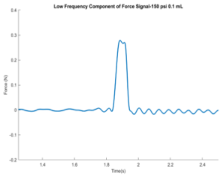

Supply Pressure = 180 psi, Injection Volume = 0.1 mL

Test 1 **Test 2** **Test 3** **Test 4** **Test 5**

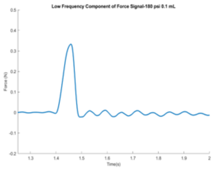

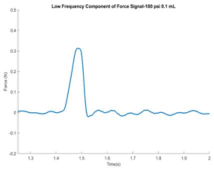

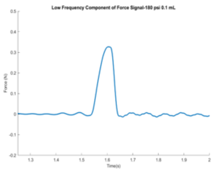

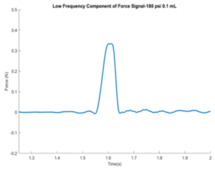

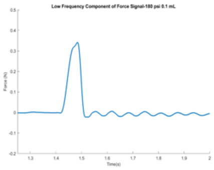

Supply Pressure = 60 psi, Injection Volume = 0.3 mL

Test 1

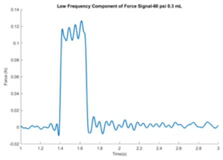

Test 2

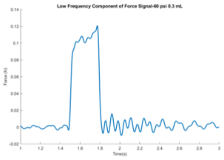

Test 3

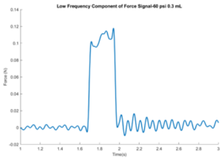

Test 4

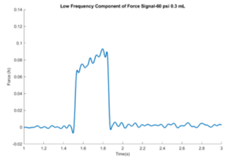

Test 5

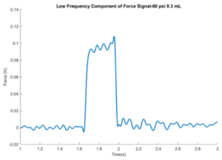

Supply Pressure = 90 psi, Injection Volume = 0.3 mL

Test 1

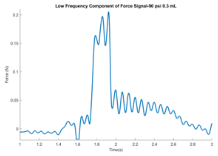

Test 2

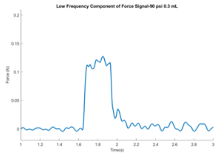

Test 3

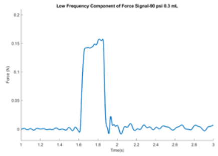

Test 4

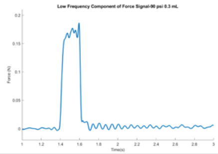

Test 5

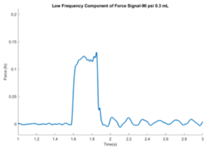

Supply Pressure = 120 psi, Injection Volume = 0.3 mL

Test 1

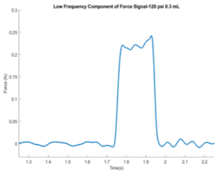

Test 2

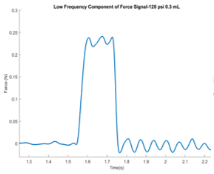

Test 3

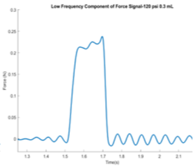

Test 4

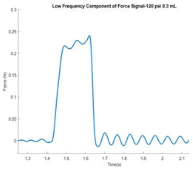

Test 5

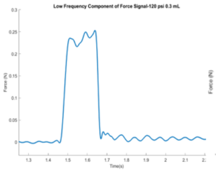

Test 6

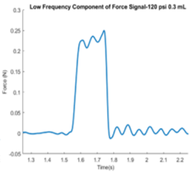

Supply Pressure = 150 psi, Injection Volume = 0.3 mL

Test 1

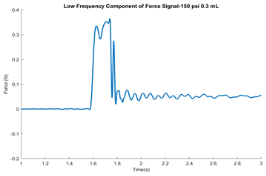

Test 2

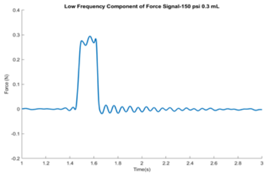

Test 3

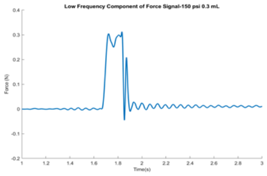

Test 4

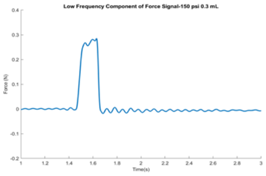

Supply Pressure = 180 psi, Injection Volume = 0.3 mL

Test 1

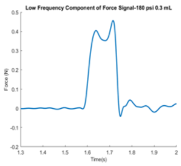

Test 2

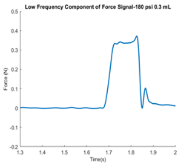

Test 3

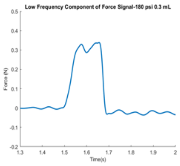

Test 4

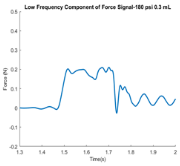

Test 5

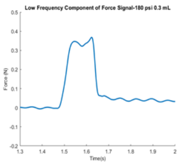

Test 6

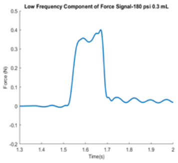

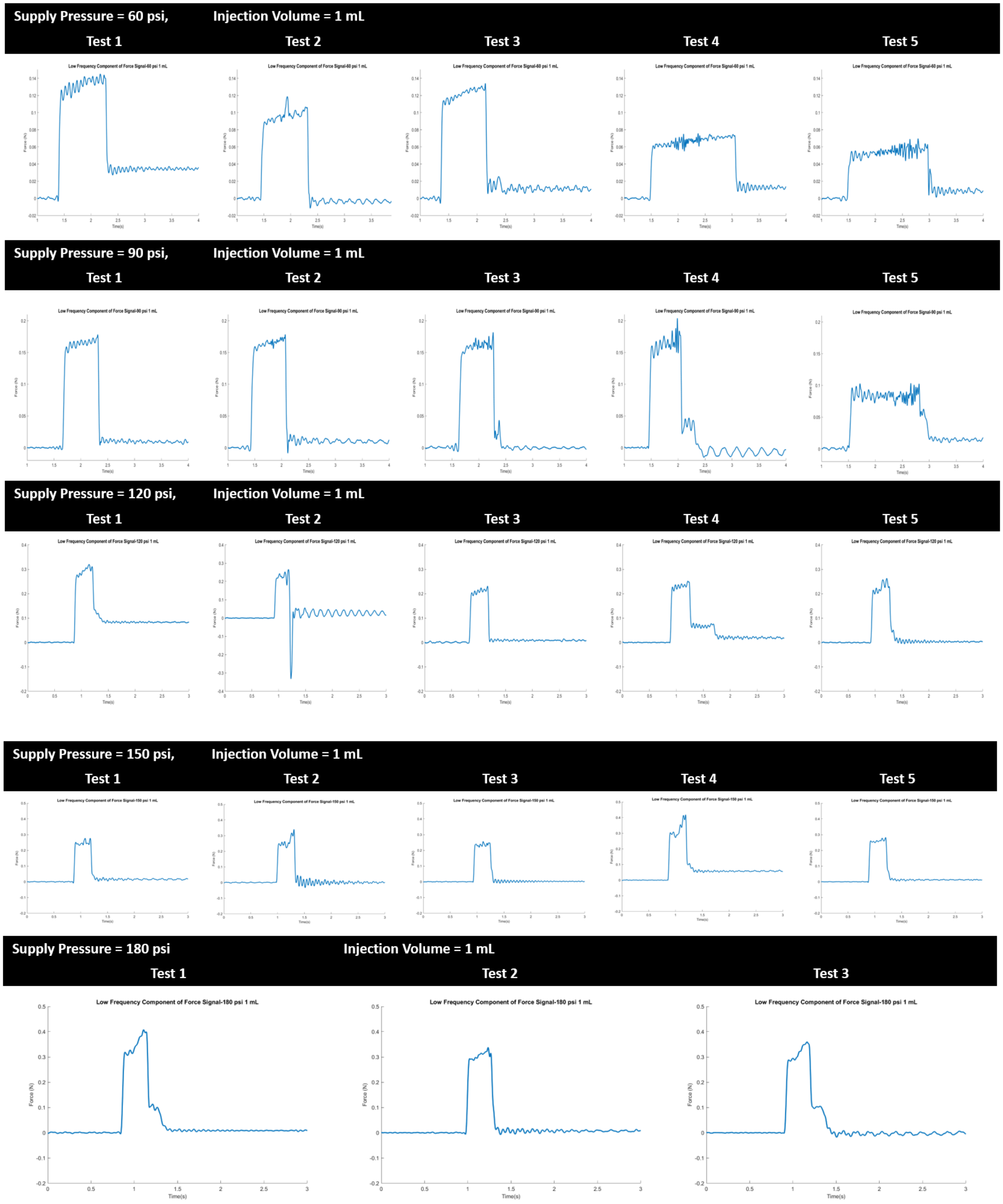

Figure 59: Time history of measured force (in Newtons) for each jet injection performed.

8.3.2 Penetration Depth vs. Time

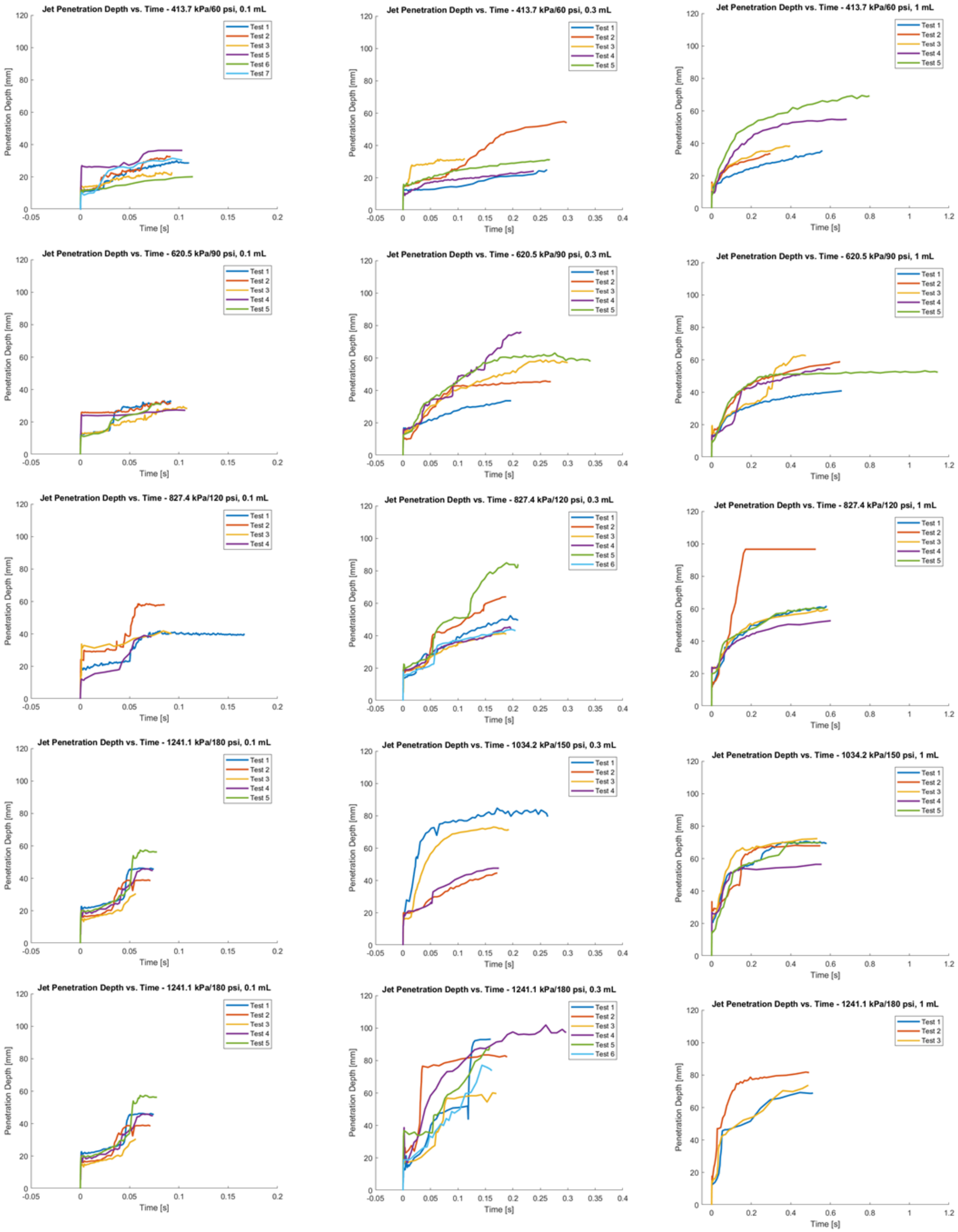

Figure 60: Time history of penetration depth (in millimetres) for each jet injection performed.

8.3.3 Force vs. Penetration Depth

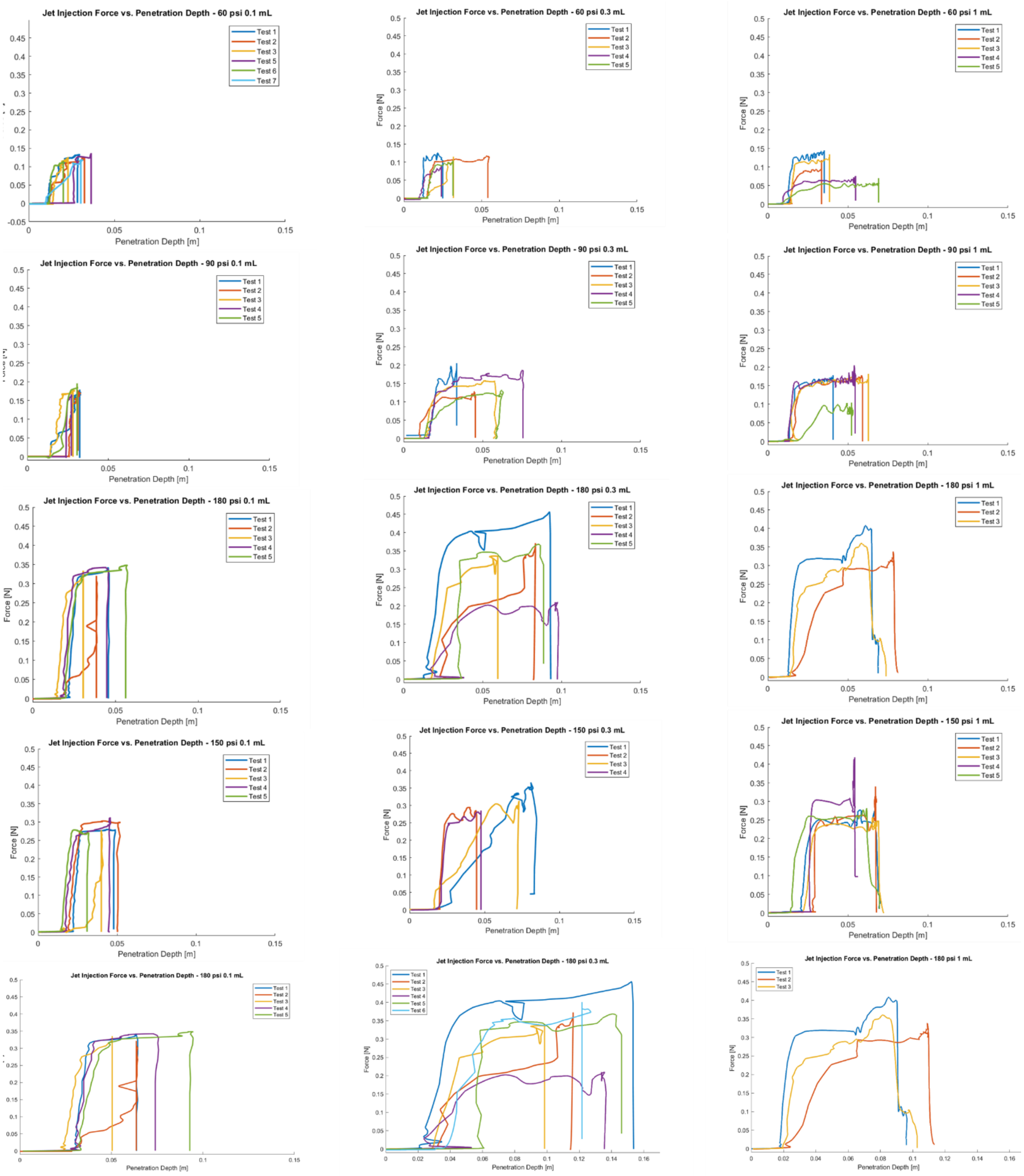

Figure 61: Force (in Newtons) vs. Penetration Depth (in metres) for each jet injection performed.